

Durham E-Theses

The pomeron and the multiperipheral model

Kamal Seyed-Yagoobi

How to cite:

Seyed-Yagoobi, Kamal (1976) The pomeron and the multiperipheral model. Doctoral thesis, Durham University.

Use policy

The full-text may be used and/or reproduced, and given to third parties in any format or medium, without prior permission or charge, for personal research or study, educational, or not-for-profit purposes provided that:

- a full bibliographic reference is made to the original source
- a <https://etheses.durham.ac.uk/id/eprint/8143/> is made to the metadata record in Durham E-Theses
- the full-text is not changed in any way

The full-text must not be sold in any format or medium without the formal permission of the copyright holders.

Please consult the [full Durham E-Theses policy](#) for further details.

THE POMERON
AND
THE MULTIPERIPHERAL MODEL

by

Kamal Seyed-Yagoobi

The copyright of this thesis rests with the author.
No quotation from it should be published without
his prior written consent and information derived
from it should be acknowledged.

A thesis presented for the degree of
Doctor of Philosophy
at the
University of Durham
April 1976

Mathematics Department,
University of Durham,
Science Site,
Durham City DH1 3LE,
England.



PREFACE

The work presented in this thesis was carried out in the Department of Mathematics of the University of Durham between October 1973 and December 1975 under the supervision of Professor E.J. Squires.

The material in this thesis has not been submitted previously for any degree in this or any other university. No claim of originality has been made for chapter one and most of the chapters two and three and where referenced.

The author wishes to express his sincere thanks to Professor Squires for his continuous help, guidance and patience throughout the stages of the present work, and also, for critically reading the manuscript and correcting the English. He, furthermore, wishes to extend his gratitudes to the lecturers of the Mathematics and Theoretical Physics Departments whom he benefited from a great deal by attending their lectures. Miss A. Yeates is also thanked for skillfully typing the thesis. A partial financial support from the British Council is also acknowledged. Finally, he would like to kindly thank his parents for their guidance and help.

ABSTRACT

In general this thesis is concerned with high energy elementary particle physics and in particular it discusses the interactions in the framework of the multiperipheral context.

The first chapter is a general introduction to the field where different observables of interest, such as cross-section and multiplicity, are defined and discussed.

In the second chapter after introducing different multiparticle production mechanisms, such as multiperipheral and diffractive models, we put more emphasis on the former and study different models of the type.

The impact parameter space is a suitable place to work in, so we transform the multiparticle amplitude to this space and extract interesting results out of it in chapter 3. Especially the works of Henyey and Jedach-Turnau are emphasized in this chapter. We show that it is hard to reconcile the model with the experimentally observed radius of elastic scattering as a function of energy.

The fourth chapter is about the interference diagrams of the multiperipheral model in the unitarity equation. As energy increases the number of such terms increases rapidly. We have estimated their effect in Henyey and Jedach-Turnau types of calculation and have added them to the 'standard' result. It is found that, as far as the radius is concerned, these extra terms ($n!-1$ of them) do not make a significant contribution.

In chapter five a modification of the basic multiperipheral amplitude is introduced in order to improve agreement with experiment. This successfully reproduces the known results.

CONTENTS

	<u>Page</u>
Preface	
Abstract	
CHAPTER 1 Phenomenology	
1.1 Opening	2
1.2 Introduction	4
1.3 Amplitudes	5
1.4 Cross-Sections	9
1.5 Multiplicities	15
1.6 Definition of Variables	19
1.7 Inclusive Cross-Sections	23
1.8 Correlations	33
1.9 Regge Theory	39
CHAPTER 2 Multiperipheral Models	
2.1 Introduction	43
2.2 Diffractive and Non-Diffractive Models - a general survey	44
2.3 Multiperipheral Models	49
CHAPTER 3 Many Body Amplitudes and Elastic Scattering	
3.1 Introduction	63
3.2 Impact Parameter Space (Henyeu Work)	64
3.3 The Work of Jedach-Turnau	67
3.4 The Random Walk Picture	76
CHAPTER 4 Interference Diagrams	
4.1 Introduction	79
4.2 Some Earlier Works	80
4.3 General Treatment of the Diagrams	84
4.4 Transverse Momentum Distribution	94
4.5 The Jedach and Turnau Effect	100
4.6 The Effect of Interference Diagrams	101
CHAPTER 5 A Link Dependent Model	
5.1 Introduction	111
5.2 What has happened during the last two years?	112
5.3 The Model	114
5.4 On the parameter γ	126
5.5 Conclusions	128

APPENDIX A	Poissonian σ_n and f_2	129
APPENDIX B	The inverse transformation of (3.8)	131
APPENDIX C	An integration (corresponding to 4.10)	134
APPENDIX D	An integration (corresponding to 4.3b)	136
APPENDIX E	A general integration	138
REFERENCES		141

CHAPTER ONE

PHENOMENOLOGY



1.1. Opening

Physics has been defined long time ago as the science that studies nature. Nature consists of different sorts of matter. Some 150 years ago man happened to discover that matter itself was made of smaller bits and later called these bits 'elements'. Elements are neatly classified in Mandaleev table according to their atomic quantum numbers. This was the realm of 'modern' physics till late eighteen hundred. The theory of relativity of Einstein and quantum mechanics of Dirac were two pushing forces that made Physics to change its stationary state to a mobile one. The resulting motion brought physics to the territory of discovery of new particles. Thus a new set of particles were added to the previously established proton, neutron, electron and photon collection. According to the latest data particle group¹ information there are nearly 150 'elementary' particles now. The dazzling attraction of simplicity once more hinted man to suggest that these elementary particles themselves were made of just three 'more' elementary particles, called quarks. Indeed, apart from recently discovered Ψ particles² all of the presently established particles could be described in terms of the standard quarks! Since quarks are not experimentally seen, this fact casts some doubts as to whether or not they are physically existing objects. There is, however another method of classifying the elementary particles, never mind this is not as plausible as the quark model classification scheme. This invokes the idea of the way the particles interact. Hence particles are nested in strong, weak and electromagnetic cages. What the thesis is concerned about is a small section of a huge subject called strong interaction.

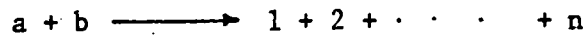
What one observes during an experiment in a high energy laboratory

is that two colliding beams of particles produce some outgoing ones. The information that one extracts from such scattering processes, at a given lab. momentum, includes the number of produced particles, the number and angles at which the secondaries emerge, momenta and energies the produced particles carry out and the type of particles. The next step is that these rather raw information are transformed into the language which is understandable to the theorists. The usage of the translated information is that, for example, it guides phenomenologists to the most appropriate way of simplifying the phase space. In a later stage, data is a test that confirms how 'reasonable' a specific model is.

The outline of the present chapter is to briefly summarize the situation of data at high energies which is of direct interest to us. By 'high energy' one thinks of those energy ranges in which the effect of masses of incoming particles are immaterial and we are well above the resonance region. The chapter will serve to define notation and conventions which we try to use consistently throughout the present work.

1.2. INTRODUCTION

The result of two or more particles interaction is the emission and production of some secondaries which obey a set of conservation laws. The secondaries could be studied upon in different ways. One way is to consider every individual of the produced particles. This corresponds to the following type of interaction,



This is referred to as an exclusive process. As the energy of the system increases, n grows too (fig. 1.1) and it gets more difficult to study all of the particles one by one. Hence the idea of one particle inclusive process, introduced by Feynman. Here one considers only one type of particle. The process is,



where x represents anything which does not include c -type particles. There is, however, another type of process which is less inclusive. This is referred to as semi inclusive process. A typical example would be the following,

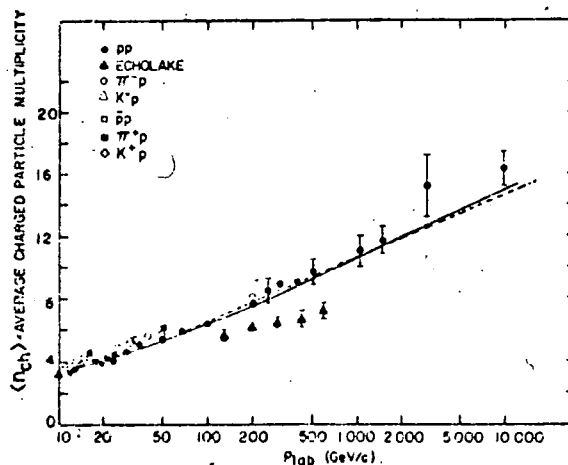


Fig 1.1 The average charged particle multiplicities per inelastic collision for all available data above 10 GeV/c. The dashed curve is the result of a $\ln S$ fit to data.

1.3. AMPLITUDES

Let us suppose that $|i\rangle$ and $|f\rangle$ show respectively the state of particles before and after collision takes place. These two states are related through a scattering amplitude which is defined as $\langle f|S|i\rangle$. As the quantum mechanics indicates, the square of the amplitude, $|\langle f|S|i\rangle|^2$ is proportional to the probability of initial state $|i\rangle$ being scattered into the final state $|f\rangle$. The conservation of probability imposes a very strong constraint upon the scattering amplitudes in general. This could be formulated as the following,

$$\sum_n \langle f|S|n\rangle \langle n|S|i\rangle = 1.$$

The complete intermediate state $|n\rangle$ covers all possible states that $|i\rangle$ could get transformed into. A pictorial representation of this constraint is given in fig. 1.2. This is referred to as the unitarity condition. In operator notations, the condition takes the familiar form

$$S S^\dagger = S^\dagger S = 1.$$

It is customary to separate the probability amplitude for no interaction by defining the A matrix,

$$S = I + i A$$

A could be related to measurable quantities. Mandelestam analyticity demands that at most only isolated singularities, poles or cuts, could be accommodated in A, provided that they are required by unitarity. Elastic amplitudes occupy a particular place and deserve more attention. Therefore we shall say one word or two about elastic scatterings.

Elastic scattering is a diffractive process. This means that $(d\sigma/dt)_e$ has an energy independent, or at most weakly dependent, structure. This fact has been displayed in fig. 1.3 for proton - proton elastic scattering which extends up to ISR energy range.

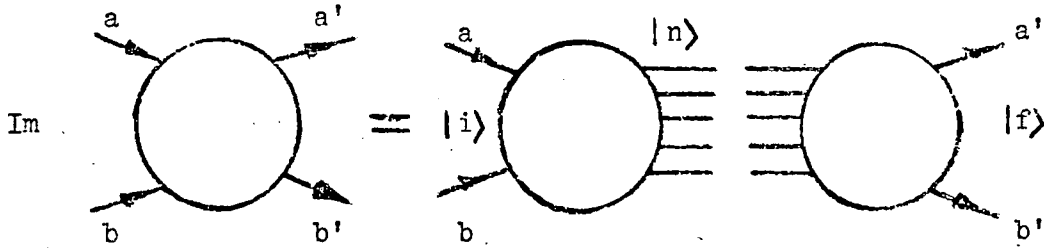


Fig 1.2

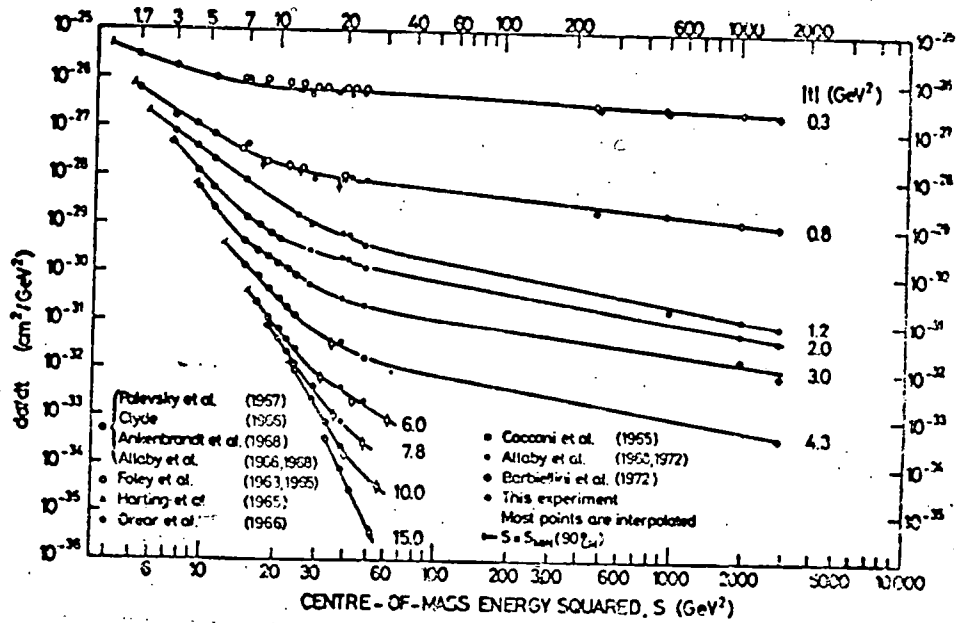


Fig 1.3 pp elastic scattering

Shrinkage of (PP) diffractive peak is also a phenomenon associated with elastic scattering. The rate of shrinkage, which is measured according to a 'slope parameter' $b(s)$, defined by,

$$b(s) = \frac{\partial}{\partial t} \ln \frac{d\sigma/dt}{(d\sigma/dt)_{t=0}},$$

is a slowly varying function of energy (fig. 1.4). A final remark to be added is the dominance of imaginary part of the elastic amplitude over the real part of it at high energies. This could be inferred by a comparison of σ_{tot} and $d\sigma/dt$ and is supported by data⁴ (see Fig. 1.5).

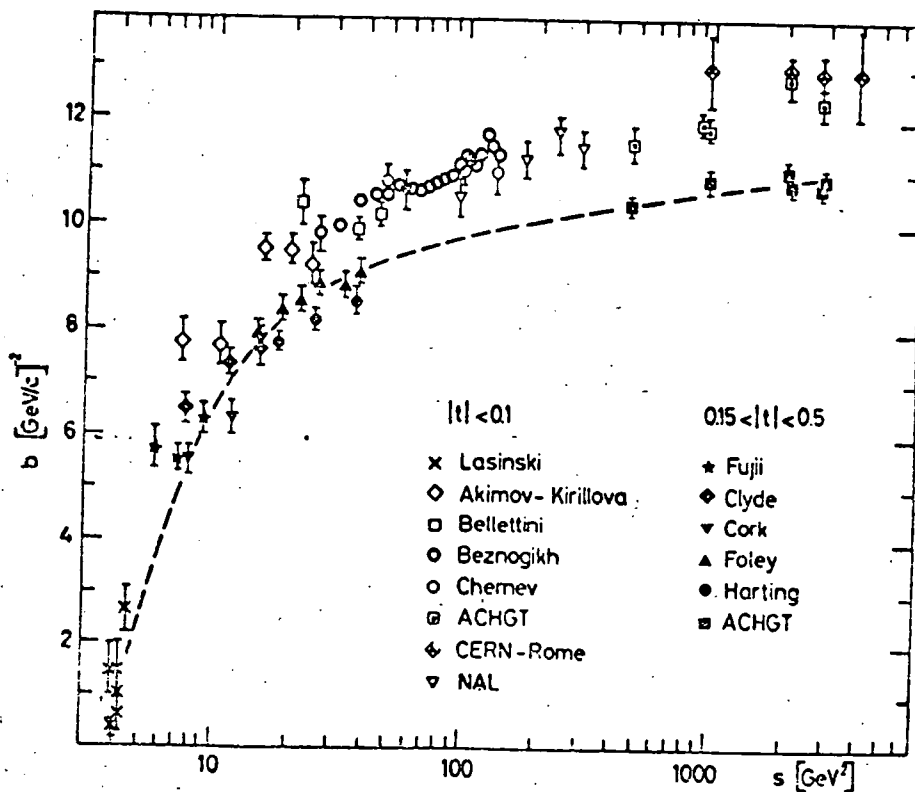


Fig 1.4 Slope parameter in pp scattering for different t regions.

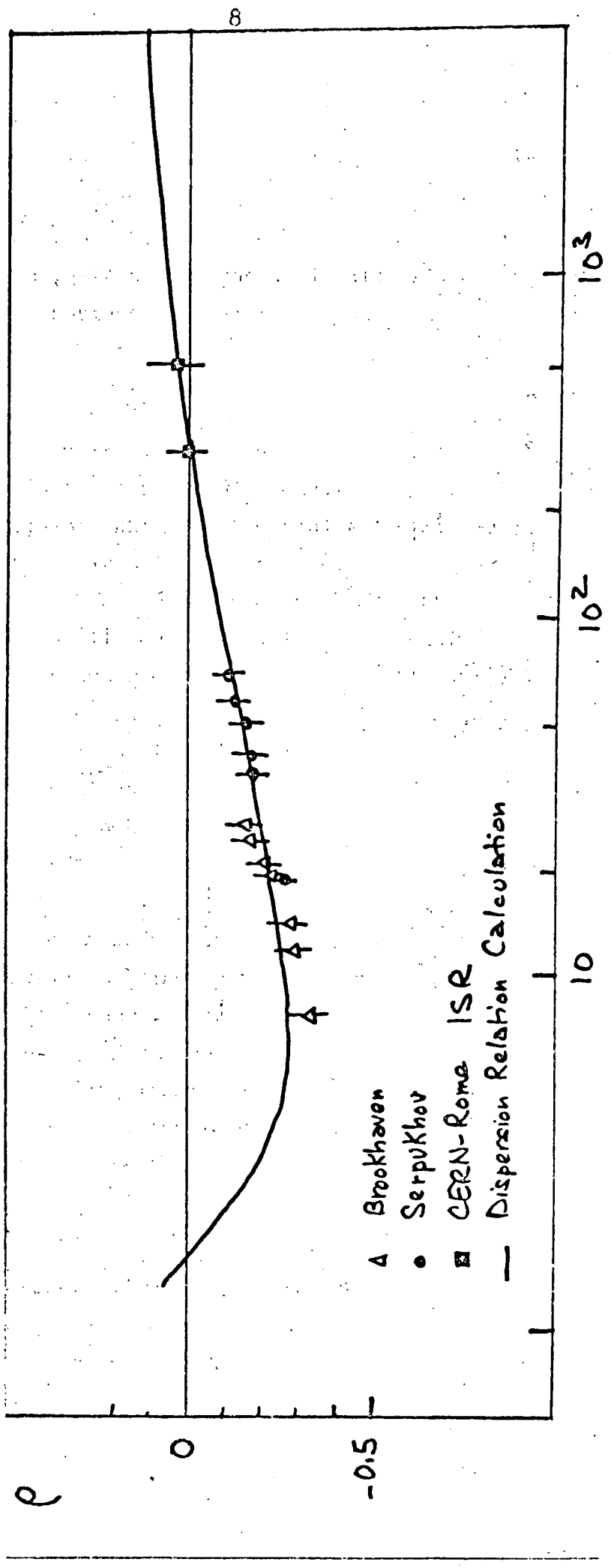


Fig 1.5 The ratio of the real to the imaginary part of the forward scattering amplitude.

1.4. CROSS-SECTIONS

Total cross-section, σ_{tot} is one of the measurable quantities, which helps to clarify the hadrons interactions as well as their structures. For instance, the fact that σ_{tot} of hadrons are of the order of tens of millibarns suggests that hadrons are objects with characteristic dimension of a fermi.

The total cross section is defined as

$$\sigma_{tot}(s) = \frac{1}{2s} \sum_{n=2}^{\infty} \int d\Phi_n |A(P_1 P_2 \rightarrow q_1 \dots q_n)|^2,$$

where $d\Phi_n$ is the n-particle phase space element,

$$d\Phi_n = \prod_{i=1}^n \left[\frac{d^3 q_i}{2\omega_i (2\pi)^3} \right] \delta^4(P - \sum q_i).$$

The kinematics is defined in fig. 1.6.

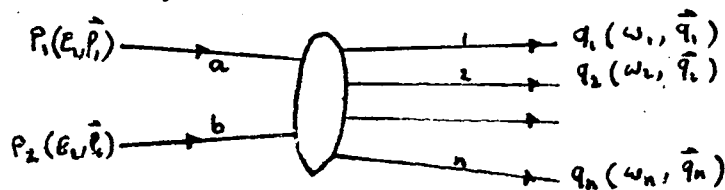


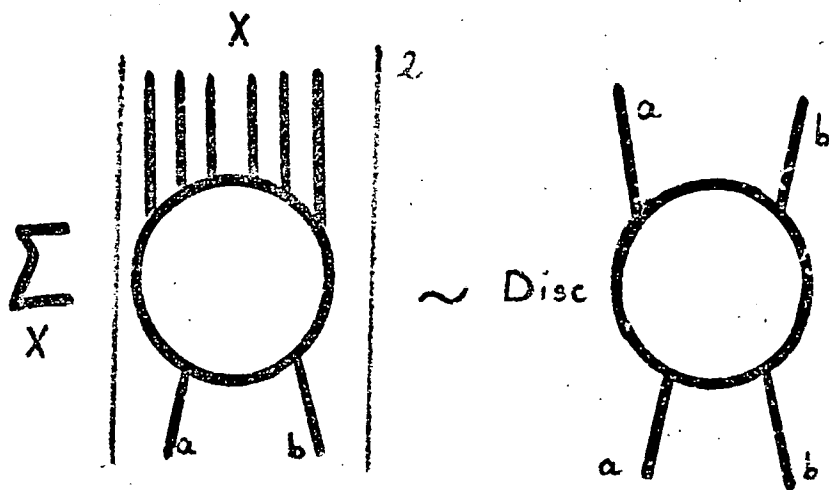
(Fig. 1.6)

Imposing unitarity conditions upon forward elastic scattering, one arrives at the optical theorem. The theorem relates total cross-section, which is experimentally measurable quantity, to the forward elastic scattering amplitude,

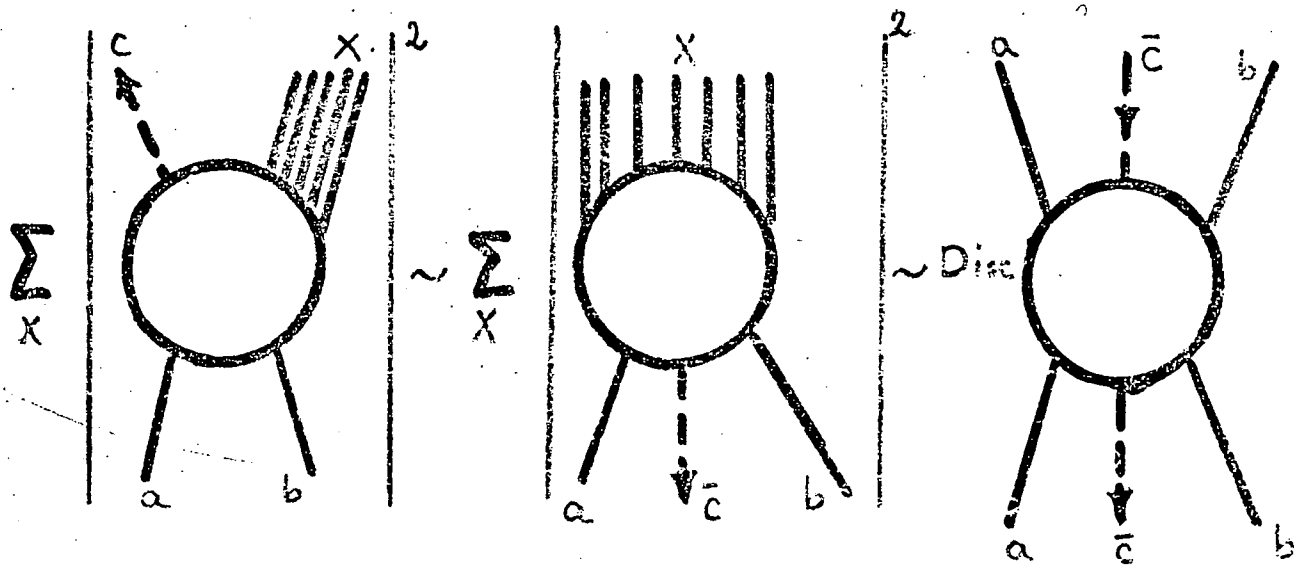
$$\text{Im } A^{\text{el}}(s, t=0) = s \sigma_{tot}(s).$$

Mueller⁴ has generalized this theorem to a far more complicated case, that is one particle inclusive reaction. His generalization connects inclusive cross sections to the forward multiparticle amplitudes. The generalized theorem has been extensively used in the phenomenology of multiparticle processes jointly with Regge phenomenology. Diagrammatically one could show these two theorems as in figure 1.7.

There are a number of general and model independent theorems



optical theorem



generalised optical theorem

Fig 1.7

which are observed by cross sections. The first one, which puts a limit on the growth of σ_{tot} is called Froissart bound.⁵

The beauty of this theorem is that it is a general and model independent statement. It states that the total cross section for any process cannot grow faster than $(\ln s)^2$ as $s \rightarrow \infty$,

$$\sigma_{\text{tot}}(s) \leq \text{const} (\ln s)^2.$$

The second one is known as the Pomeranchuk theorem.⁶ This simply states that the total cross-section of either particle and anti-particle become asymptotically equal,

$$\sigma_{ab}(s) \xrightarrow{s \rightarrow \infty} \sigma_{\bar{a}\bar{b}}(s).$$

The last statement is that total cross-sections of particles belonging to the same isospin multiplets are the same,

$$\sigma_{\text{tot}}(a_i b_j) = \sigma_{\text{tot}}(a_k b_l),$$

where a_i , a_k as well as b_j and b_l belong to the same isospin multiplets.

Experiments,⁷ done within a broad range of energy, indicate that total cross-section is a very slowly varying function of s , fig. 1.8, and that about twenty per cent of it is due to elastic scattering channel (fig. 1.9). At this stage it would be interesting to ask the following question: What is a total cross-section built up of? The total cross-section is made up of some prong cross-sections which, following Horn and Zachariasen,⁸ are called topological cross-sections, σ_n . The topological cross-sections are changing rapidly with energy⁹ (fig. 1.10), but this happens in such a way that when adding up all σ_n to produce σ_{tot} the result becomes roughly constant.

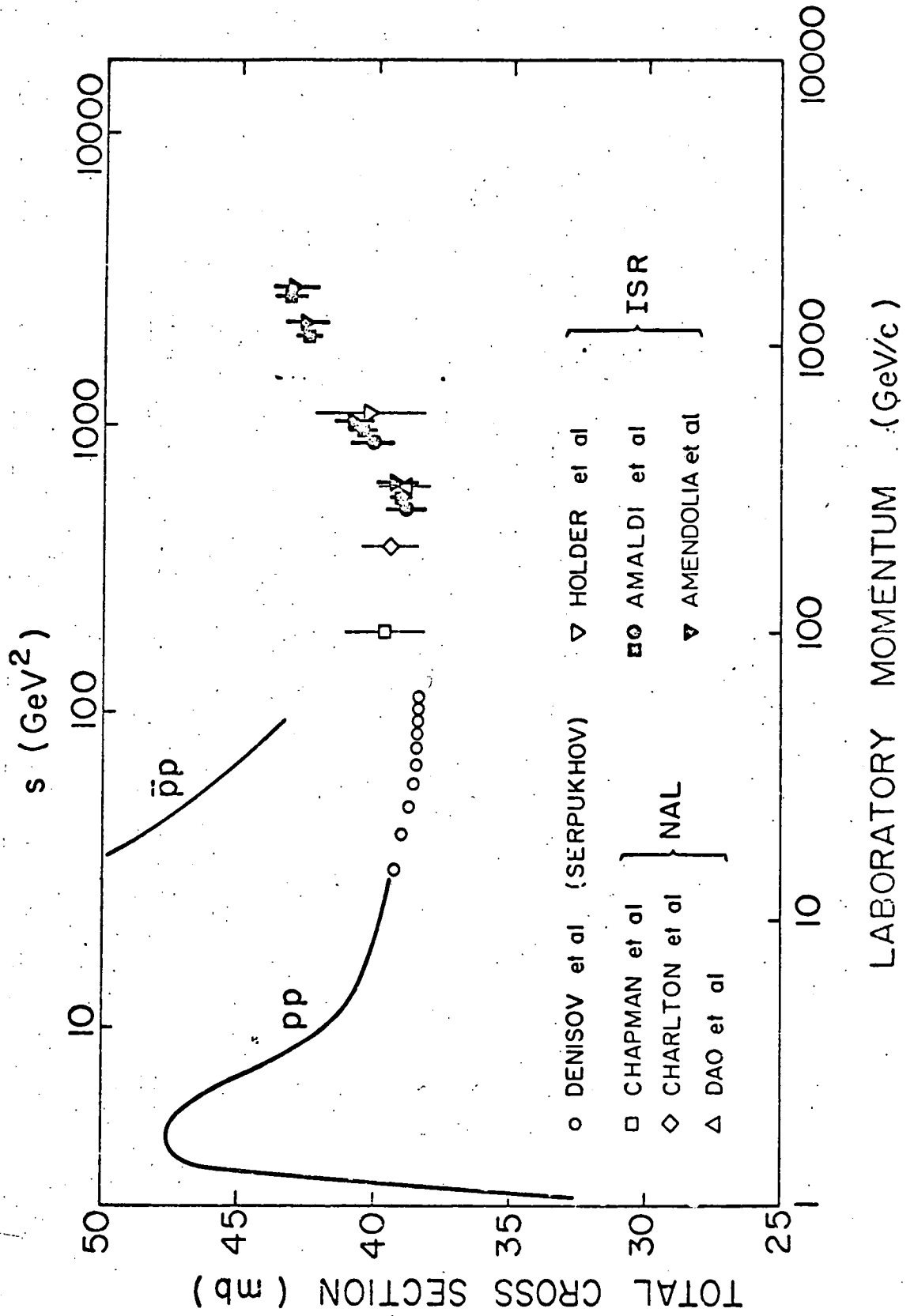


Fig 1.8

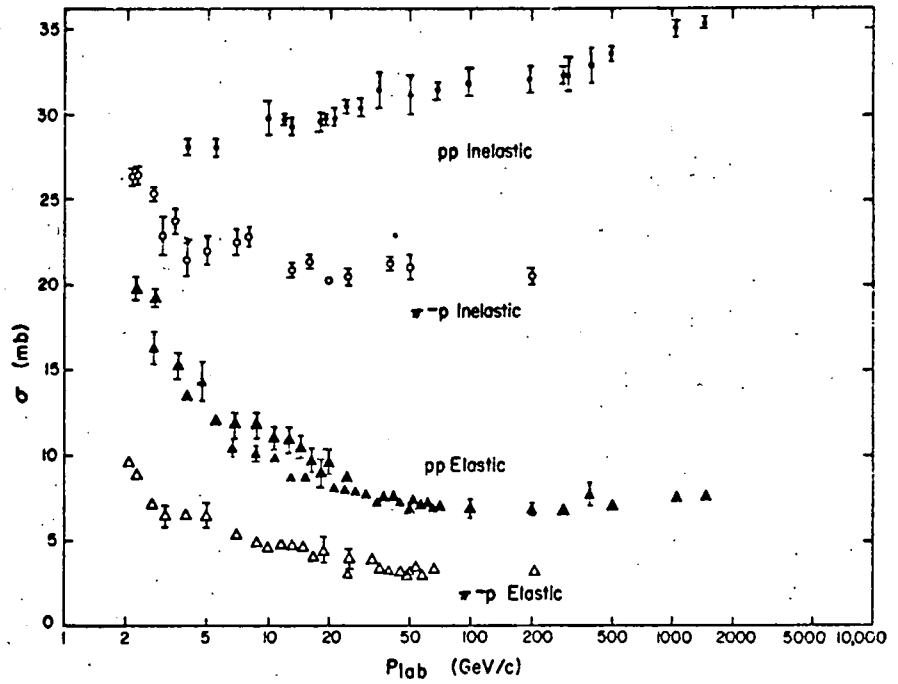


Fig. 1. The elastic and total inelastic cross sections in pp and π^-p interactions.

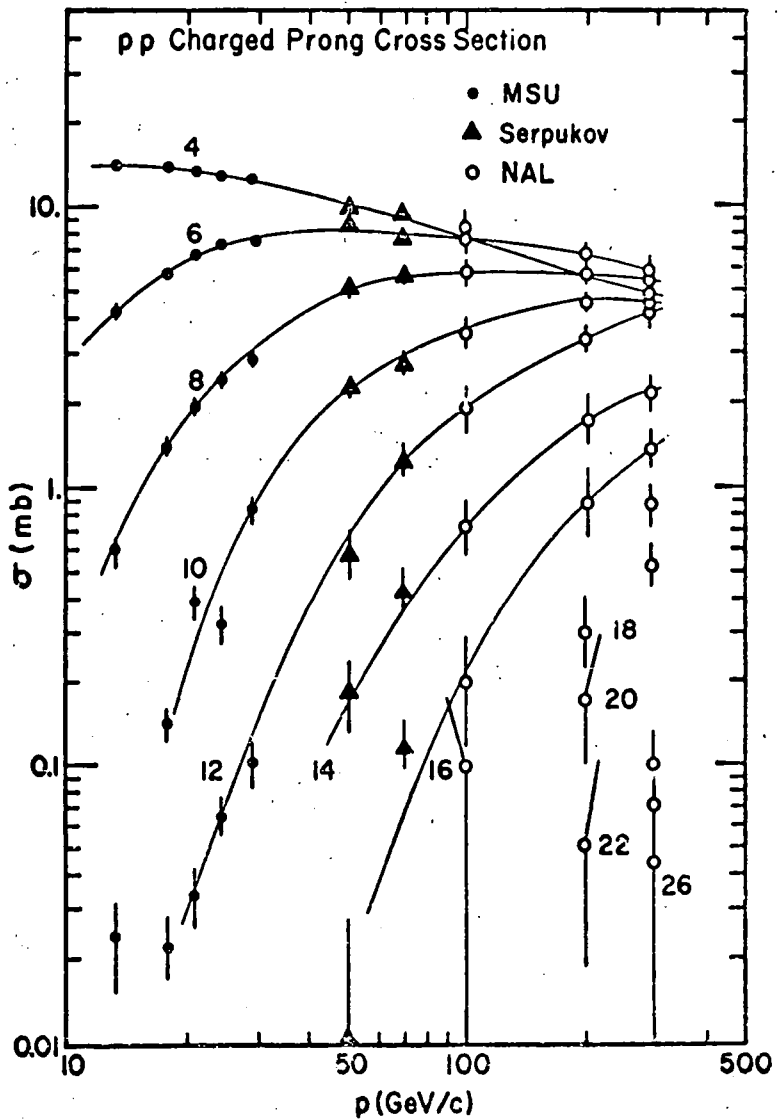


Figure 1.10

Energy dependence of cross-sections for different numbers of charged particles as now observed in proton-proton collisions up to 300 GeV.

It is worth mentioning that as energy increases the more important σ_n comes from higher prongs.

To close this section we end up by plotting σ_n versus n for proton-proton scattering.¹⁰ It is customary to compare this with a poissonian distribution. If the difference between these two curves is not very distinct at medium energy (50 gev/c) one certainly gets broader tails at ISR energy range as shown in fig. 1.11.

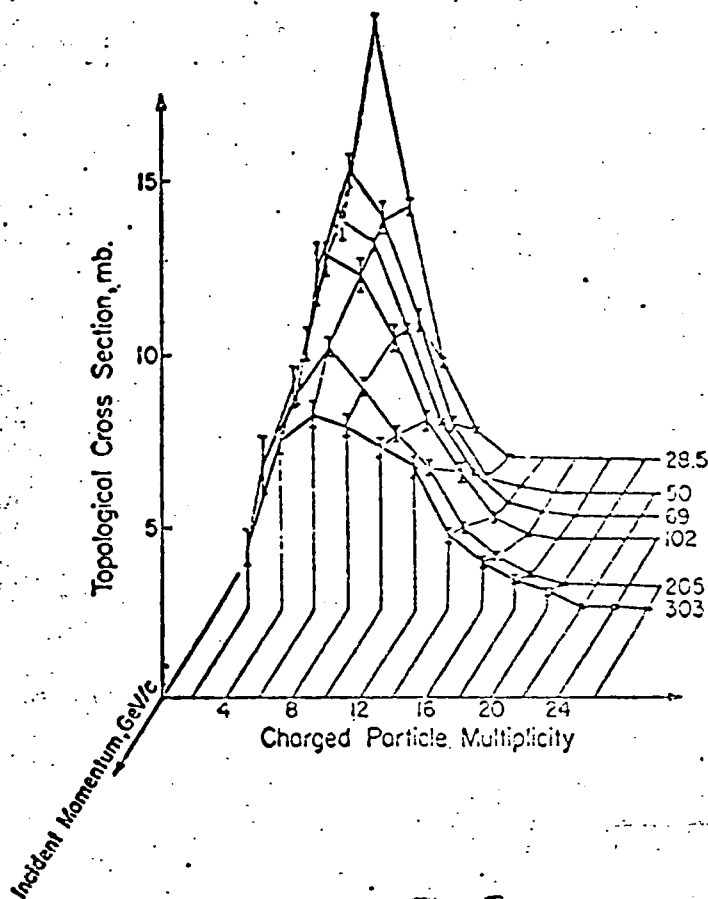


Fig 1.11

1.5. MULTIPLICITIES

The average multiplicity, $\langle n \rangle$, is defined as

$$\begin{aligned} \langle n \rangle &= \frac{\sum_{n=2}^{\infty} n \sigma_n}{\sum_{n=2}^{\infty} \sigma_n} \\ &= \frac{1}{\sigma_{\text{tot}}} \sum_{n=2}^{\infty} n \sigma_n \end{aligned}$$

Fig. 1.12 indicates that, roughly speaking, the average number of charged particles in PP inelastic collision is about 12 at ISR energy range. One expects that the bulk of this is pions. It is clear, then, that at low energies protons are dominant. As we go to higher energies pions take over the protons at a quite early stage and later rise in proportion to the total multiplicity. The number of protons does not increase rapidly at ISR as compared to that of pions. Of course we must observe an increase in $\langle n_p \rangle$ simply because antiproton shows a rising. A way to explain this is by invoking the idea of leading particle effect to be described in the seventh section. The leading particle takes the bulk of the available energy and what remains is not enough to create a heavy $P\bar{P}$ pair.

Detecting neutrally charged particles was a difficult process. So it was no surprise that until three years ago data on charged particles multiplicity, $\langle n_c \rangle$, was available only. It was also generally believed that $\langle n_{\text{tot}} \rangle = \frac{3}{2} \langle n_c \rangle$ was a good estimate of the total multiplicity. The first evidence on the neutral multiplicity came out during the Batavia conference in 1973. The represented results showed that $\langle n_0 \rangle$, as long as it is kinematically allowed, increases with energy, very much in the same way as $\langle n_c \rangle$ does. The corresponding data have been summarized in fig. 1.13. Fig. 1.14 shows that $\langle n_- \rangle$

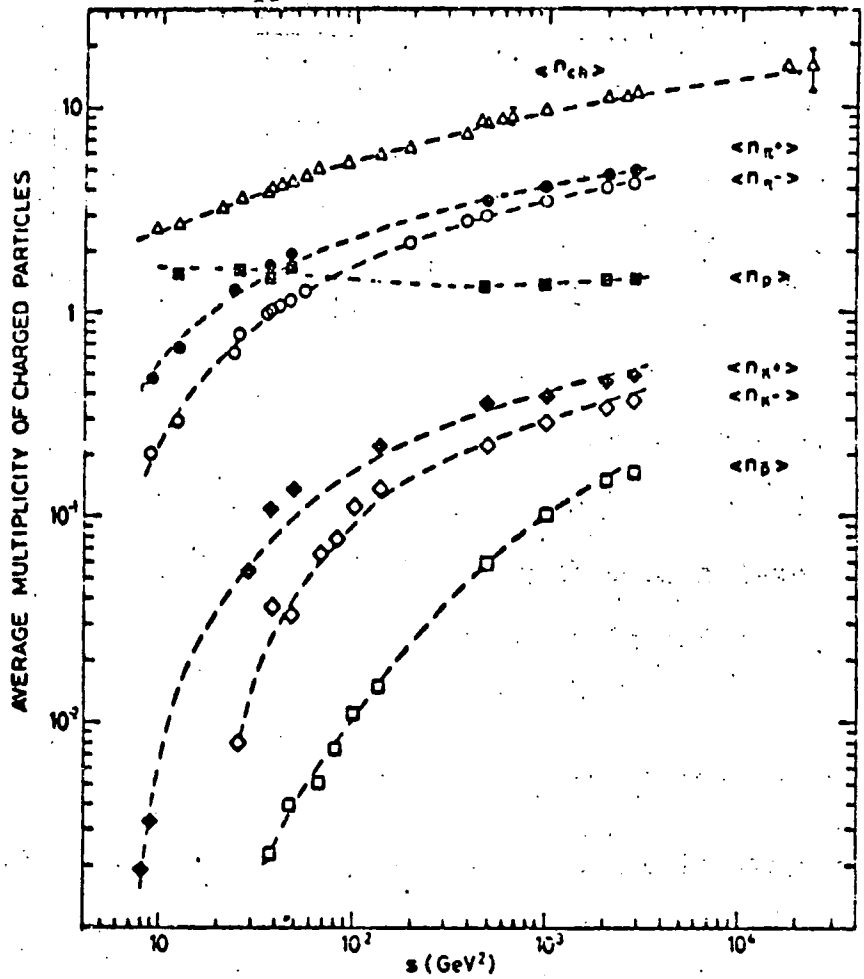


Fig 1.12 Average multiplicity of various charged particles per inelastic pp collision versus s (GeV^2) on a ln-ln plot.

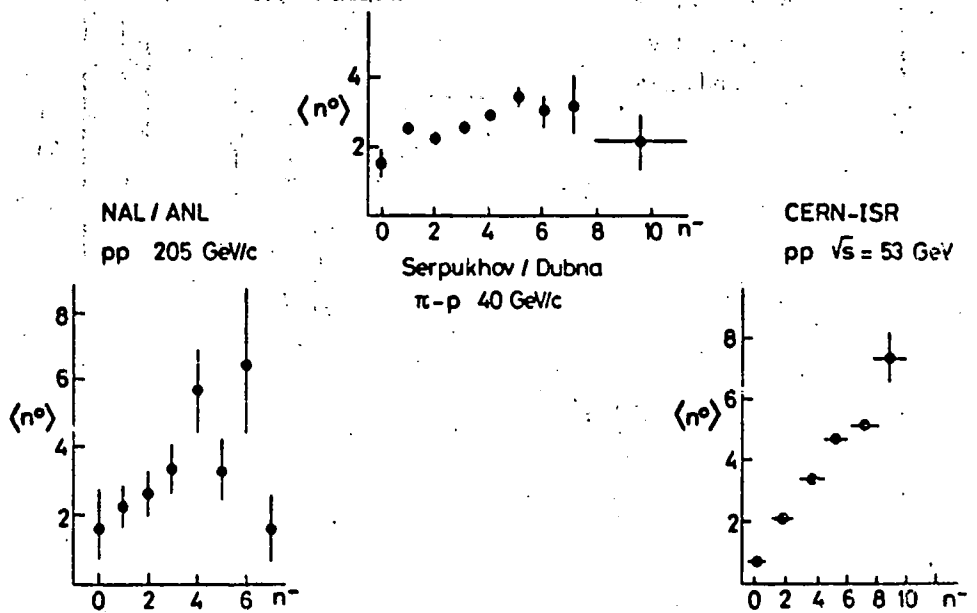


Figure 1.13

The mean number of π^0 as a function of the observed number of charged particles. Data from a Dubna collaboration at 40 GeV/c, the Argonne-NAL experiment at 200 GeV and an ISR experiment are combined together. The observed ISR multiplicities are limited to a particular solid angle.

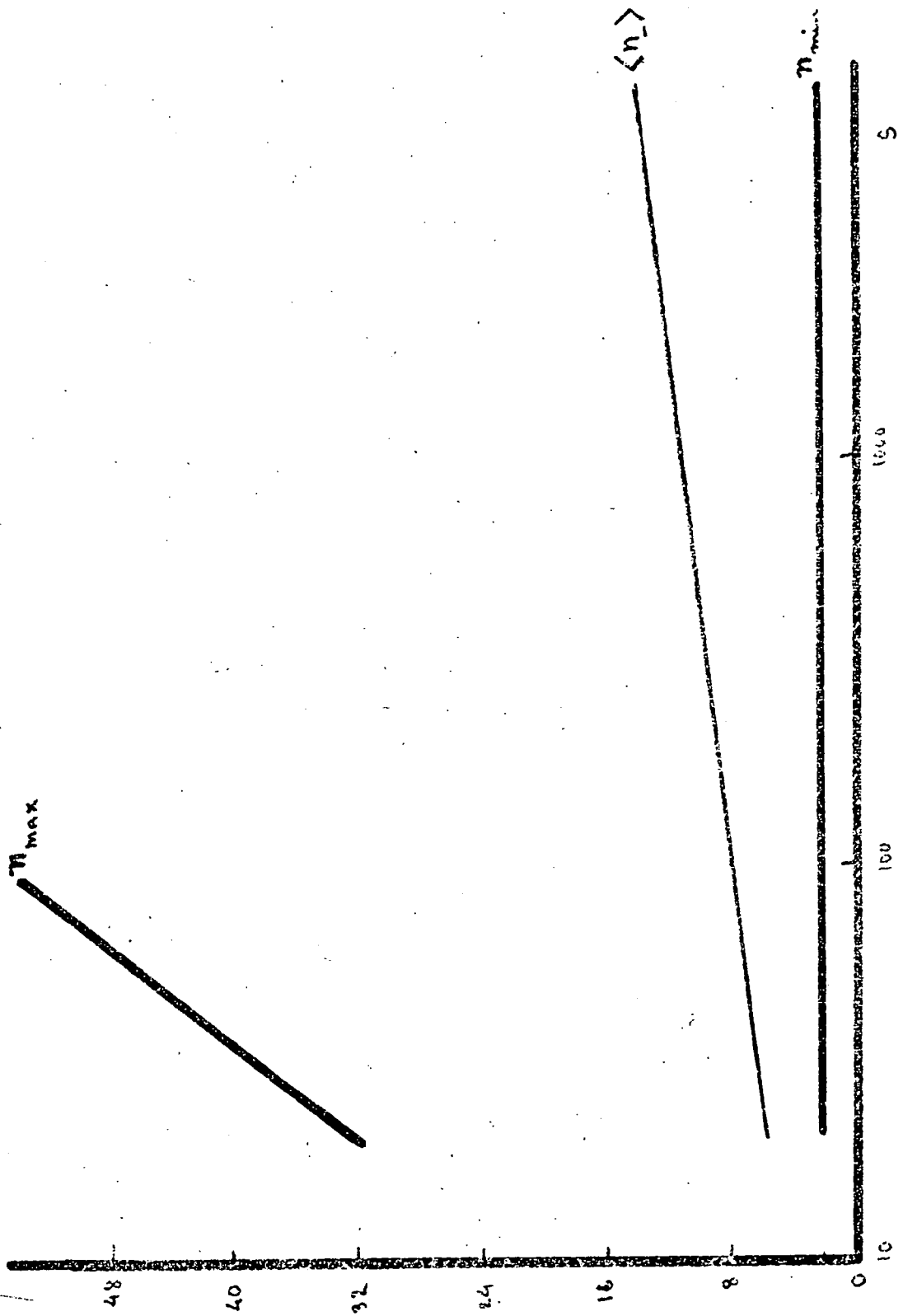


Fig 1.14

grows very slowly with energy,¹¹ more likely as $\ln S$,

$$\langle n_- \rangle = a + b \ln S .$$

This relationship is one of the predictions of a multiparticle model, namely multiperipheral model, which is going to be the subject of the following chapter. Comparing the data with the top and bottom lines, the kinematically allowed maximum and minimum number of produced particles, in fig. 1.14, one concludes that the production mechanism uses a small amount of its available energy in creating particles, the bulk of it manifests itself in the kinematical energy form of the secondaries.

1.6. DEFINITION OF VARIABLES

The representation of data should be regarded carefully. This depends quite a lot on the type of variables one chooses. The choice of variables thus will result on the conclusion that whether or not some features are important. To understand this better, a known animal is plotted on different scales.¹⁰ As one could see in fig. 1.15, different parts of the pig have been emphasised less or more according to the type of the plane he uses. The situation is more or less like this in the high energy particle physics.

The frame of reference we are mainly going to work in is the centre of mass frame, unless otherwise indicated. The incoming particles A and B have four momenta P (E, \underline{P}) those of the secondaries are q (ω, \underline{q}). The three momenta \underline{q} could be further decomposed into two components, q_L and \vec{q}_T . q_L is called the longitudinal component and is parallel to the colliding axis of particles A and B; \vec{q}_T is the transverse part of \underline{q} and is perpendicular to the longitudinal axis. The usefulness of this decomposition more or less lies on the fact that the transverse momenta are highly suppressed as data¹² show (fig. 1.16). This, clearly, reduces the three dimensional phase space to one dimension and, therefore, greatly simplifies the calculations.

One can, now, introduce the reduced longitudinal momentum which frequently is referred to as the Feynman¹³ variable, x . It is defined by,

$$x_i \equiv \frac{q_{L_i}}{q_{L_i}^{\max}},$$

where q_L^{\max} is the maximum value that q_L is kinematically allowed to take. At high energies, with a good approximation, one could write x_i as,

$$x_i \approx \frac{2q_{L_i}}{\sqrt{s}}.$$

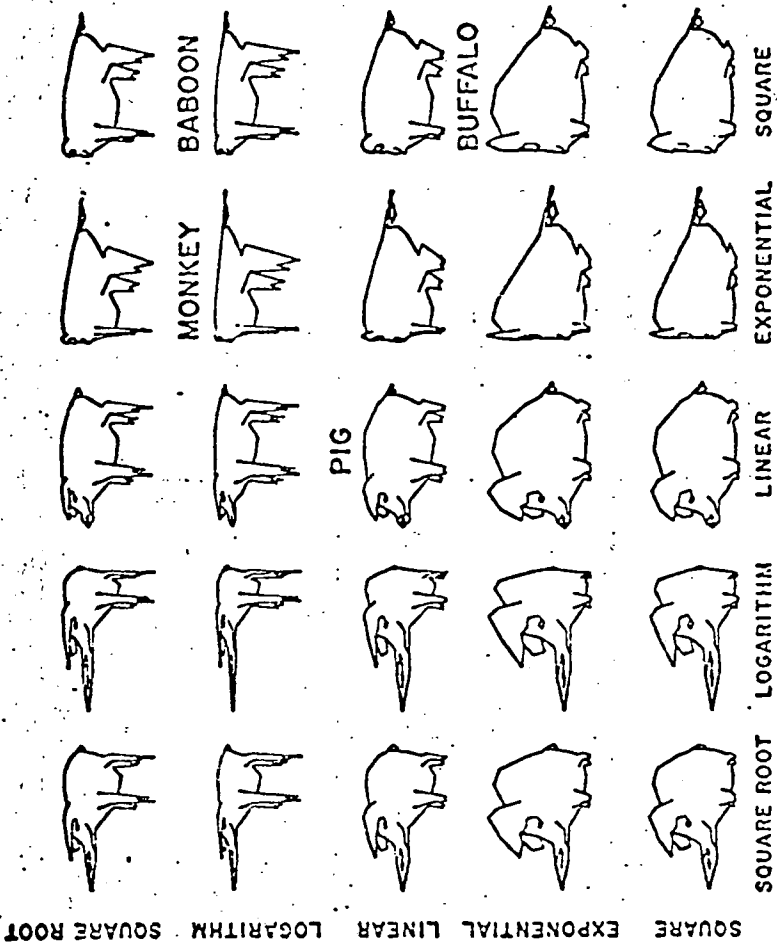


Fig 1.15 Illustration of the importance of data presentation.

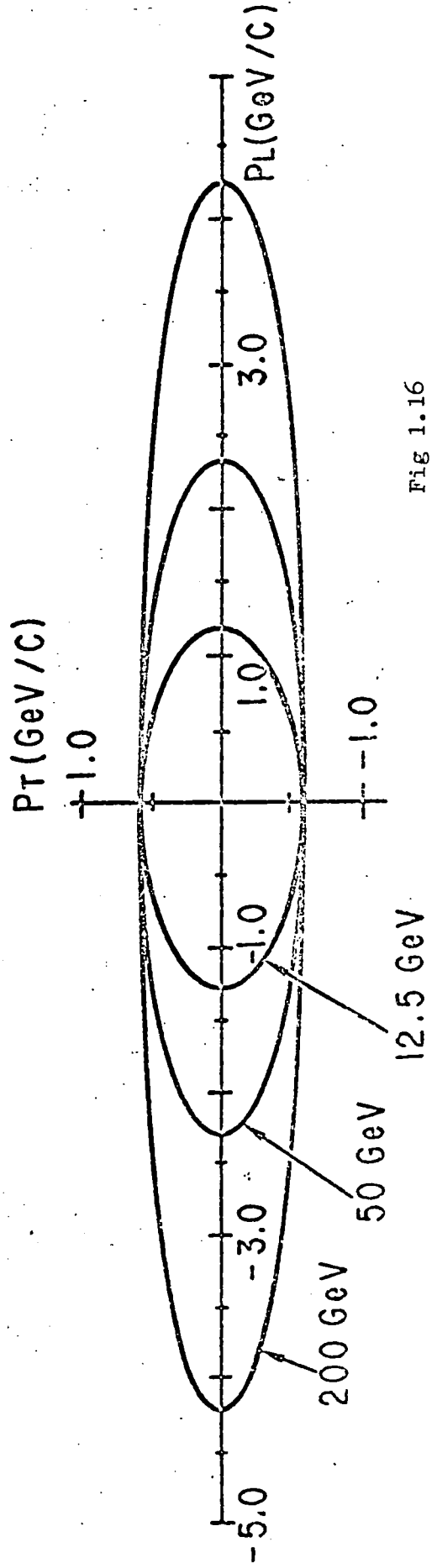


Fig 1.16

The domain of definition of X is between 1 and -1, $-1 < X < +1$.

Particles A and B have X values 1 and -1 respectively. It is evident that the particles not moving with A or B, and have definite q_L value, will end up at $X = 0$ as energy increases ($S \rightarrow \infty$).

Phenomenologically speaking, it does not seem to be so interesting to map almost all particles to one point. Hence, one introduces a new one dimensional variable Y ,

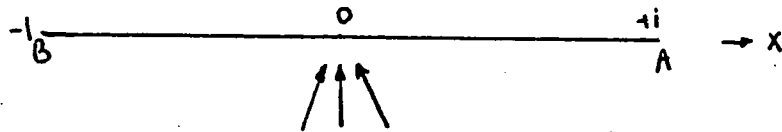


Diagram 1 particles not moving with A or B are mapped to the centre at S.

often called the rapidity, It is defined as

$$y_i = \frac{1}{2} \ln \frac{\omega_i + q_{Li}}{\omega_i - q_{Li}}$$

$$= \ln \frac{\omega_i + q_{Li}}{m_i^\pi}$$

where the transverse mass, m_i^π is defined as

$$m_i^\pi = (m_i^2 + q_{T,i}^2)^{1/2},$$

m_i being the mass of the i th particle. The growth of Y takes place according to $\ln S$ as energy increases. The maximum and minimum values of y_i are determined by $\frac{1}{2} \ln \frac{S}{m_i^\pi}$ and $-\frac{1}{2} \ln \frac{S}{m_i^\pi}$, respectively.

The rapidity has two advantages over Feynman X variable. The first one is that all particles are evenly located in the rapidity space. The second advantage is that under Lorentz boost with velocity v , the rapidity changes additively, that is

$$y_i \rightarrow y_i' = y_i + \tilde{y}_i,$$

where

$$\tilde{y}_i = \sinh^{-1} \beta v.$$

In any case, either of $(S, \chi_i, \vec{q}_{T_i})$ and $(S, \psi_i, \vec{q}_{T_i})$ make a complete set of variables which are capable of describing the high energy phenomenon.

With due regard to a $2 \rightarrow 2$ process, the reason why we require three parameters for one particle inclusive reaction, rather than two, that is one extra parameter, to describe a process is that the missing mass, M , is a variable itself and is not fixed by $M = m_c$.

1.7. INCLUSIVE CROSS-SECTIONS

As mentioned before, inclusive processes correspond to reactions like



The corresponding invariant cross section, which is sometimes called single particle distribution is defined by,

$$\begin{aligned} f_{AB}^C &= \omega \frac{d\sigma}{d^3q} \\ &= \frac{1}{2s} \sum_{n=2}^{\infty} \sum_k \int \prod_{i=1}^n [d\Phi_i] \omega_k \delta^{(3)}(\vec{q}_k - \vec{q}) |A(p_1, p_2; q_1, \dots, q_n)|^2, \end{aligned}$$

where summation over K is done over particles of type C . The invariant cross-section is experimentally a measurable quantity, since $d\sigma/d^3q$ is the probability per unit incident flux of C being produced in momentum element d^3q . In order to make the quantity $d\sigma/d^3q$ frame independent one multiplies that by ω . The phase space element could be written in terms of other variables already defined as follows:

$$\frac{d^3q}{\omega} = d^2q_T \frac{dq_L}{\omega} = d^2q_T dY.$$

The fact that the phase space could be written in the form of rapidity times transverse momentum and that kinematics does not permit Y to exceed a certain limit, given an energy of course, and that data suppress the growth of \vec{q}_T , suggests that one could think of the phase space as a bottle where the particles momenta are the position vectors of gas molecules, namely Feynman - Wilson gas, inside it (fig. 1.17). As the energy increases, the length of the bottle gets bigger and essentially in the asymptots the motion of gas molecules inside could be considered one dimensional.

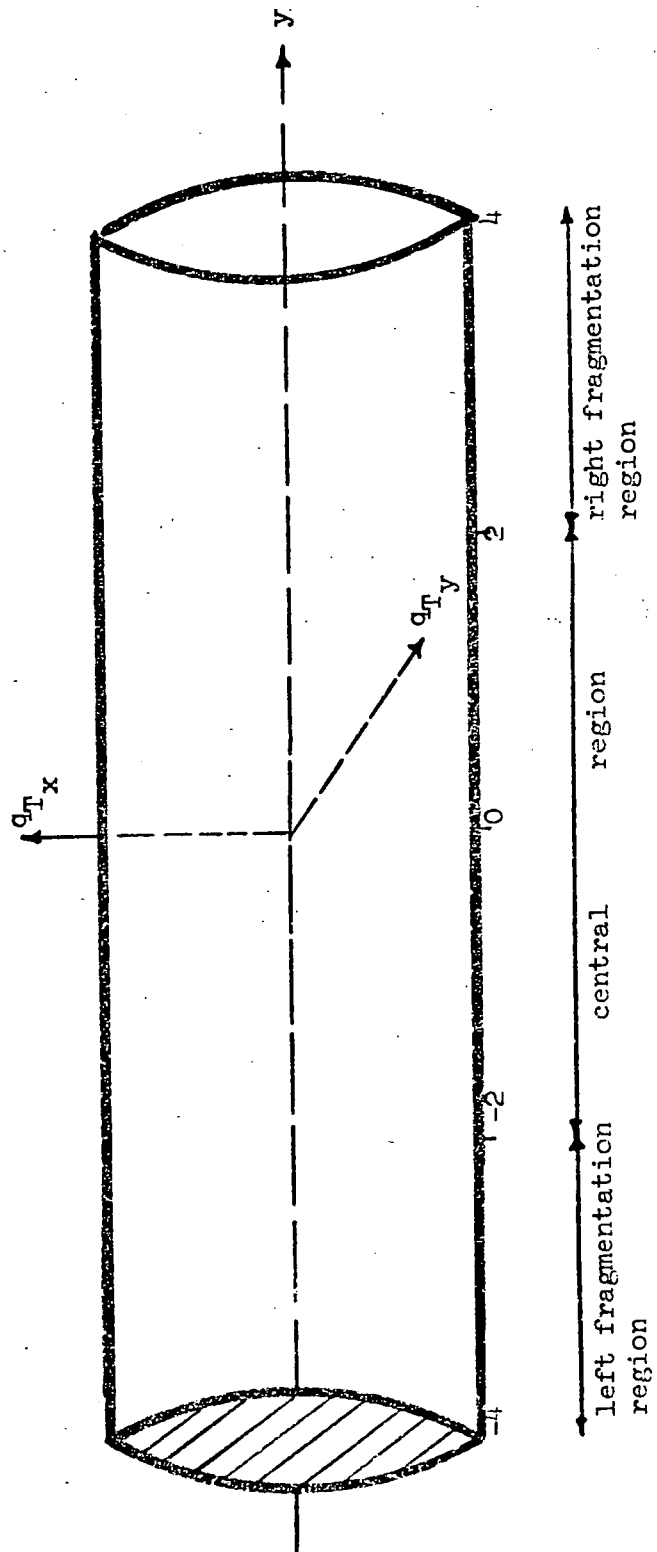


Fig 1.17

Let us see now what one could understand from the experiments. First of all, data¹⁴ show that there is a strong exponential fall off in the transverse momentum (fig. 1.18). This is one of the striking features of multiparticle reactions at high energy. Plotting q_L against \hat{q}_T one finds that events cluster along the longitudinal axis indicating that transverse components are strongly damped. The average value one finds for $\langle \hat{q}_T \rangle$ from a fit to data, whether the fit is $\exp(-\lambda \hat{q}_T^2)$ or $\exp(-\lambda \hat{q}_T)$, is that it is roughly .33 geV/c for π and .45 geV/c for K and P. The situation for q_L is somehow different. For instance the type of particles plays a role here. For example, plotting PP inclusive cross-section versus x , one finds that proton stays relatively flat as compared to pions or kaons (fig. 1.19). What this means is that a final particle, which has some quantum numbers as those of one of the initial particles, retains an important fraction of the available energy. This situation is often referred to as the 'leading particle effect'.

In general, ρ , the inclusive distribution, is a function of S , q_L and \hat{q}_T . Data¹⁴ supports the idea that at higher energies the invariant cross-section becomes a function of only two variables, x and \hat{q}_T ,

$$\rho_{AB}^c(S, q_L, \hat{q}_T) \xrightarrow{S \rightarrow \infty} \rho_{AB}^c(x, \hat{q}_T).$$

This is referred to as the Feynman¹³ scaling. The statement could be verified empirically by comparing the low energy and ISR energy range data. This has been shown in fig. 1.20. Perhaps it is worth mentioning that the scaling region is reached sooner for pions, and possibly kaons whereas for other particles one must go towards higher energies (fig. 1.21).

Koba et al¹⁶ three years ago suggested the following form of scaling

$$\langle n \rangle \frac{\sigma_n}{\sigma_{\text{inel}}} \xrightarrow{S \rightarrow \infty} f\left(\frac{n}{\langle n \rangle}\right).$$

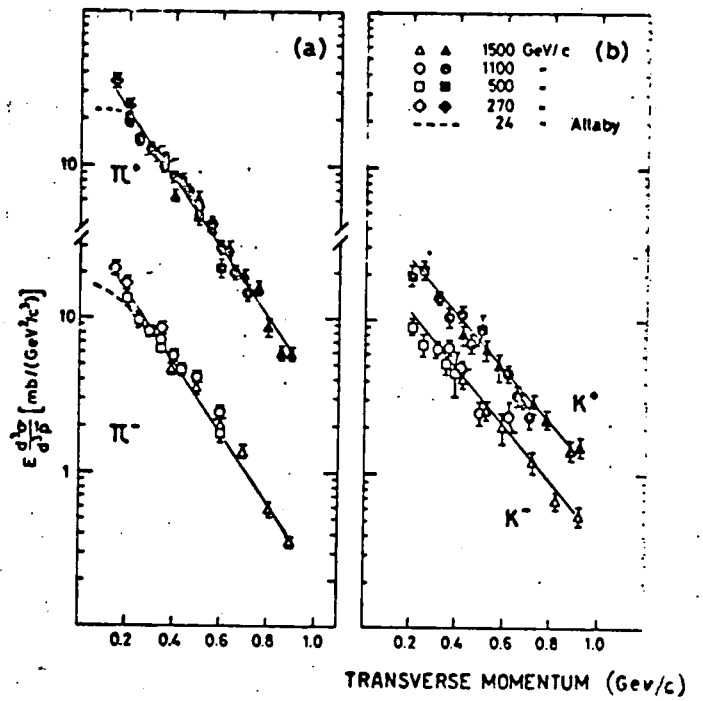


Fig 1.18 Invariant inclusive cross-sections plotted versus q_T .

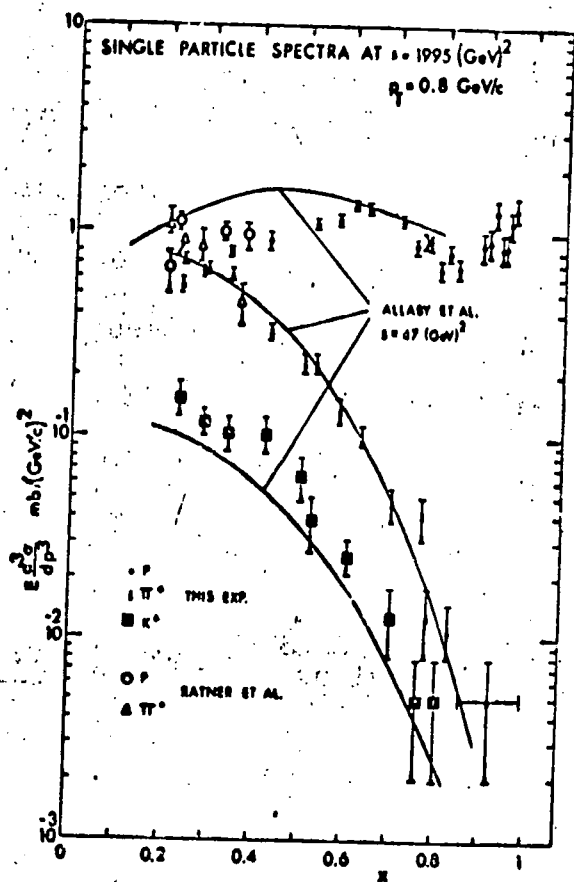


Fig 1.19 Inclusive invariant cross-sections for $pp \rightarrow c + X$ where $c=p, \pi^+, K^+$ at $s=1995 \text{ GeV}^2$.

$$\omega \frac{d\sigma}{dq^2}$$

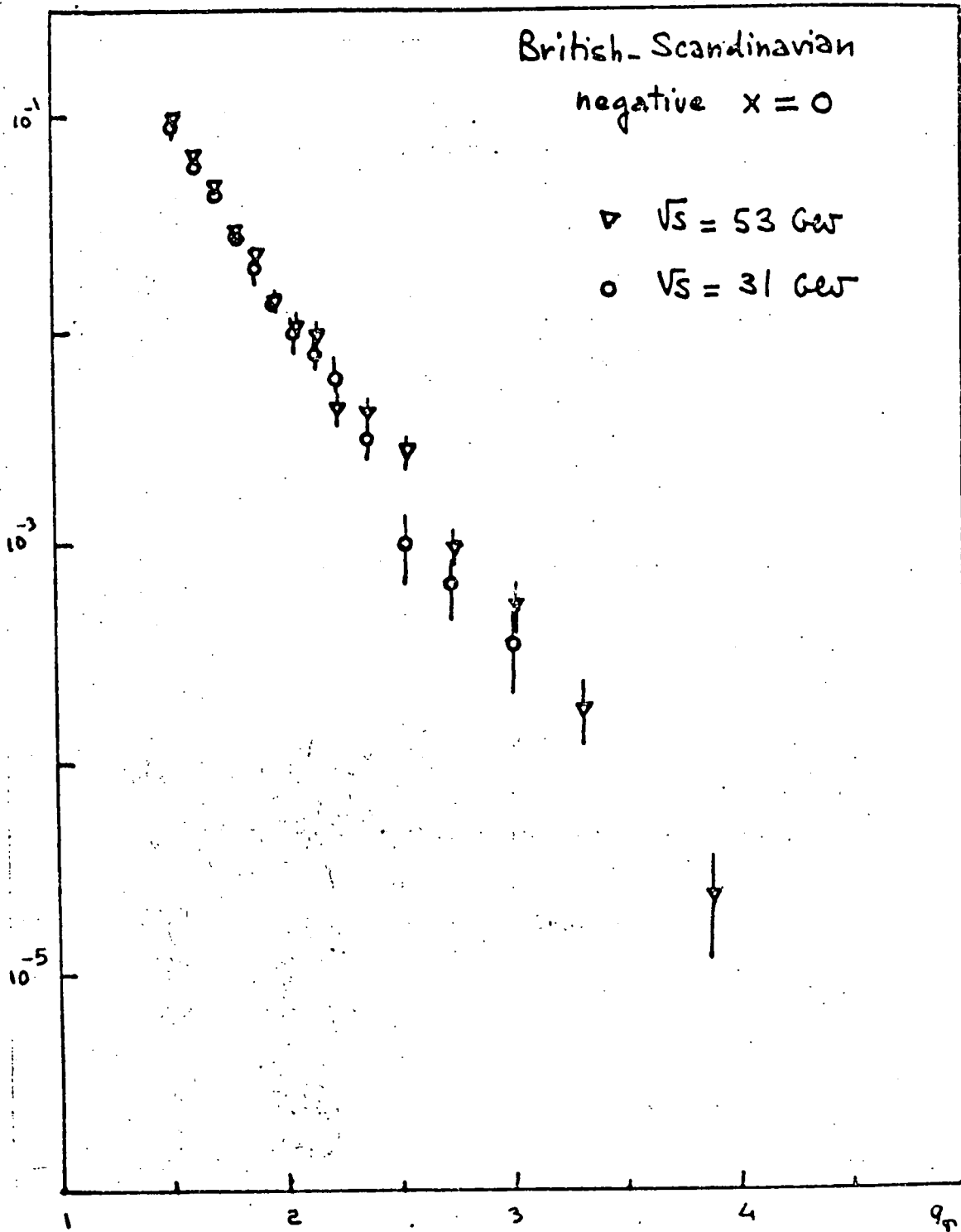


Fig 1.20 Approximate scaling of the negative particles

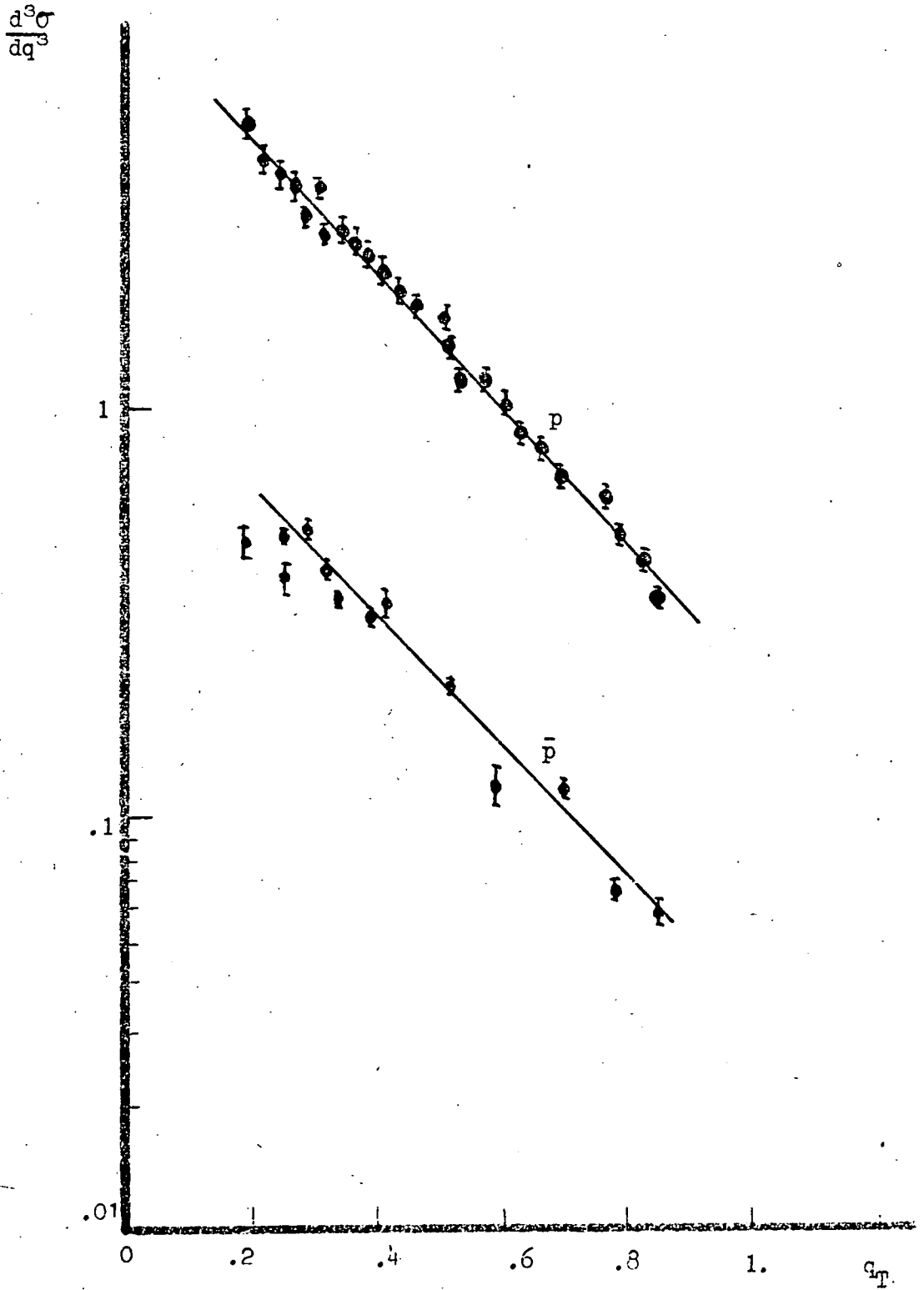


Fig 1.21
(see also fig. 1.18)

This gives a very good fit to the PP data if one supposes that

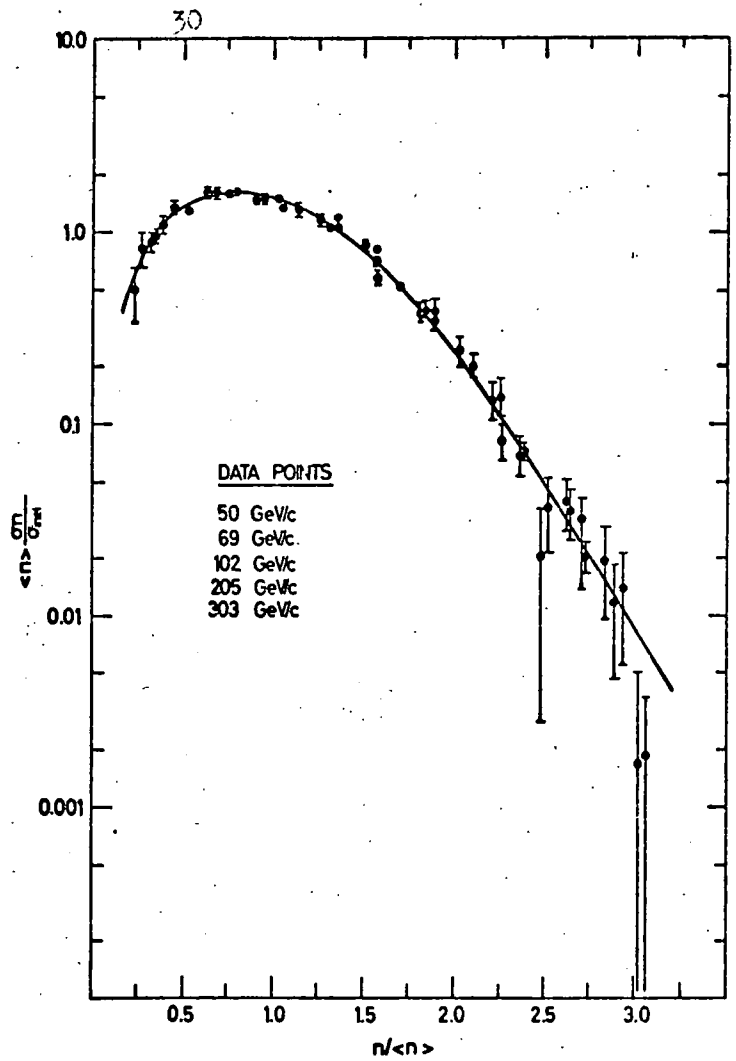
$$f\left(\frac{n}{\langle n \rangle}\right) = \frac{n}{\langle n \rangle} .$$

Figure 1.22 displays an excellent agreement with data.

As energy increases the inclusive distributions tend to a limiting value for any q^{lab} asymptotically. This was first observed by the authors of reference¹⁷ who thought of the secondaries as some fragments of the initial particles. This is called limiting fragmentation. Surprisingly this already holds at low energies (fig. 1.23).

Viewing the role of projectile as a mere catalyzer which enables the fragmentation to occur, one comes across to the statement that the inclusive distribution is independent of the projectile in the target fragmentation region, apart from an overall normalization factor proportional to $\sigma_{tot}(AB)$. The figure 1.24 is a supporting fact to the above mentioned statement.

Another interesting thing to observe is the development of a plateau if one plots the inclusive cross-section versus rapidity as in figure 1.25. This happens in the central region which is far from the target as well as the projectile region. The central region is sometimes called pionization region. This is because in this region pion inclusive distribution is more dominant. Perhaps it should be added that some ninety per cent of the secondaries are pions. A comparison between different produced charged multiplicities in PP scattering is given in fig. 1.12.



Plot of $\langle n \rangle \frac{\sigma_n}{\sigma_{inel}}$ as a function of $\frac{n}{\langle n \rangle}$ for bubble-chamber data with $p_{lab} \geq 50$ GeV/c

Fig 1.22

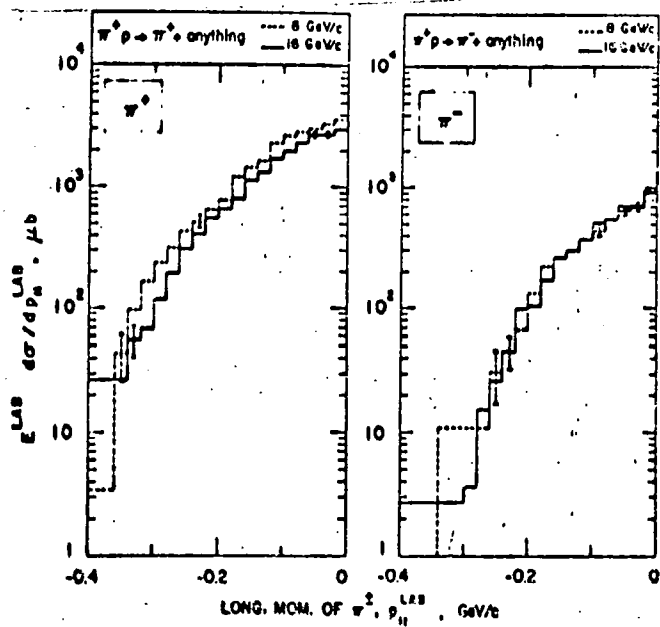


Fig 1.23 Limiting fragmentation observed for accelerator data at lab. momenta of 8 and 16 GeV.

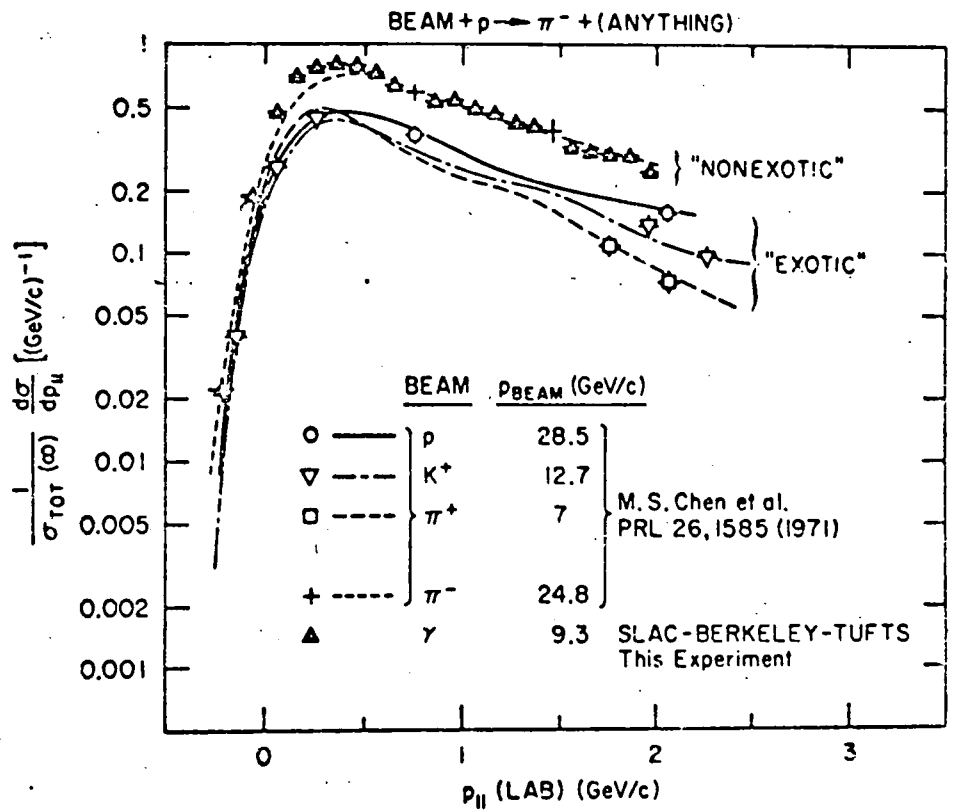


Fig 1.24

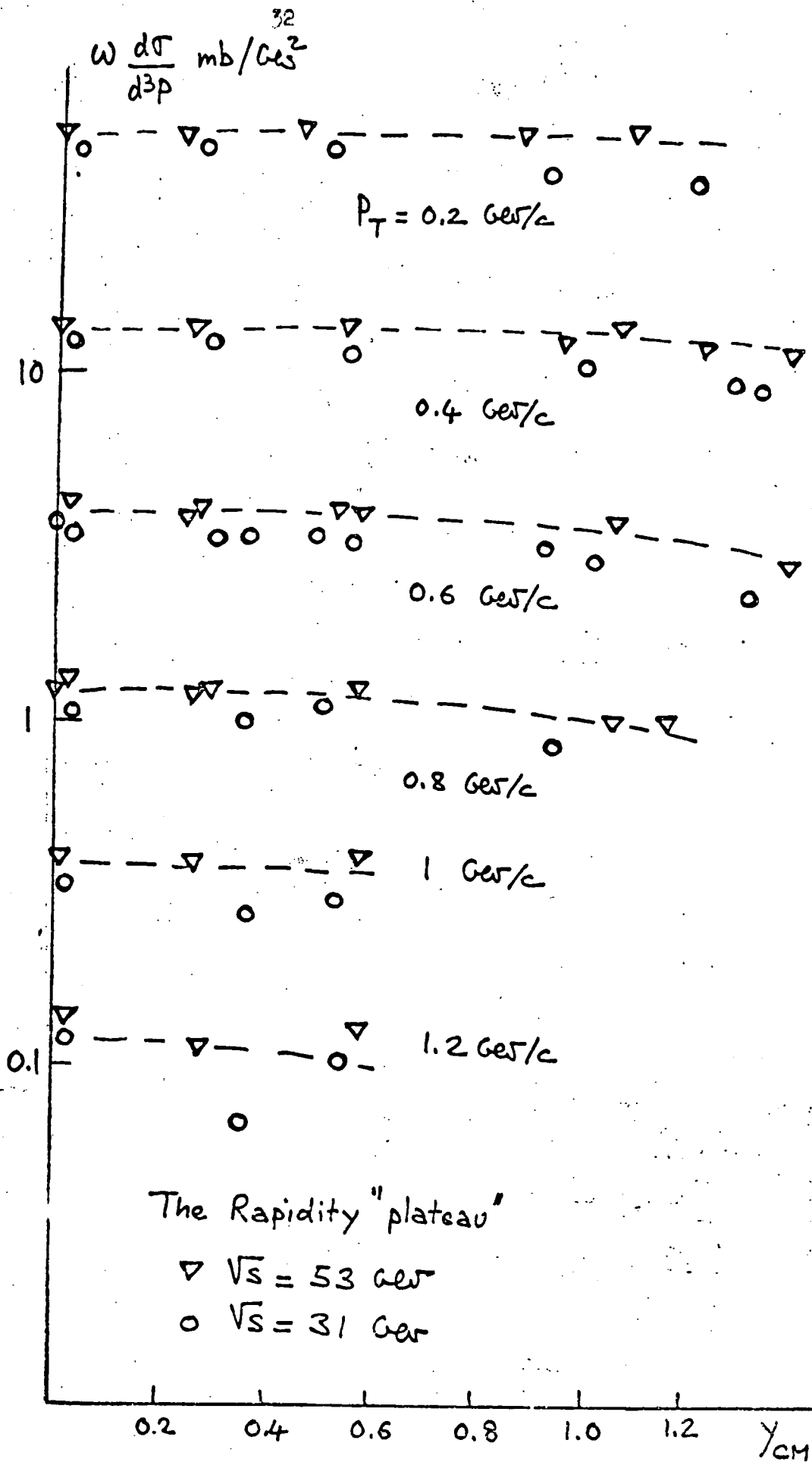


Fig 1.25 rapidity plateau for π^- as seen at two different energies.

1.8. CORRELATIONS

The purpose of introducing correlations is to discover some regularities, additional to what have been previously discussed, which data may seem to possess. The way to study correlation is by means of a correlation function. The two particle correlation function is defined in analogy of Feynman gas:

$$C_2(Y_1, Y_2) = \frac{1}{\sigma_{gr}} \frac{d^2\sigma}{dY_1 dY_2} - \left(\frac{1}{\sigma_{gr}} \frac{d\sigma}{dY_1} \right) \left(\frac{1}{\sigma_{gr}} \frac{d\sigma}{dY_2} \right)$$

Noting that the first term on the right hand side is the probability of finding simultaneously gas molecules on the locations 1 and 2 (i.e. particles with momenta q_1 and q_2) and that the second term is the multiplication of the probabilities of finding a single molecule in 1 and another one in 2 one gains some insight into the meaning of correlations. For example, if $C_2(Y_1, Y_2) = 0$ for all values of Y_1 and Y_2 , then this means that the two particles are uncorrelated in Y_1 and Y_2 . Of course different conservation laws correlate the particles,¹⁷ therefore practically no-correlation is not likely to occur in nature.

To have an overall estimate of the correlation one may introduce an integrated correlation function

$$f_i(s) = \int \left[\prod_i d\vec{q}_i \right] C_i(\vec{q}_1, \vec{q}_2, \dots, \vec{q}_i) \dots$$

A poissonian fit to the topological cross-sections reveals that f_2 , the multiplicity moment, is zero suggesting the absence of correlations. Therefore, f becomes a useful tool in evaluating the strength of correlations between the particles. In other words, f_2 measures the deviations of a multiplicity distributions from a poissonian fit

since $f_2 = \langle n(n-1) \rangle - \langle n \rangle^2$. To see how f_2 looks like we plot it against S . The rise of it indicates correlations amongst secondaries. (fig. 1.26).

In general there are two types of correlations : short range and long range correlations. Short range correlation (SRC), as is implied by its name, says that the correlation function will be negligible if the particles under consideration exceed a certain distance in the rapidity space (fig. 1.27). One way to formulate this is the following

$$C_2(\eta_1, \eta_2) \propto \exp[-|\eta_1 - \eta_2|/\lambda] \quad , \quad \lambda \neq 0 \quad ,$$

where λ is defined as the correlation length and theoretically is around 2.

The confrontation of SRC idea with data indicates the presence of long range correlations. This is because SRC predicts f_2 to grow like $\ln S$ but data increases faster, possibly as $\ln S^2$ (fig. 1.26).

As short range correlation is known to exist, it suggests that the emitted secondaries should form some sort of clusters. Another way to look at this is as follows. The leading particle takes away a huge amount of energy and what remains must be shared amongst a considerable number of pion secondaries. This suggests that these pions will have almost same rapidities, therefore they are forced to come out in clusters. So, briefly speaking, the production mechanism proceeds in the following manner. From the collision of initial particles some clusters get produced. These clusters subsequently decay into the final particles. To estimate number of particles per cluster would be an interesting item to study as we shall do it now.

Let us put the problem in a slightly different way and ask the following question. What is the adequate energy to produce n clusters? Had there been just one particle per cluster the calculation of energy

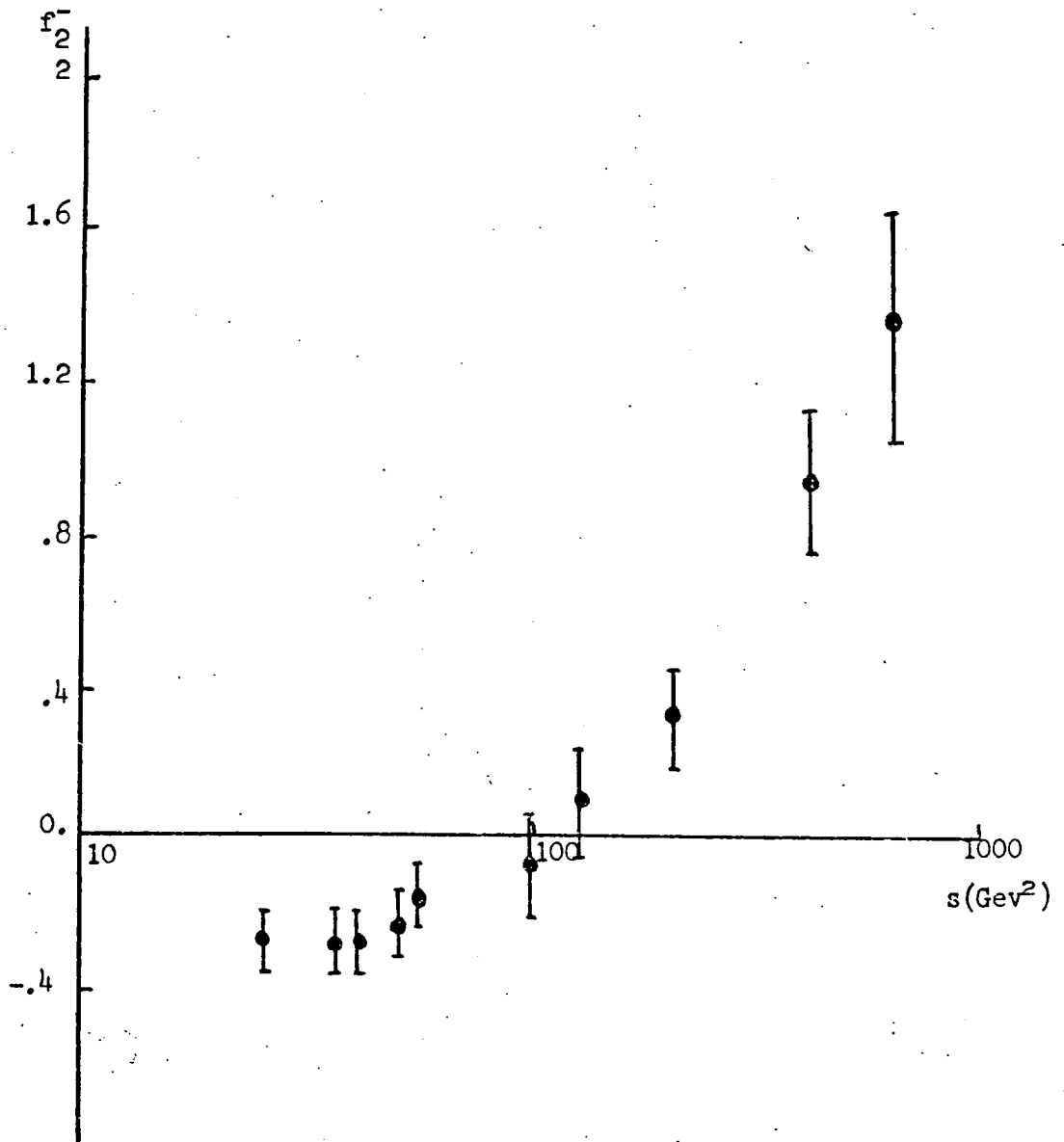


Fig 1.26 The integrated two particle correlation function as a function of energy in pp interaction.

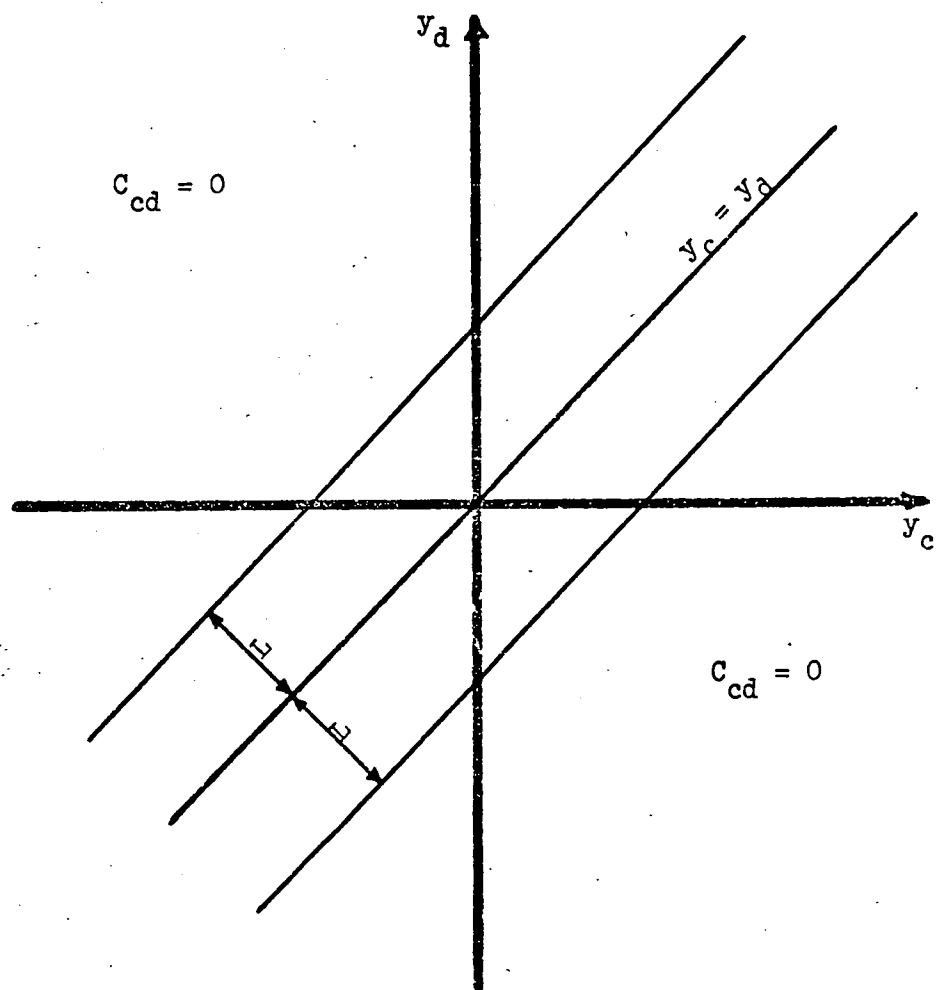


Fig 1.27

would have been easier:

$$S = A e^{\frac{n-d}{3a}}$$

where a and b are the coefficients in $\langle n \rangle = a \ln S + b$ and $A = \exp(-\frac{b}{a})$.

d is 2 (0) if initial particles have positive (zero) overall charge.

In deriving this equation one has assumed that there are as many neutral particles as positive or negative ones. It is, however, unlikely this situation to happen. Thus, to determine the average number of (negatives) particles we introduce the following method. Using charge conservation law for, e.g. $n_{cl} = 3$ in PP scattering case, we see that the only possible formation likely to happen is

Cluster one	Cluster two	Cluster three
overall charge	+	0

Bearing in mind that clusters can decay in such a way that each of them preserves charge conservation law, one can write the following possible decay modes

Cluster one	Cluster two	Cluster three
overall charge	+	0
decay modes	+	0
$\frac{1}{2} + + -$	$\frac{1}{2} + + -$	$\frac{1}{2} + - 0$
$\frac{1}{2} 0 0 +$	$\frac{1}{2} 0 0 +$	$\frac{1}{2} 0 0 0$

where the numbers (P_i) are to serve the 'weighing' purpose. The calculation of energy is straightforward now:

$$S = A \exp\left(\frac{\sum_{i=1}^{n_{cl}} P_i \bar{n}_i}{a n_{cl}}\right),$$

with A as defined above. For the example under study, using Harari's fit $\langle n \rangle = .84 \ln S - 2.14$, we find $S = 102.6 \text{ geV}^2$, as the energy for producing three clusters in PP scattering.

For the sake of completeness we would like to state that in the

section we implicitly realized that the integrated correlation functions were connected to the topological cross-sections. The suspicion arose when we noted that if σ_n was poissonian f_2 became zero. To try to connect those two quantities together explicitly we come across to the so called generating function,¹⁸ $Q(z)$. The function is defined as

$$Q(z) = \sum z^n \sigma_n$$

with

$$Q(1) = \sigma_{\text{tot.}}$$

The knowledge about σ_n will determine the form of $Q(z)$. The multiplicity momenta could easily be derived from $Q(z)$,

$$f_m = \frac{d^m \ln Q(z)}{dz^m} \Big|_{z=1}$$

The relationship between $Q(z)$ and σ_n is

$$\sigma_n = \frac{1}{n!} \frac{d^n Q(z)}{dz^n} \Big|_{z=0}$$

The above three equations provide the explicit connection we were looking for.

1.9. REGGE THEORY

The idea of analytically continuing a physical t-channel partial wave scattering amplitude in complex angular momentum j , plane was introduced by Regge in 1959 for the first time in his pioneering work concerning the potential scattering. This continuation is the foundation of building a theory, namely Regge theory, which describes qualitatively most of the asymptotic phenomenological features of high energy physics. For a comprehensive review of the subject, out of a very vast amount of reviews available in the literature, one of the references mentioned in 19 may be consulted.

As we are more interested in the elastic scattering we shall very briefly outline below the Regge theory for a $2 \rightarrow 2$ process. In this theory the amplitude takes the following form

$$A(s,t) \sim \beta(t) \left(-e^{-i \frac{\pi}{2} \alpha(t)} \right) s^{\alpha(t)},$$

where $\beta(t)$ is a product of some residue functions and $\alpha(t)$, the so called Regge trajectory which is a function of t , is characteristic of the exchanged channel. Obviously we must have $\alpha(0) \leq 1$ in order not to violate the Froissart bound. Studying the trajectories in a Chew -Frautschi plot ($\text{Re } \alpha$ versus t) data suggests that the trajectory is a straight line (fig. 1.28), so that we may write

$$\alpha(t) = \alpha(0) + \alpha' t.$$

It is clear from the figure that bosons are located where the trajectory passes through integer (half integer for fermions) values.

For 'ordinary' trajectories data is compatible with the following,

$$\alpha(0) \approx 1/2$$

$$\alpha' = 1$$

Considering the optical theorem we can calculate the total cross-section,

$$\begin{aligned}\sigma_{\text{tot}} &\sim \frac{1}{s} \text{Im} A(s, t=0) \\ &\sim s^{\alpha(0)-1}\end{aligned}$$

The constancy of σ_{tot} in the intermediate energy range suggests that,

$$\alpha(0) = 1,$$

corresponding to an object named Pomeron, called after Pomeranchuk. The two immediate implications of this for elastic scattering are as follows. The ratio of real to imaginary parts of the elastic amplitude, for small t with the assumption of vacuum quantum numbers for the Pomeron, is related to the Pomeron slope,

$$\frac{\text{Re} A}{\text{Im} A} = \frac{\pi}{2} \alpha'_P t + \dots,$$

suggesting that the flatter the pomeron the less real part there is. The second implication concerns the differential cross-section. It is easy to see that,

$$\frac{\frac{d\sigma}{dt}}{\frac{d\sigma}{dt}|_{t=0}} \sim e^{2\alpha' t \ln s},$$

which displays the shrinkage property of the differential cross-sections, since t is negative. The shrinkage is conveniently studied by a slope parameter $b(s)$,

$$b(s) = 2\alpha' \ln s,$$

which has been previously seen (fig. 1.4). It seems clear, by a comparison with data, that α' for the pomeron is around .3, which makes it rather different from other Regge trajectories.

With due regard to fig. 1.2, we have mentioned a few words about the left hand side of the equation. In the next chapter

we shall study some of the proposed models related to the right hand side of the equation. In the third chapter a comparison of the both sides of the unitarity equation will be given. We shall see that there are cases where the equality does not always hold. Thus to improve the situation we consider the interference terms in the fourth chapter. This we find to be not the answer to the problem. In the final chapter an improvement to the (multiperipheral) model will be suggested. It will be seen that this will preserve the equality sign.

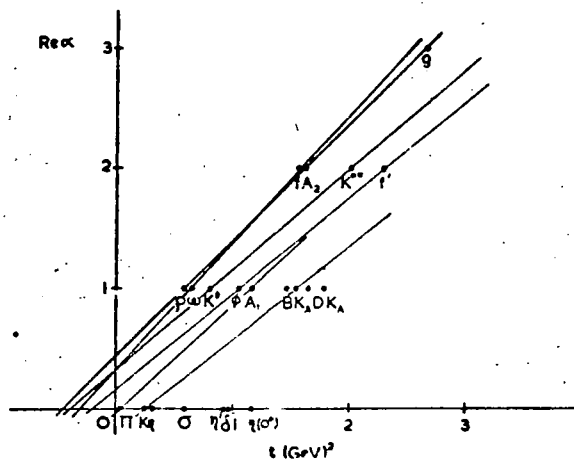


Fig 1.28 A Chew-Frautschi plot for the well established meson resonances.

CHAPTER TWO

MULTIPERIPHERAL MODELS

2.1. INTRODUCTION

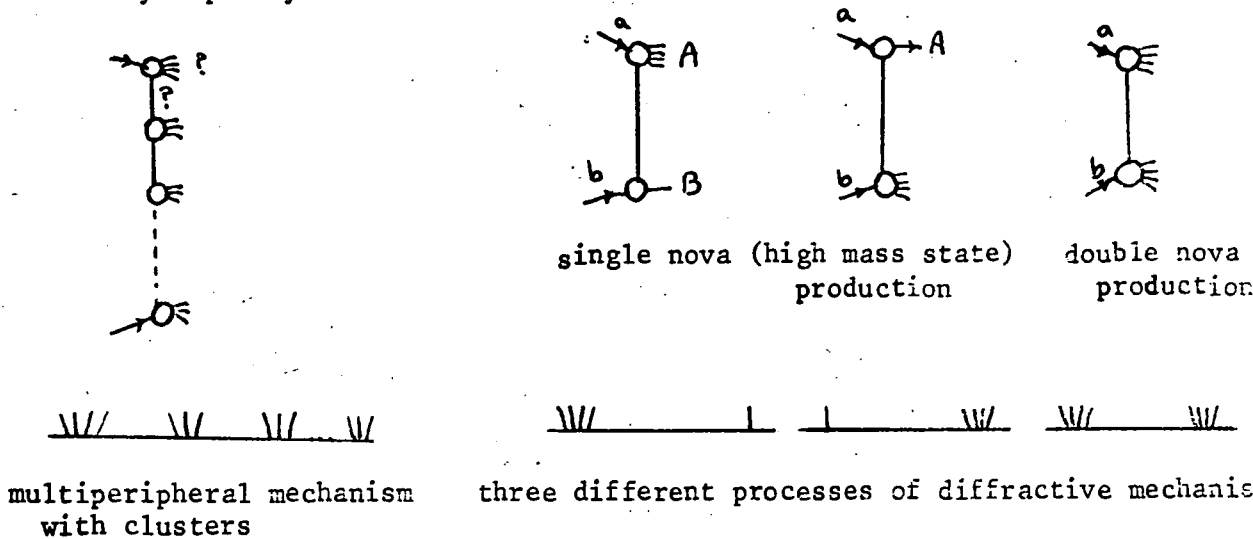
It has always been interesting to try to describe and explain different and frequently occurring phenomena in terms of a very few basic things. For example, since the time of Isaac Newton till the beginning of the present century, almost everything occurring in the domain of physics could have been satisfactorily explained by a very simple formula : $F = m \ddot{x}$.

In theoretical physics the way by which we explain a set of events (data) is through constructing models (either theoretical or phenomenological). Some models were found to be more popular than the others. These were the ones which, as they stood or after some refinements and improvements, succeeded in explaining more phenomena. Or, even they had the power to predict things which were not known then! The best example I could think of is the quark model and the prediction of the Ω particle.

In high energy elementary particle theory, amongst very many types of models, essentially two models seem to be of particular interest. They are the so-called diffractive and non-diffractive models. In this chapter we shall study in some details different types of non diffractive, explicitly speaking multiperipheral, models and see how they cope with data. A few words will also be mentioned about the other model.

2.2. DIFFRACTIVE AND NON-DIFFRACTIVE MODELS - A GENERAL SURVEY

It is generally believed to be the case that there are two different production mechanisms at high energy, namely diffractives and multiperipheral, which are responsible to describe the data. These are the two extremes of the production mechanisms. The picture below shows how these processes look like, together with their secondary rapidity distributions.



The multiperipheral model is a straightforward generalization of the peripheral approach to two particle production amplitudes. The multiperipheral amplitude has contributions from S -channel resonances or t -channel exchanges. Regardless of what are exchanged or what are produced (the two question marks in the figure), which are refinements in the amplitude in order to have a better agreement with data, all fall in the category of multiperipheral model. The multiperipheral model is of short range correlation nature. Once the interaction occurs the secondaries lose all knowledge of the initial colliding particles, contrary to the fragmentation models which have the idea that the initial states maintain much of their identity throughout the collision processes. Just from the topological configuration of the multiperipheral model the following remarks could be made,

- i) in its simplest form the distribution of topological cross-section (σ_n) versus n is Poissonian.
- ii) logarithmic growth of $\langle n \rangle$ in energy variable.
- iii) constant rapidity gaps of the secondaries.
- iv) scaling

The other mechanism is the diffractive model. In the Regge language diffractive process means Pomeron exchange. As it is clear from the picture the colliding particles a and b become excited under impact to produce high mass objects and then break up to give the observed secondaries. The fragments are grouped together in rapidity with a big gap separating them. Assuming that the total cross-section remains finite,

$$\sum_n \sigma_n = \text{finite}$$

one can still get a logarithmic increase for average multiplicity,

$$\frac{1}{\sigma_{\text{tot}}} \sum_n n \sigma_n \propto \ln s$$

A natural way of consistency preservation is to assume that,

$$\sigma_n \propto \frac{1}{n^2}$$

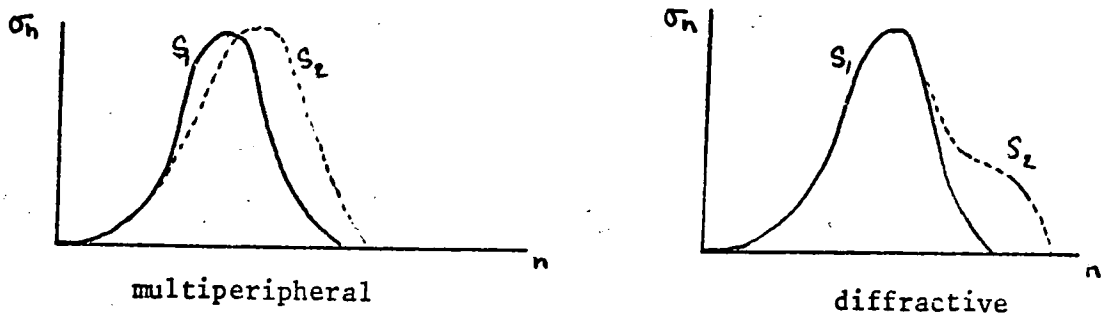
Let us compare some of the properties of these two models below.

- i) We know that outgoing particles carry very little transverse momentum. Neither short range correlation nor fragmentation models predict this effect. This is a basic input of the model in both cases.
- ii) As a direct consequence of $\alpha(0) = 1$ one gets a central plateau in the multiperipheral model. In the second mechanism the plateau does not occur so straightforwardly, but of course it is quite possible to accommodate this in the model. In other words the central plateau is an input for fragmentation models.

Once one gets the flat central plateau, the logarithmic increase of the average multiplicity follows easily, since

$$\langle n \rangle = \frac{1}{\sigma_{\text{tot}}} \int \frac{d\sigma}{dy} dy$$

iii) σ_n is one of the places where the prediction of the mechanisms differ. Particles in the multiperipheral model are produced almost independently (i.e. a roughly poisson shape is n for σ_n), with the peak moving slowly to higher values as S increases. Whereas in the other model the peak of σ_n in n remains constant. The increase in σ_n is coming only from the extension of the tail at high n (see fig. below).



The total cross-section, at higher energies, tends to be constant in this diffractive model. In the framework of multiperipheral model, adjusting the coupling constant and α_{in} , it is possible to have either a constant or a variable σ_{tot} .

iv) Diffractive and multiperipheral models differ profoundly at the level of two particle inclusive reactions. For instance the integrated correlation function,

$$f_2(y) = \int dy_1 dy_2 C_2(y_1, y_2, y)$$

where

$$C_2(y_1, y_2, y) = \frac{1}{\sigma_{\text{tot}}} \frac{d\sigma}{dy_1 dy_2} - \left(\frac{1}{\sigma_{\text{tot}}} \frac{d\sigma}{dy_1} \right) \left(\frac{1}{\sigma_{\text{tot}}} \frac{d\sigma}{dy_2} \right)$$

has different behaviours, depending on the type of model under study.

The short range correlation models give,¹⁸

$$f_2(Y) \xrightarrow{Y \rightarrow \infty} aY + b + e^{-(1-\alpha_S(s))Y}$$

$\alpha(s)$ being the leading angular momentum singularity next to the Pomeron. Fragmentation models predict,⁴⁵

$$f_2(Y) \xrightarrow{Y \rightarrow \infty} c e^{Y/2}$$

which is not linear in Y .

Just by noting the strong energy variation of data in two and four prong topological cross-sections (Fig. 2.1), it seems inappropriate to think of the diffractive models as the sole production mechanism.

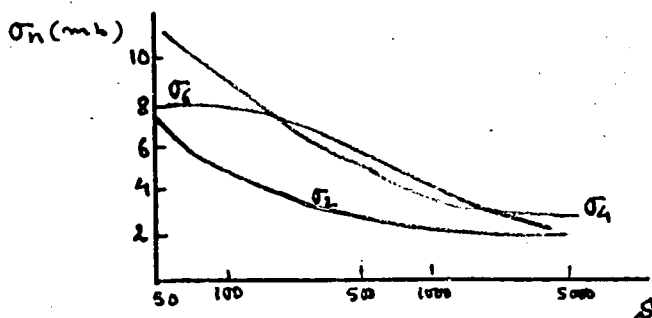
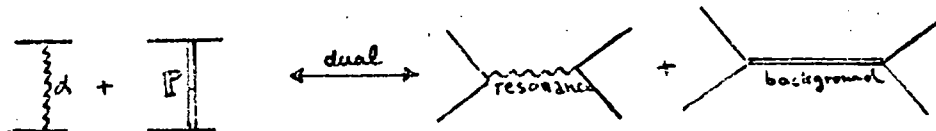


Fig. 2.1

Incorporating the two production mechanisms into one, Harari and Poliwici as well as Fiollawiski and Miettinen²⁰ introduce a new model, a two component model (multiperipheral and diffractive models as the components) which produces nice results. Their procedure is to write σ_n as

$$\sigma_n = \underbrace{m_n}_{\text{multiperipheral}} + \underbrace{d_n}_{\text{diffractive}}$$

En passant, it is interesting to see that when $n = 2$ one gets the familiar old two component duality²¹ :



Next they define parameters D and M by

$$\sum_n dn = D \sigma_{inel} ,$$

$$\sum_n m_n = M \sigma_{inel} ,$$

with the obvious constraint that

$$D + M = 1 .$$

Using seven parameters to fit different sections of data they find

$$\sigma_{tot} = 40 \text{ mb},$$

$$\sigma_{el} = 7 \text{ mb},$$

$$\sigma_{inel} = 33 \text{ mb} .$$

But, perhaps most interesting of all is the value they get for D and M:

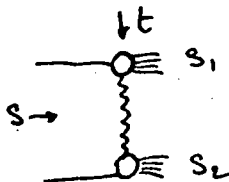
$$D = .16$$

$$M = .84,$$

which is indicative of the fact that the contribution of multiperipheral model to the production mechanism is almost 5.5 times more than that of the diffractive part. This is a good support of approximating the production mechanism by the multiperipheral model.

2.3. MULTIPERIPHERAL MODELS

The multiperipheral model is a generalization of the singly peripheral description of high energy scattering. For a multiparticle final state, such as



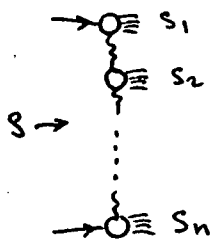
the collision is called (singly) peripheral if for that process the momentum transfer, $|t|$, is smaller than a given number, say $\tau \approx 5 \mu^2$,

$$|t| \ll \tau$$

The calculation of t_{min} with the high energy approximations, results in the following criterion,

$$\frac{s_1 s_2}{s} \ll \tau$$

Generalising this to a multi-peripheral process of n-blobs,



one requires,

$$\frac{1}{s} \prod_{i=1}^n s_i \ll \tau^{n-1}$$

(τ could be interpreted as some mean inter blob momentum transfer).

To show, for example, how the logarithmic increase of mean multiplicity arises naturally in these models, we make the approximation that

$$s_i \approx s_0 \quad \forall i = 1, n$$

Then

$$\frac{s_0^{(n)}}{s} \ll \tau^{(n)-1}$$

which, taking the logarithm of both sides, shows that

$$\langle n \rangle \sim \ln S$$

In the remaining of this section we shall study three different models belonging to this category.

2.3a ABFST MODEL

Interest in a multiperipheral model like that of Amati-Bertocchi-Fubini-Stanghellini and Tonin (ABFST) which was proposed in 1962²² derives from its relevance in describing such features of high energy scattering as Regge behaviour for elastic amplitudes and total cross-sections, scaling and logarithmic growth of the multiplicity in multiparticle production reactions.

The basic idea of the model is that the absorptive part of the elastic scattering amplitude can be computed from a multiparticle production amplitude which factors into a product of unspecified blobs, the number of which is restricted by the amount of the input energy (\sqrt{s}), connected by single particle propagators. In the original model the outgoing particles as well as the internal lines are pions. As it is clear from the picture (Fig. 2.2) the final state particles emerge in pairs. The reason for this is due to the G-parity conservation rule. This, in a sense, implies that in the ABFST model cluster formation is built in automatically.

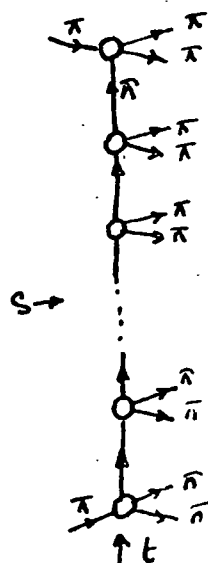


(Fig. 2.2)

The repetitive nature of the production amplitude together with the s-channel unitarity give rise to an integral equation for elastic scattering (s-channel absorptive part, to be more precise),

$$\tilde{A}(p, k, q) = \int \alpha^4 p' V(p, p', q) S(p, q) \tilde{A}(p', k, q) \quad (2.1)$$

where $\tilde{A} = \text{Im}A$ and $S(p, q)$ is a multiplication of the propagators,

$$S(p, q) = \frac{1}{m^2 - (\frac{q}{2} + p')^2} \frac{1}{m^2 - (\frac{q}{2} - p')^2} ,$$

and the four momenta are defined as illustrated in fig. 2.3 which also exhibits a diagrammatic representation of the equation (2.1).

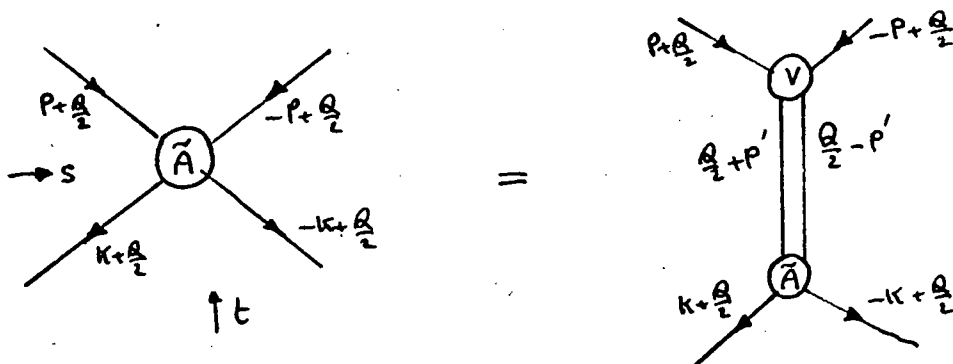


Fig. 2.3

V is the input to the model which most of the times is formulated by considering the phenomenology. For instance Amati et al had supposed the imaginary part of the low energy $\pi\pi$ scattering amplitude for V^* .

The integral equation (2.1) is of a particular importance. Since its solution gives rise to a lot of interesting results, described at the beginning of this subsection, which are compatible with data. Indeed by allocating a power dependence to the amplitude $A = S^\alpha \phi$ they²² arrive at the conclusions that asymptotically,

- i) cross sections behave as a power of the energy.
- ii) multiplicities grow logarithmically with the energy.
- iii) constant inelasticity.

To stretch the analytical solution for the integral equation (2.1) as much as possible in order to express the high energy properties of physical scattering amplitudes in terms of singularities in the partial

* Other models include inclusion of a high energy tail represented by Pomeron exchange or the use of duality to replace the low energy direct channel resonances by the exchange of lower lying Regge trajectories (P' , ρ) in the t-channel in addition to the P exchange.

wave parameter plane. one should be prepared to do some sacrifices. This is due to the fact that the eigenvalue equations for the Regge trajectory involve fairly complicated kernels and cannot be solved exactly. The sacrifices represent themselves in two standard approximations usually one meets at this stage. It, however, turns out that once the approximation is made the rest of the calculation can be carried out more or less exactly. It will be fair to say that the best support for validity of the two approximations is that their results are similar to the exact numerical calculations.

Let us very briefly describe here what the approximations are. We first partial wave project the equation (2.1) in the t-channel with the first term of the sum separated:

$$\tilde{A}_L(i, f) = V_L(i, f) + \int \tilde{V}_L(i, int) \tilde{A}_L(int, f) dint,$$

where A_L and V_L are the t-channel partial wave projections of A and V. V_L includes the propagators. i, f and int are the abbreviations for initial, final and inter-mediate states respectively.

The first approximation is called factorizable kernel approximation.²³ The method is just to write the kernel as something similar to the following equation:

$$\tilde{V}_L(i, int) = \tilde{V}_L^{(i)}(i) \tilde{V}_L^{(e)}(int).$$

The factorization is subject to the condition that it retains the correct behaviour at the physical boundary. The method gives a (Fredholm) denominator, D_L ,

$$\tilde{A}_L \propto \frac{g^2 (m^2)^{-l-1}}{D_L}$$

from which Regge trajectory of real and complex poles can be derived ($D_L = 0$).

The second approximation,²⁴ that is the trace approximation, for the eigenvalues of an integral equation with (Fredholm) denominator $D_L(g^2)$ is to write

$$\begin{aligned} D_L(g^2) &= 1 - g^2 \text{Tr } \check{V}_L + \dots \\ &= 1 - g^2 \int \check{V}_L(i\pi, i\pi) d\pi \end{aligned}$$

and to incorporate the full kernel singularity structure in the first term and to ignore higher terms in the denominator. The Regge poles, again, occur as the zeros of D_L in the L variable.

The calculations show that the slope is always proportional to $\ln m_\pi^2$. Supposing that the intermediate states have masses 1 and those of i and f states are m_π , one arrives at the following numerical results for the leading trajectory (Pomeron) with $\alpha_0 = 1$,

$$\alpha'_0 = .27 \text{ gev}^{-2}, \quad g^2 = 2.2 \text{ gev}^{-2}, \quad \sigma_{\pi\pi} = 33 \text{ mb}.$$

It could be worth stating that there is one secondary pole near every negative integer ℓ ($t = 0$).

Finally we summarize the section at the following diagram.

ABFST equation

$$V = g^2 \delta(s - M^2)$$

Approximate the kernel as one or
a sum of resonances.

Partial wave project
in t

Trace approximation

Factorizable kernel
approximation

Regge trajectory content of ABFST

2.3b CtA Model

Another multiperipheral model, with Reggeized rungs was introduced by Chan Hong-Mo, Loskiewicz and Allison.²⁵ The modulus of the n-particle amplitude corresponding to the model is

$$|A_n| \sim \prod_{i=1}^{n-1} \left(\frac{g_i S_i + c \alpha}{S_i + a} \right) \left(\frac{S_i + a}{a} \right)^{\alpha_i} \left(\frac{S_i + b_i}{b_i} \right)^{t_i} \quad (2.2)$$

where

$$S_i = (\bar{q}_i + \bar{q}_{i+1})^2 - (m_i + m_{i+1})^2$$

$$t_i = \left(p_a - \sum_{r=1}^i q_r \right)^2$$

and α_i is the intercept of the Regge trajectory with the $t = 0$ axis. The constants b_i , g_i , c and a determine the t_i dependence, the coupling constant, the strength of Regge type and phase space contributions and the energy scale respectively.

The idea behind the parametrization of the amplitudes was three fold,

- i) the amplitude is fully Reggeized if the S_i of the final particles are large.
- ii) the amplitude is partly constant whenever some S_i are small.
- iii) there is a smooth interpolation between (i) and (ii).

It is not difficult to see that the amplitude (2.2) fulfills these criteria For instance when all S_i are large, that is,

$$S_i \gg a$$

$$S_i \gg b_i$$

the amplitude takes the following form

$$|A_n| = \prod_i g_i \left(\frac{S_i}{a} \right)^{\alpha_i} e^{\lambda_i t_i} \quad (2.3)$$

where

$$\lambda_i = \ln \frac{S_i}{b_i}$$

The equation (2.3) has the form of a fully Reggeized amplitude.

Studying the $\vec{\pi} p \rightarrow p + (n-1) \pi$ reaction, CtA fit very successfully

the data for the single particle distributions of $\hat{\kappa}$ and P such as $\langle \hat{q}_T \rangle$ and q_L distributions at energies up to 16 gev/c.

One of the points that was not discussed in the paper is the effect of the phases. In fact the inclusion of phases changes some of the predictions of the model drastically.²⁷⁻²⁸ For example, a Reggeized phase gives a steeper slope for the overlap function as shall be seen later.

2.3c CHEW-PIGNOTTI MODEL

The model was proposed in 1968 and is one of the most popular multiperipheral models.²⁶ We shall study the model in some details and end up the chapter by saying a few words about the multiperipheral bootstrap.

The figure (2.4) shows a pictorial form of the model. The rungs are Reggeized and therefore give a contribution of $S_{i,i+1}^{\alpha(t)}$ to the amplitude and it shall be exploited later.

In the laboratory frame of reference where particle a is at rest and b is moving along a direction, say z , we have the following,

$$P_a = (m_a, \vec{0}, 0),$$

$$P_b = (m_b \cosh \gamma, \vec{0}, m_b \sinh \gamma),$$

$$q_i = (m_{T_i} \cosh \gamma_i, \vec{q}_{T_i}, m_{T_i} \sinh \gamma_i),$$

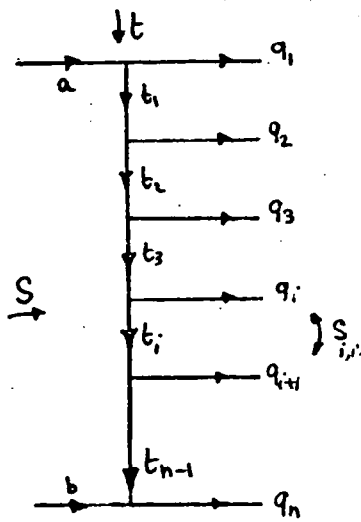


Fig. 2.4

where the transverse mass m_T is defined as,

$$m_T = (m^2 + q_T^2)^{1/2},$$

and also

$$e^{-\gamma} = 1/S.$$

The phase space element is

$$d\Phi_n = \prod_{i=1}^n \frac{d^3 q_i}{\omega_i} \delta^{(4)} \left(\sum_{i=1}^n q_i - P_a - P_b \right),$$

which, because of the separation of longitudinal and transverse kinematics could be written as

$$d\Phi_n = \frac{1}{2} \prod_{i=1}^n d^2 q_{T_i} d\gamma_i \delta^2 \left(\sum_{j=1}^n \vec{q}_{T_j} \right) \delta \left(\sum_{j=1}^n m_{T_j} e^{-\gamma_j} - m_a - m_b e^{-\gamma} \right) \\ \cdot \delta \left(\sum_{j=1}^n m_{T_j} e^{-\gamma_j} - m_a - m_b e^{-\gamma} \right)$$

In the strong ordering approximation ($Y_{i+1} \gg Y_i$) and also ignoring the $\vec{q}_{T_i}^2$ terms in the m_{T_i} , we can approximate the last two delta functions of the phase space by

$$\frac{e^{-Y}}{m_a m_b} \delta(Y - X_a) \delta(Y_b - Y_n - X_b)$$

where

$$X_a = \ln \frac{m_{T_1}}{m_a},$$

$$X_b = \ln \frac{m_{T_n}}{m_b}.$$

Writing the phase space in terms of the rapidity gap variable, $Z_i = Y_i - Y_{i-1}$, and making use of the first δ function above to do the integration over Y_i , we get,

$$d\Phi_n = \frac{e^{-Y}}{2m_a m_b} \prod_{i=1}^n d^2 q_{T_i} \prod_{k=2}^n dz_k \delta\left(\sum_{j=1}^n \vec{q}_{T_j}\right) \delta\left(X - \sum_{j=1}^n z_j\right)$$

where

$$X = Y - X_a - X_b \\ = Y$$

The squared amplitude in the model is written as

$$|A_n|^2 = g^{2n} \prod_i^{n-1} (S_{i,i+1})^{2\alpha_i},$$

with

$$S_{i,i+1} = (q_i + q_{i+1})^2 \stackrel{Y_{i+1} \gg Y_i}{\approx} \frac{m_{T_i} m_{T_{i+1}}}{Y_{i+1} Y_i} e^{Y_{i+1} - Y_i} = \frac{m_{T_i} m_{T_{i+1}}}{Y_i} e^{z_i}$$

Hence the calculation of σ_n ,

$$\sigma_n \propto e^{-Y} \int g^{2n} \prod_{i=1}^{n-1} (S_{i,i+1})^{2\alpha_i} d\Phi_n,$$

is easy now:

$$\begin{aligned} \sigma_n &\propto e^{-Y} g^{2n} e^{Y(2\alpha_i - 1)} \int \prod_{i=1}^n dz_i \delta(Y - \sum z_i) \\ &= g^{2n} e^{Y(2\alpha_i - 2)} \frac{Y^n}{n!} \\ &= S^{2\alpha_i - 2} \frac{(g^2 \ln S)^n}{n!} \end{aligned} \quad (2.4)$$

Summing over n one gets the total cross-section

$$\begin{aligned}
 \sigma_{tot} &= \sum_n \sigma_n \\
 &= S^{2\alpha_{in}-2} \sum_n \frac{(g^2 \ln S)^n}{n!} \\
 &= S^{2\alpha_{in}-2} e^{g^2 \ln S} \\
 &= S^{2\alpha_{in}-2+g^2} \quad (2.5)
 \end{aligned}$$

Supposing that the total cross section is constant one gets

$$2\alpha_{in} - 2 + g^2 = 0$$

Putting this back into (2.4) one obtains a poissonian type of distribution for the topological cross sections:

$$\sigma_n = (g^2 \ln S)^n \frac{e^{-g^2 \ln S}}{n!},$$

with an average multiplicity which grows logarithmically:

$$\langle n \rangle = g^2 \ln S \quad (2.6)$$

The fact that σ_n turns out to be poissonian is suggestive of there being no correlations amongst the secondaries, $f_2 = 0$ (see Appendix A).

The equation (2.5) shows a sort of bootstrap model. It is a well known fact that the dominance of a Regge pole results on

$$\sigma_{tot} \sim S^{\alpha_{out}-1} \quad (2.7)$$

The comparison of (2.5) and (2.7) yields,

$$\alpha_{out} = 2\alpha_{in} - 1 + g^2, \quad (2.8)$$

where α_{in} is the input Regge trajectory. The equation clearly indicates that not all α_{in} could be pomeron (unless $g^2 = 0$). Calculating α_{in} in terms of the others

$$\alpha_{in} = \frac{1}{2} (\alpha_{out} + 1 - g^2),$$

with the numerical values

$$\alpha_{out} = 1$$

$$g^2 = 1.5$$

one gets

$$\alpha_{in} = .25$$

which does not seem to be too good. A way round this is a lower value for g^2 ($g^2 \approx 1$), which means, considering the equation (2.6), the introduction of clusters.

We end the section by summing up the multiperipheral bootstrap model in fig. (2.5).

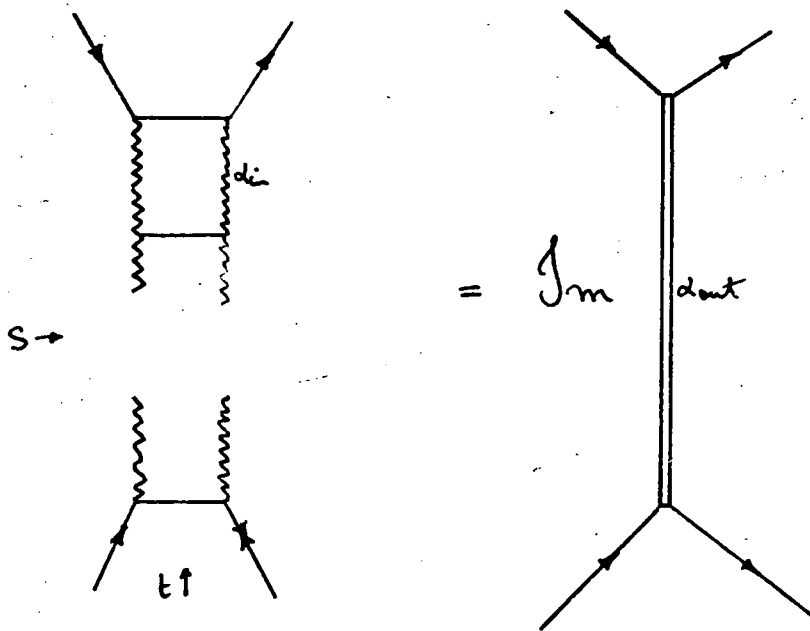


Fig 2-5

CHAPTER THREE

MANY BODY AMPLITUDES AND ELASTIC SCATTERING

3.1. INTRODUCTION

The present chapter, in a way, is a confrontation of the first two chapters in a specific case study which we hinted in the last section of the first chapter. Let us introduce the problem more explicitly here.

We know that as a direct consequence of the S-matrix unitarity the following could be written,

$$\text{Im } A^{\text{el}}(p_a, p_b, p_a', p_b') = \sum_{n=2}^{\infty} \int d\Phi_n A_n(p_a, p_b; q_1, \dots, q_n) A_n^*(p_a', p_b'; q_1, \dots, q_n) \quad (3.1)$$

where A^{el} is the elastic scattering amplitude describing $a + b \rightarrow a' + b'$ and A_n is the n-particle production amplitude for $a + b \rightarrow 1, 2, \dots, n$ and $d\Phi_n$ is the phase space element.

In theory, as one understands from the equation, a 'nice' multiparticle amplitude inserted to the right hand side of (3.1) must be able to generate the correct elastic scattering process. So, the problem we are going to study here is to see if a Chew-Pignotti type of model, which adequately describes the main features of the inelastic scattering data, is eligible to produce the correct forward diffraction peak as well. In the next section we shall deal with the problem in the impact parameter space.

3.2. IMPACT PARAMETER SPACE (HENYEV WORK)

As in the $2 \rightarrow 2$ processes one could guess that the impact parameter space is perhaps one of the suitable places to study multiparticle processes at high energies. Thinking of the impact parameter as the transverse position of a scattering particle one could go from (q_L, \hat{q}_T) space to (q_L, \vec{b}) space.²⁹ The Fourier type of transformation establishes a relationship between the multiparticle amplitudes in these two spaces (see Fig. 3.1 for the notations)

$$\tilde{A}(\vec{b}_j, q_{Lj}) = \int \prod_{j=1}^n \left[\frac{d^2 \vec{q}_{Tj}}{(2\pi)^2} e^{i \vec{q}_{Tj} \cdot \vec{b}_j} \right] A(\vec{q}_{Tj}, q_{Lj}) \delta^2(\sum \vec{q}_{Tj}) \quad (3.2)$$

The transverse momentum conservation δ -function has made the transformation a little different from an ordinary Fourier transformation. The inverse form of the equation (3.2) is written as follows (see the Appendix B for its derivation),

$$A(\vec{q}_{Tj}, q_{Lj}) = (2\pi)^2 \int \prod_{j=1}^n \left[d^2 b_j e^{-i \vec{q}_{Tj} \cdot \vec{b}_j} \right] \tilde{A}(\vec{b}_j, q_{Lj}) \delta^2(\sum \vec{b}_j) \quad (3.3)$$

Using the unitarity relation together with the separation of longitudinal kinematics from that of transverse, one ends up with,

$$\text{Im } A_{el}(\hat{\Delta}) = \frac{(2\pi)^4}{2} \sum_n \int \prod_{j=1}^n \left[\frac{d^2 q_{Tj}}{(2\pi)^2} \frac{d^4 y_j}{4\pi} \right] A^*(q_{Lj}, q_{Tj})$$

$$A(q_{Lj}, q_{Tj}) \delta^2(\sum_{j=1}^n \vec{q}_{Tj}) \delta(\sum_{j=1}^n q_{Lj})$$

$$\delta(\sum_{j=1}^n \omega_j - \sqrt{s})$$

(3.4)

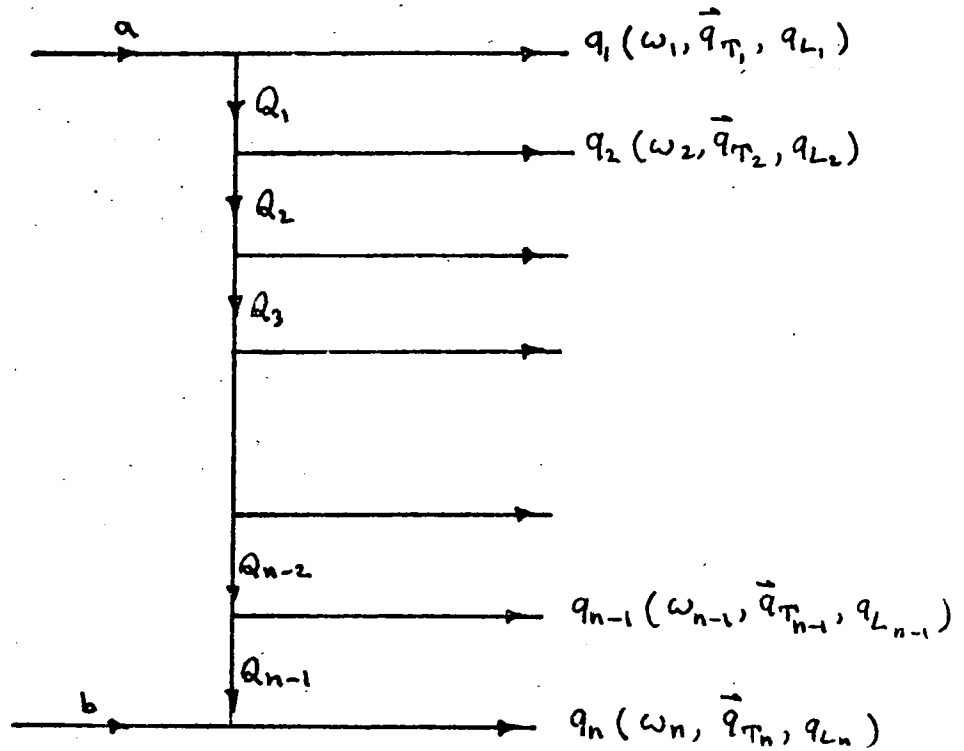


(Fig. 3.1)

where

$$q'_{Lj} = q_{Lj} - \frac{\vec{q}_{Tj} \cdot \vec{\Delta}}{\sqrt{s}/2} \approx q_{Lj}$$

$$\vec{q}'_{Tj} = \vec{q}_{Tj} + \frac{q_{Lj}}{\sqrt{s}/2} \vec{\Delta}$$

$\vec{\Delta}$ is the momentum transfer in elastic scattering ($t \approx -\Delta^2$).

The transformation of A and A^* to the impact parameter space in the equation (3.4) (b and b' respectively) by using equation (3.3) and doing the integrations over q_{Tj} and \vec{b}_j in turn yields

$$\text{Im } A^{\text{el}}(\vec{\Delta}) = \sum_n \frac{(2\pi)^4}{2} (2\pi n)^2 \int \prod_{j=1}^n \left[d^2 b_j \frac{d^4 y_j}{4\pi} \right] \delta(\Sigma \vec{q}_{Tj}) \delta(\Sigma \omega_j - \sqrt{s}) \exp\left[i \vec{\Delta} \cdot (\Sigma \vec{b}_j \frac{q_{Lj}}{\sqrt{s}/2})\right] \delta^2(\Sigma \vec{b}_j) |\tilde{A}(\vec{b}_j, q_{Lj})|^2$$

The application of equation (3.2) on (3.5) results on

$$\begin{aligned} \text{Im } \tilde{A}_{el}(\vec{b}) = \sum_n \frac{(2\pi)^4}{2} (2\pi n)^2 \int \prod_{j=1}^n \left[d^4 b_j \frac{d^4 y_j}{4\pi} \right] \\ \delta(\sum q_{Lj}) \delta(\sum v_j - \sqrt{s}) \delta^{(4)}(\sum \vec{b}_j) \\ \delta^{(4)}(\vec{b} - \sum \frac{q_{Lj}}{\sqrt{s/2}} \vec{b}_j) | \tilde{A}(\vec{b}_j, q_{Lj}) |^2. \end{aligned} \quad (3.6)$$

The equation (3.6) is the central result of the reference 10. It resembles an optical theorem at each impact parameter. The equation states that the imaginary part of the elastic scattering is given by the sum of all cross-sections at each impact parameter. The application of the result on an exponential multiperipheral model for the multiparticle amplitude with the approximation that momentum transfers do not include the longitudinal part results on the following form for the $\text{Im } A^{el}$,

$$\text{Im } A^{el}(t) \sim \exp \left[\langle \chi^t \rangle (n-1) \frac{R^2}{4} t \right], \quad (3.7)$$

where n is the multiplicity, R is the step size in impact parameter space and $\langle \chi^t \rangle$ is an average over certain summation of Feynman type quantities. $\langle \chi^t \rangle$ and R^2 vary very slowly with energy such that they could be considered as constants (the paper uses these values for $\langle \chi^t \rangle$ and R^2 at $n = 10$: $\langle \chi^t \rangle = .6$ and $R^2 = 10.9 \text{ gev}^{-2}$).

The comparison of (3.7) with data (i.e. the overlap functions:³⁰ the imaginary part of the elastic scattering with the contribution of elastic scattering itself excluded) shows that the multiperipheral model introduces a bigger slope which grows very fast with energy (see figure 3.2).

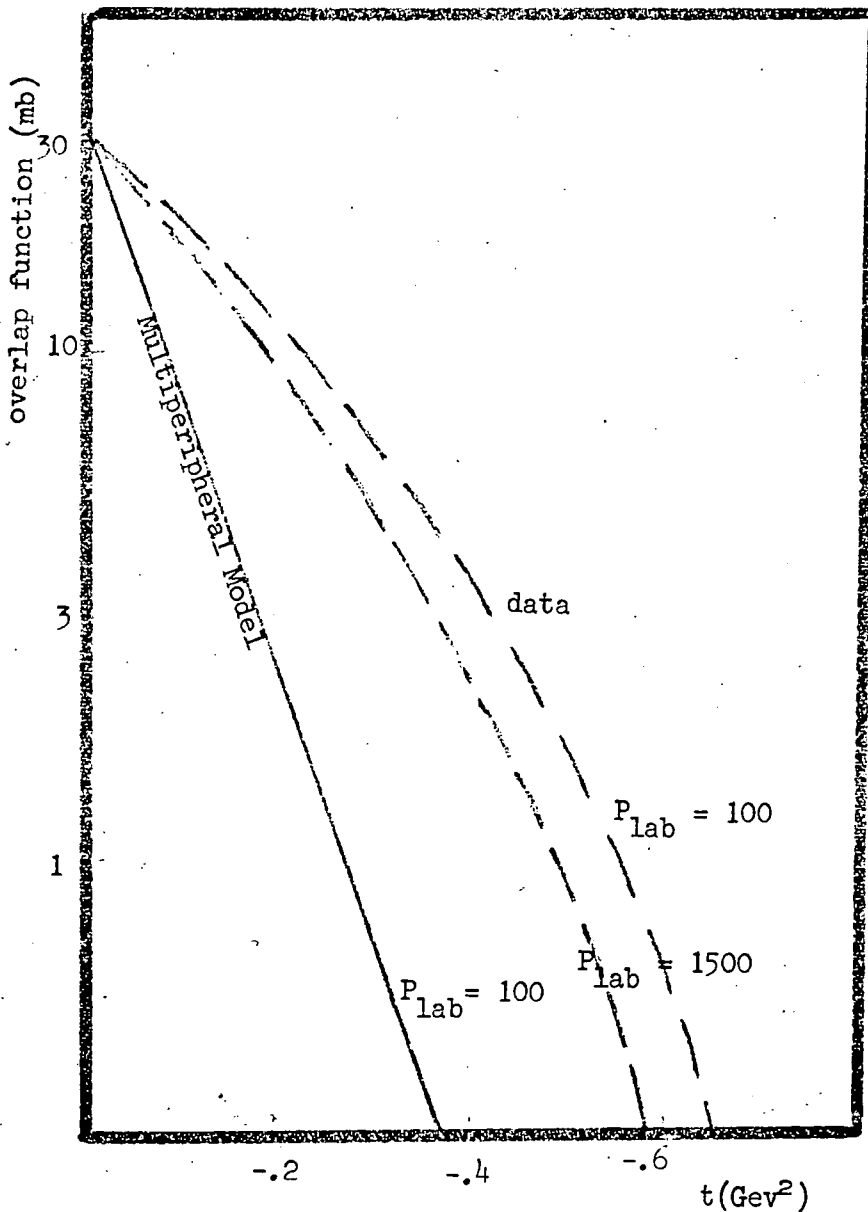


Fig 3.2

3.3. THE WORK OF JEDACH-TURNAU

The approximation of $t_i \approx t_i^T$, which was applied in the previous section, was the point of criticism by Jedach and Turnau.³¹ What they claim is that the replacement of $\exp \lambda t_i$ of each internal line of the multiperipheral chain by $\exp \lambda t_i^T$ is not at all convincing. They find that the bounds on transverse momenta are provided by the longitudinal part, t_i^L , of momentum transfer rather than its transverse part t_i^T . Let us see below how the \vec{q}_T dependence enters the calculation through t_i^L .

$$t_i = t_i^L + t_i^\pi$$

where

$$t_i^\pi = - \left(\sum_{k=1}^i \tilde{q}_{\pi k} \right)^2$$

and

$$t_i^L = \left(E_a - \sum_{k=1}^i \omega_k \right)^2 - \left(P_a^L - \sum_{k=1}^i q_{Lk} \right)^2$$

t_i^L could be written in the following form:

$$t_i^L = \left(E_a - \sum_{k=1}^i \omega_k - P_a^L + \sum_{k=1}^i q_{Lk} \right) \left(E_a - \sum_{k=1}^i \omega_k + P_a^L - \sum_{k=1}^i q_{Lk} \right) \quad (3.8)$$

The insertion of momentum and energy conservation rules

$$P_a^L - \sum_{k=1}^i q_{Lk} = -P_b^L + \sum_{k=i+1}^n q_{Lk} \quad ,$$

$$E_a - \sum_{k=1}^i \omega_k = -E_b + \sum_{k=i+1}^n \omega_k \quad ,$$

in equation (3.8) gives

$$t_i^L = - \left[E_a - P_a^L - \sum_{k=1}^i (\omega_k - q_{Lk}) \right] \left[E_b + P_b^L - \sum_{k=i+1}^n (\omega_k + q_{Lk}) \right]$$

Since

$$\omega_k \pm q_{Lk} = m_k^\pi \exp(\pm \gamma_k) \quad ,$$

where

$$m_k^\pi = \sqrt{m_k^2 + \tilde{q}_{\pi k}^2}$$

thus

$$t_i^L = - \left(m_a e^{-\gamma_a} - \sum_{k=1}^i m_k^\pi e^{-\gamma_k} \right) \left(m_b e^{\gamma_b} - \sum_{k=i+1}^n m_k^\pi e^{\gamma_k} \right) \quad (3.9)$$

To make the transverse dependence of t_i^L more explicit we do some approximations:

$$m_k^\pi = \langle m^\pi \rangle$$

supposing equal spacing in the rapidity state one gets

$$\sum_{k=1}^i m_k^\pi e^{-Y_k} = \langle m^\pi \rangle \frac{e^{-Y_i} - e^{-Y_1}}{1 - e^{-d}}$$

$$\sum_{k=i+1}^n m_k^\pi e^{Y_k} = \langle m^\pi \rangle \frac{e^{Y_{i+1}} - e^{Y_n}}{1 - e^{-d}}$$

Making use of these two relations and

$$e^{-Y_a} \approx e^{-Y_i} \ll e^{-Y_1}$$

$$e^{Y_b} \approx e^{Y_n} \ll e^{Y_{i+1}}$$

in the equation (3.9) one comes to the approximation that

$$t_i^L \approx \langle m^\pi \rangle^2 \frac{e^{-d}}{(1 - e^{-d})^2} \quad (3.10)$$

where

$$Y_i - Y_{i+1} = d,$$

is the gap size and experimentally is a small number ($d \ll 1/n$).

Therefore the transverse momentum distribution is controlled

by the longitudinal part of the momentum transfer. Thus approximating

$t_i^L = 0$ requires a bigger value for λ in order to fit the

transverse momentum distribution, hence strong shrinkage. Taking t_i^T

as well as t_i^L into consideration, Jedach and Turnau arrive at the

result that the shrinkage is in accord with data but has smaller values,

in two versions of multiperipheral model CtA and CP, (Fig. 3.3): The

same conclusion has been reached by Teper.³²

The situation becomes more interesting if we consider another paper by Henyey.³³ There he claims that data is indicative of the fact that amplitudes have either no, or at least less, dependence on the longitudinal part of the momentum transfer. Let us briefly explain the argument. Equation (3.10) shows that t_i^L is a rapid function of

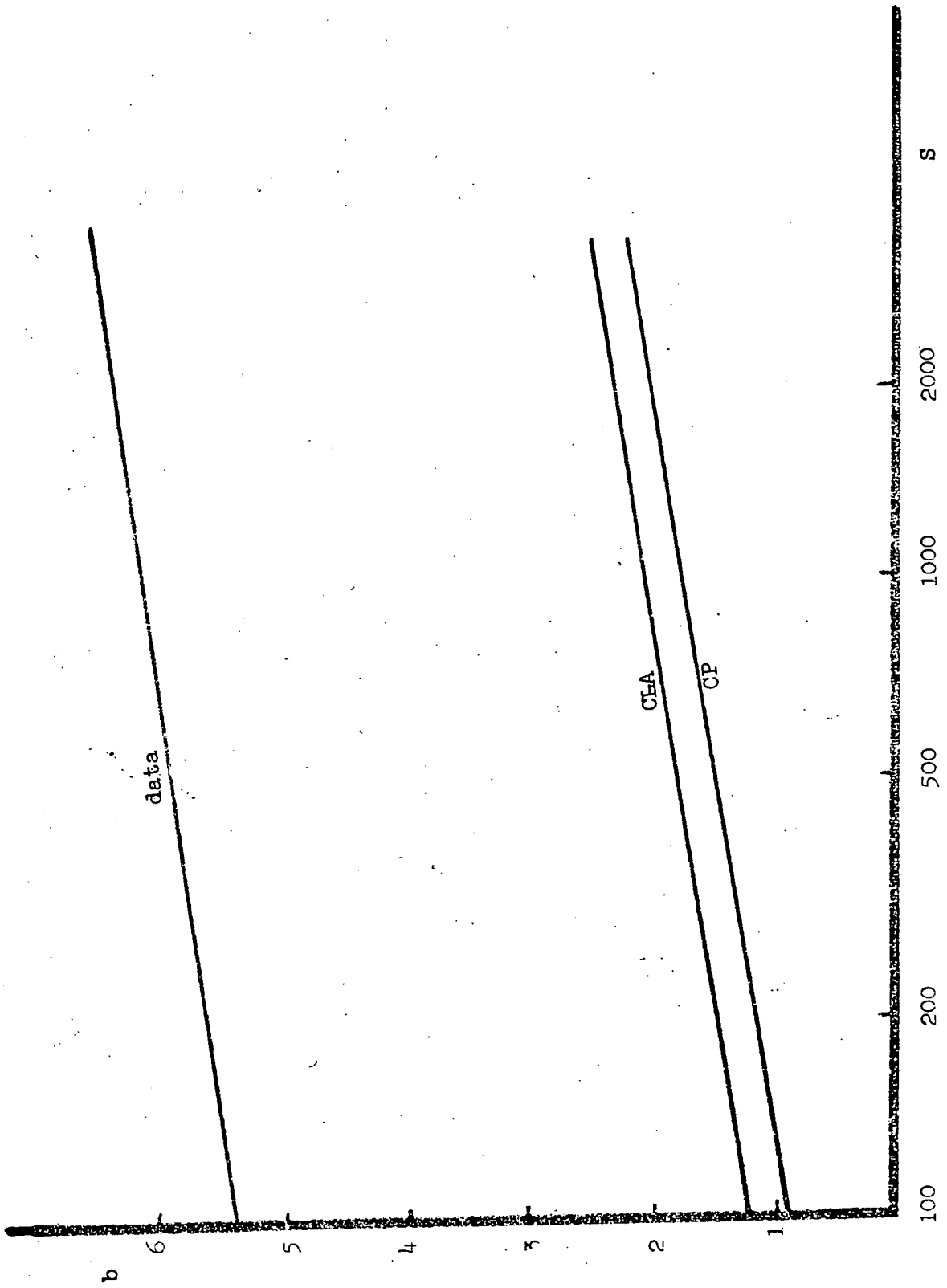


Fig 3.3

the rapidity gap d . Since experimentally d is a small number the factor

$$Z = \frac{e^{-d}}{(1 - e^{-d})^2}$$

will be a large one and therefore, if t_i^L present, will dominate t_i^T (see fig. 3.4).

Theoretically, from equation (3.10), one has

$$\langle q_T^2 \rangle \approx \frac{1}{\lambda Z}$$

Comparing this with data (fig. 3.5) one finds no similarity, so possibly the dependence of the amplitude on t_i^L is very weak.

However, the elastic slope for an amplitude of the form

$$|A|^L \propto e^{2\lambda \sum t_i}$$

where t_i is the total momentum transfer, is ³⁴

$$B = \langle (n-1) \chi R^L \rangle$$

Comparing this with the slope of equation (3.7) one concludes that the inclusion of t_i^L only replaces χ^L by χ . Since $\chi \approx .8$ the previous result of Henyey has not been modified too much. Therefore whether or not one enters t_i^L into the calculations the problem of proportionality of slope and multiplicity, which is ruled out by data but predicted by multiperipheral models (fig. 3.5), remains a mystery.

The inclusion of phases does not seem to remedy the problem either. For instance, the effect of corresponding a phase of the form of

$$\exp\left[i \frac{\pi}{2} \alpha(t_i)\right], \text{ where}$$

$$\alpha(t_i) = \alpha_0 + \alpha' t_i,$$

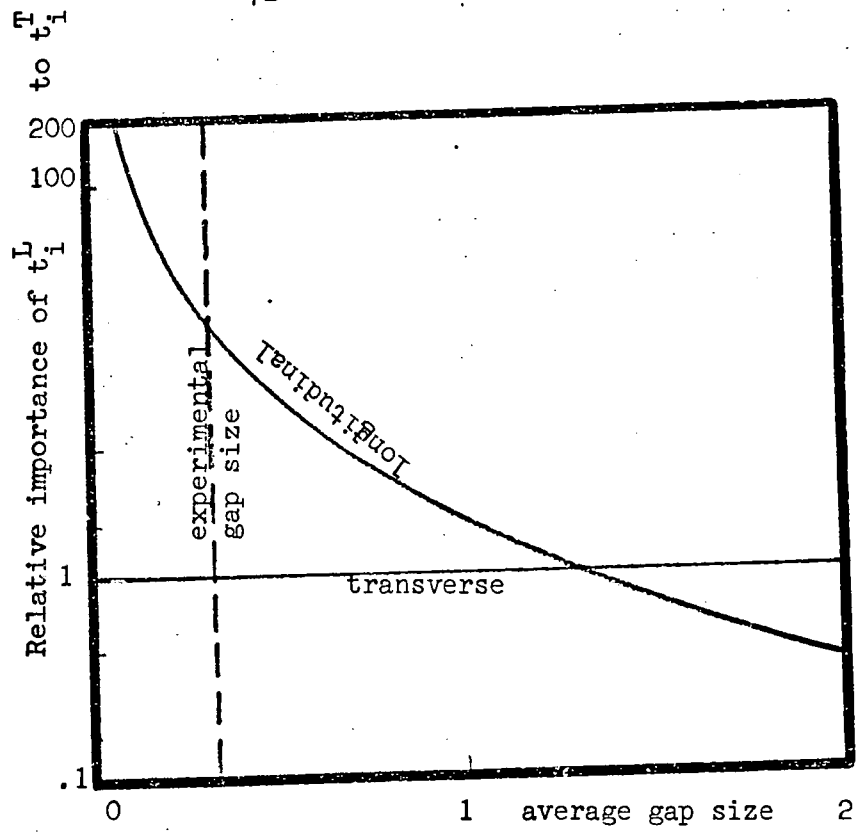


Fig 3.4

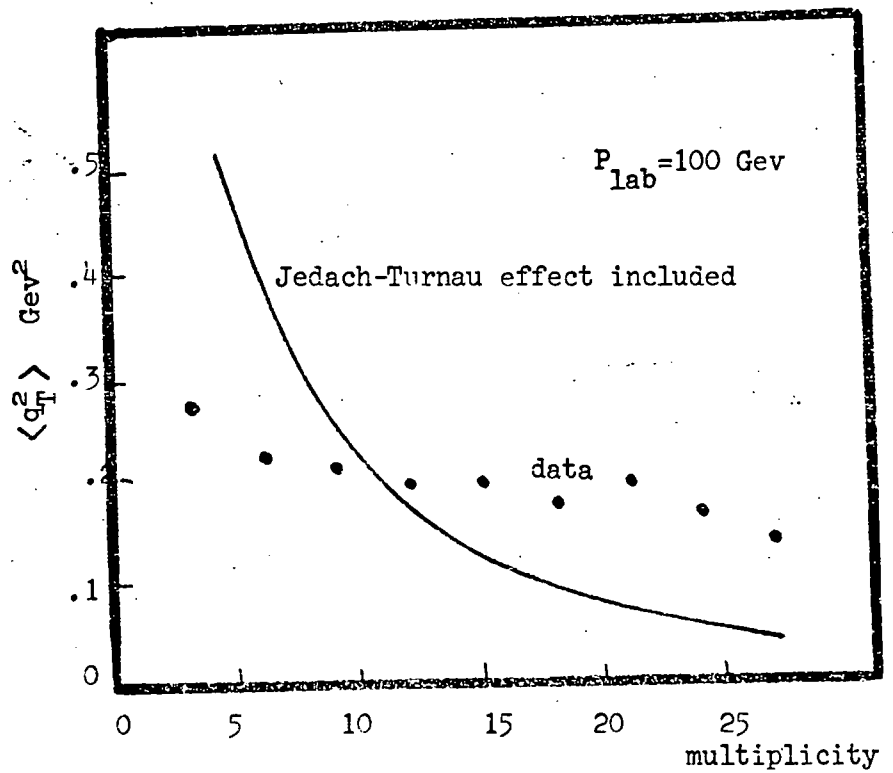


Fig 3.5

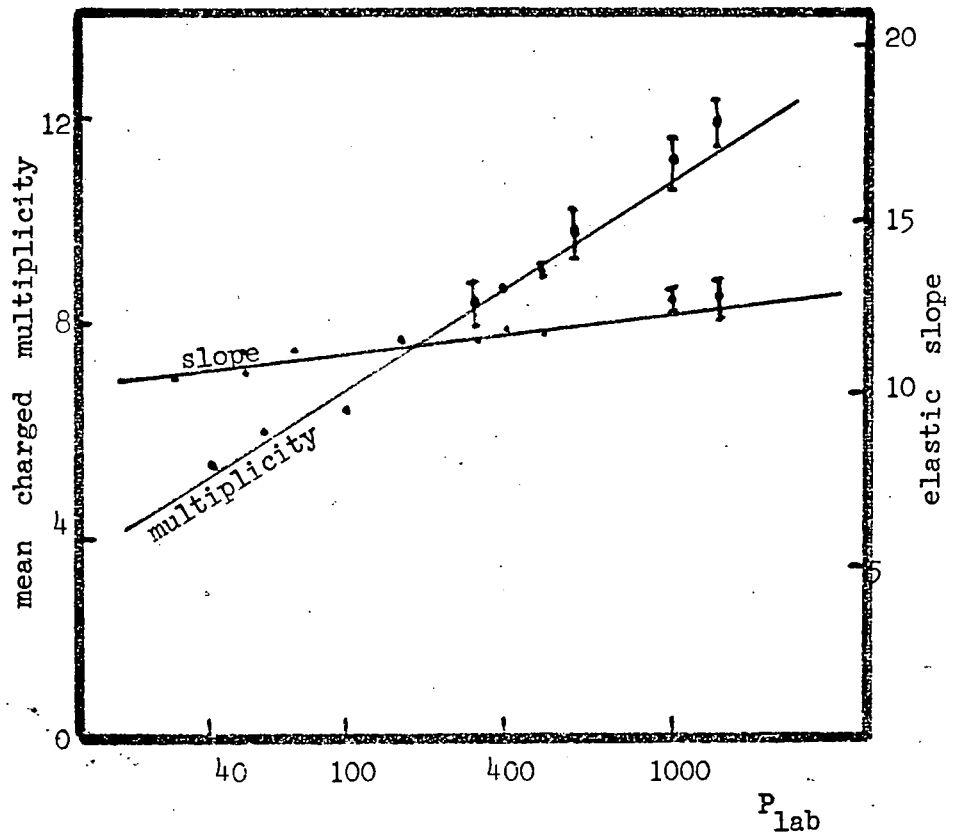


Fig 3.6

to each of the links not only does it not help to cure the problem but makes the situation worse too^(27, 32) : the slope, now, increases faster! See figure (3.7).

In the next chapter we shall investigate the effect of criss-cross diagrams in the unitarity equation to see if it could help to overcome the problem. The effect of clusters will also be studied. But before ending the chapter we would like to introduce the random walk picture.

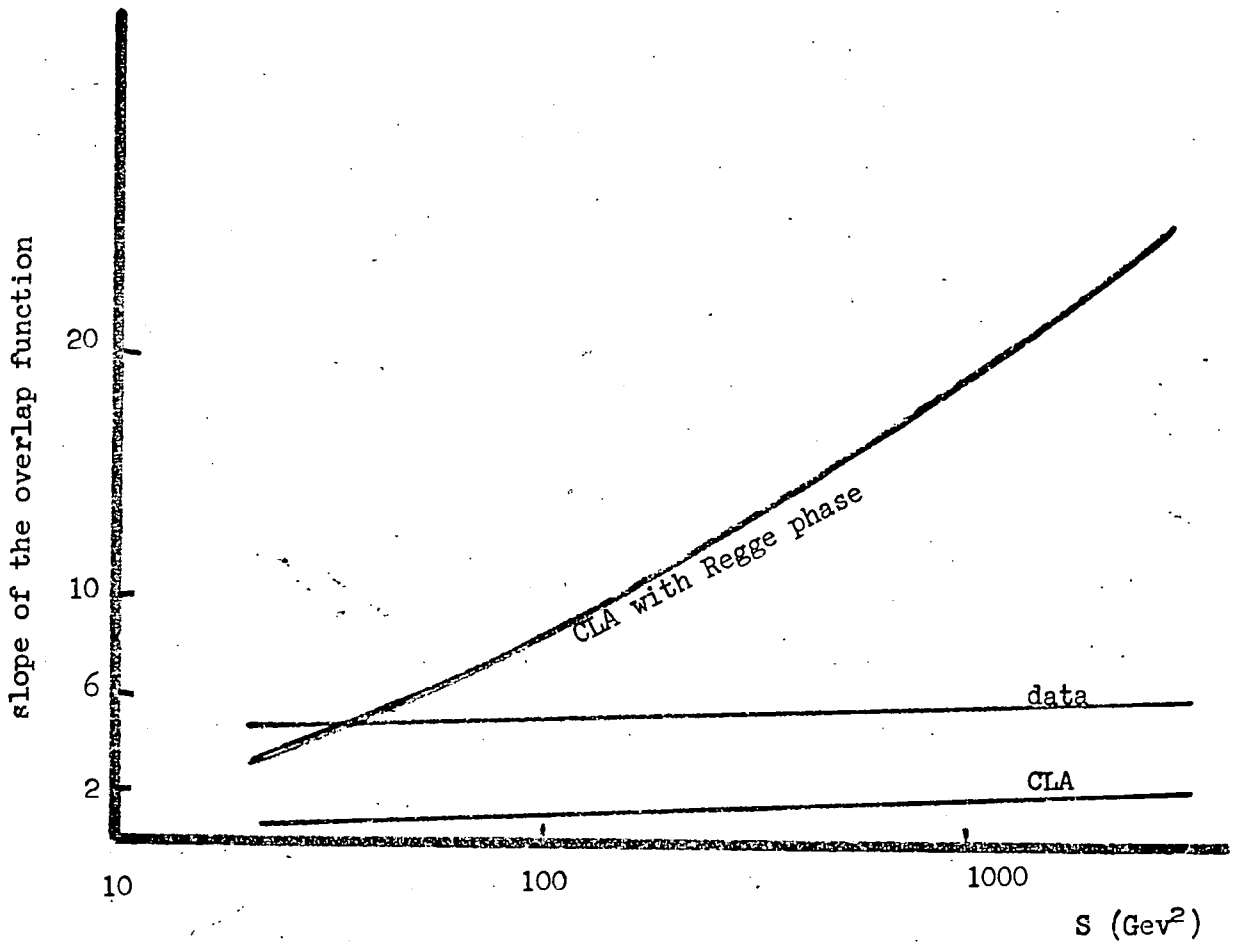


Fig 3.7

3.4. THE RANDOM WALK PICTURE

We might have introduced the idea of the random walk picture right after the equation 3.7, but we postponed it to a separate section so that not only the flow of the text was not deviated but we could also derive the equation.

The part of the multiparticle amplitude we are interested, in terms of the $(n-1)$ independent transverse momentum transfer, \vec{Q}_{T_j} , is

$$A(\vec{Q}_{T_j}) = \prod_{j=1}^{n-1} e^{-\lambda \vec{Q}_{T_j}^2}, \quad (3.11)$$

with the notations as in figure 3.1.

The overlap function is⁴⁰

$$I_m A^{\text{el}}(\vec{\Delta}) = \int \prod_{j=1}^{n-1} d^2 Q_{T_j} e^{-\lambda (\vec{Q}_{T_j}^2 + \vec{Q}'_{T_j}^2)},$$

where $\vec{\Delta}$ is the momentum transfer in elastic scattering and we have

$$\begin{aligned} \vec{Q}'_{T_j} &\underset{\Delta \text{ small}}{\approx} \vec{Q}_{T_j} - \vec{\Delta} \left(\sum_{i=1}^j \alpha_i \right) \\ &= \vec{Q}_{T_j} - \alpha_j \vec{\Delta} \end{aligned}$$

Hence

$$\begin{aligned} I_m A^{\text{el}}(\vec{\Delta}) &= e^{-\lambda \sum \alpha_j^2 \Delta^2} \int \prod_{j=1}^{n-1} d^2 Q_{T_j} e^{-\lambda (2\vec{Q}_{T_j}^2 - 2\alpha_j \vec{\Delta} \cdot \vec{Q}_{T_j})} \\ &= \prod_{j=1}^{n-1} e^{-\frac{\lambda}{2} \alpha_j^2 \Delta^2} \end{aligned}$$

Writing α_j^2 in terms of an average,

$$\sum_{j=1}^{n-1} \alpha_j^2 = (n-1) \langle \alpha^2 \rangle,$$

one obtains,

$$I_m A^{\text{el}}(\vec{\Delta}) = e^{-\frac{\lambda}{2} (n-1) \langle \alpha^2 \rangle \Delta^2},$$

which is the equivalent of (3.7) in Δ - space.

Defining the radius, R , by

$$R^2 = \frac{1}{2} \lambda \langle \alpha^2 \rangle (n-1)$$

we note that

$$R \propto \sqrt{n}$$

which is a way of presenting the random walk notion.

CHAPTER FOUR

INTERFERENCE DIAGRAMS

4.1. INTRODUCTION

Since the original paper of Michejda, Turnau and Bialas²⁸ there have been many discussions of whether the multiperipheral model of particle production gives, through unitarity, the correct t -dependence of elastic scattering. We saw in the third chapter that neither Henyey nor Jedach and Turnau type of calculations, with or without including phases, helped to improve the situation in which the predicted radius was too small in the lower energy region and augmented too rapidly as a function of energy compared to experiment.

In this chapter we shall try to investigate the effect of the interference diagrams in the unitarity equation and see if they could improve the situation. We shall begin first by reviewing some of the earlier attempts which were made along this direction. Then the way we have handled the diagrams will be presented.

4.2. SOME EARLIER WORKS

It has usually been the case that people make the assumption that the interference terms contribute to the calculations negligibly and therefore they are discarded completely. The supporting argument is that graphs with crossed lines have larger t values than the no-crossed ones and therefore because of the sharp cut off in t they are damped. This argument does not, however, show that even if a single crossed line graph is small, the sum of all of them would be small too; since there are so many of them.

Despite this argument there have been several attempts to consider the interference diagrams in different multiperipheral models. For instance Snider and Tow³⁵ discuss the problem in an ABFST type of model and Teper^{32, 36} uses a Reggeized version. The effect of the interference diagrams on rapidity correlations has also been studied.³⁷ We briefly review these calculations.

In the framework of ABFST model, Snider and Tow consider the following amplitude for $\pi\pi \rightarrow n\pi$ process corresponding to fig (4.1).

$$A_n(p_a, p_b; q_1, \dots, q_n) = \frac{T_2(q_1, q_2; p_a, q_1)}{(Q_1^2 - m_\pi^2)} \dots \frac{T_2(q_{n-1}, q_n; Q_{n-1}^2, p_b)}{Q_{n-1}^2 - m_\pi^2} \quad (4.1)$$

The four momenta of the equation (4.1) are defined in the same figure.

T_2 is the off shell $2 \rightarrow 2$ $\pi\pi$ scattering amplitude.

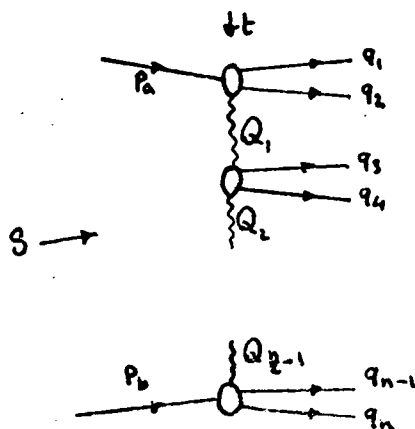


(fig. 4.1)

Insertion of this amplitude in the unitarity equation and letting the lines cross would mean that there will be some additional terms, therefore the kernel as well as the inhomogeneous term has to be modified. Considering the case where $n = 4$, they group the interference terms in three different categories as shown in fig. 4.2.

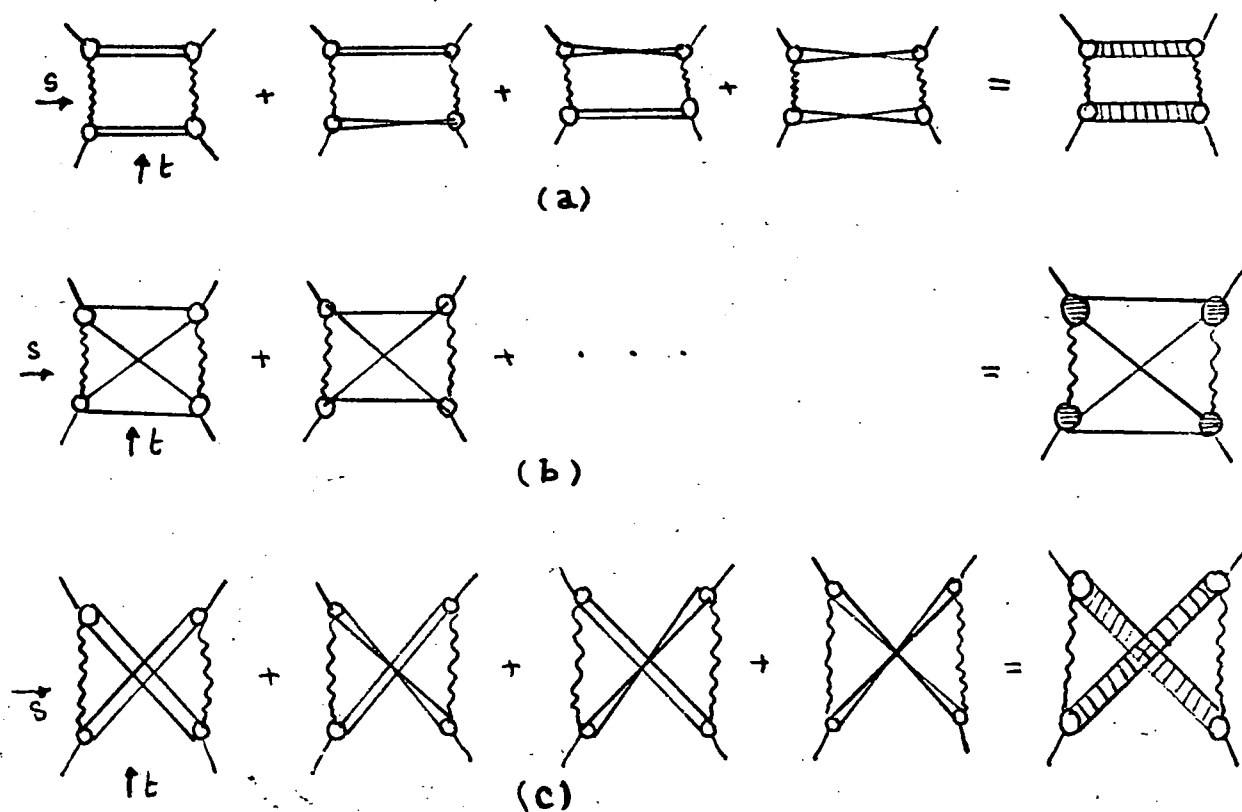
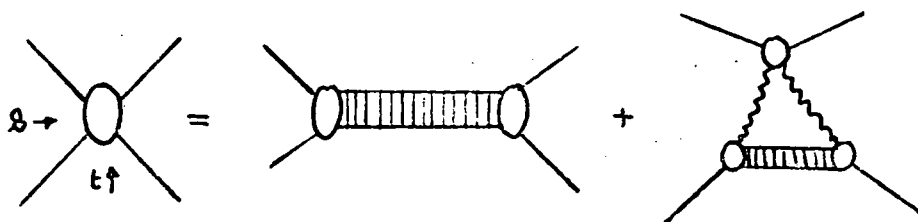
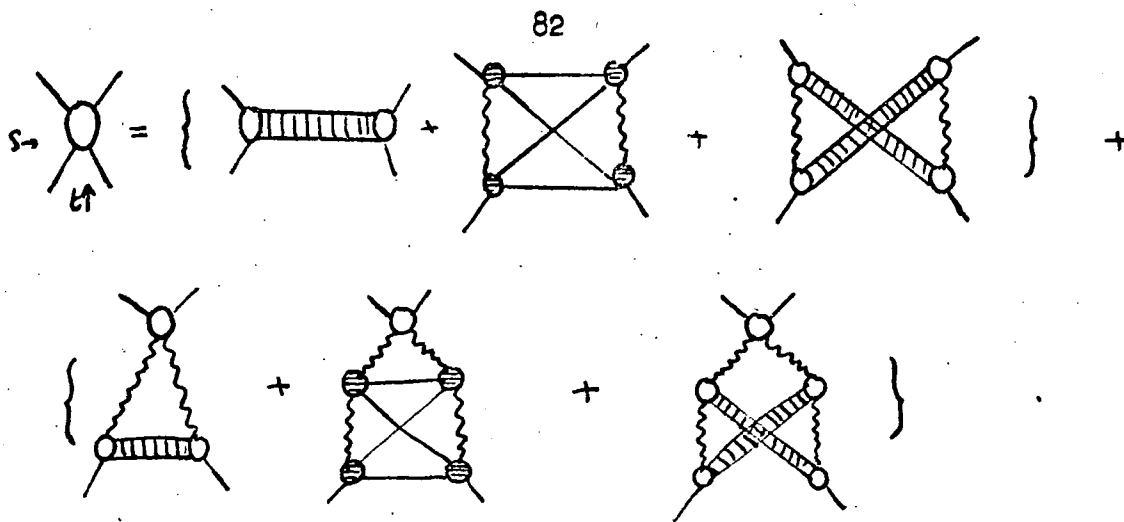


(Fig. 4.2)

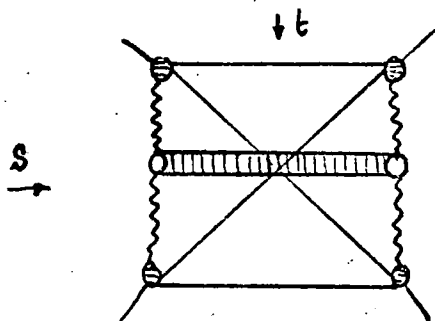
The terms on the right hand side show the sum of 4, 16, 4 graphs of the figure. They are the uncrossed, single crossed and double crossed terms. The figure shows that the integral equation, from the forward absorptive part, will be transformed from its standard form to something



more complicated such as the following,



Of course the new kernel is not complete in that it is not capable of generating terms like



The authors believe that the contribution of terms similar to these will be very small, which in turn means that there is no need to have infinite number of terms in the kernel. Using the trace approximation to get the position of the pole and comparing that with the result one could get from the standard kernel they conclude that the effect of criss cross diagrams as far as the output vacuum pole position is concerned is not important. Of course it is quite straightforward to note that this small change will amount to a larger change in the topological cross sections at high energies. This is part of the story. The other part concerns those arguments which are in favour of the importance of the interference diagrams. In reference 37, for example, one finds that the inclusion of these terms in the integrated six prong rapidity correlation function of χ^- pairs in $K^+p \rightarrow$ six charged prong states

brings the theory to match very well with the experiment (fig. 4.3).

In a similar way to Snider and Tow, Teper³² also considers diagrams which are a mixture of only neighbouring crosses and the uncrossed ones. He uses a Reggeized model and concludes that the additional terms have the effect that they bring the energy dependence of the slope of the overlap function closer to that of the elastic scattering but with the drawback that the absolute size of the slope is now much less than the one observed experimentally.

In this work we add together the effect of the interference diagrams. We first describe our method of calculation on a particular diagram.

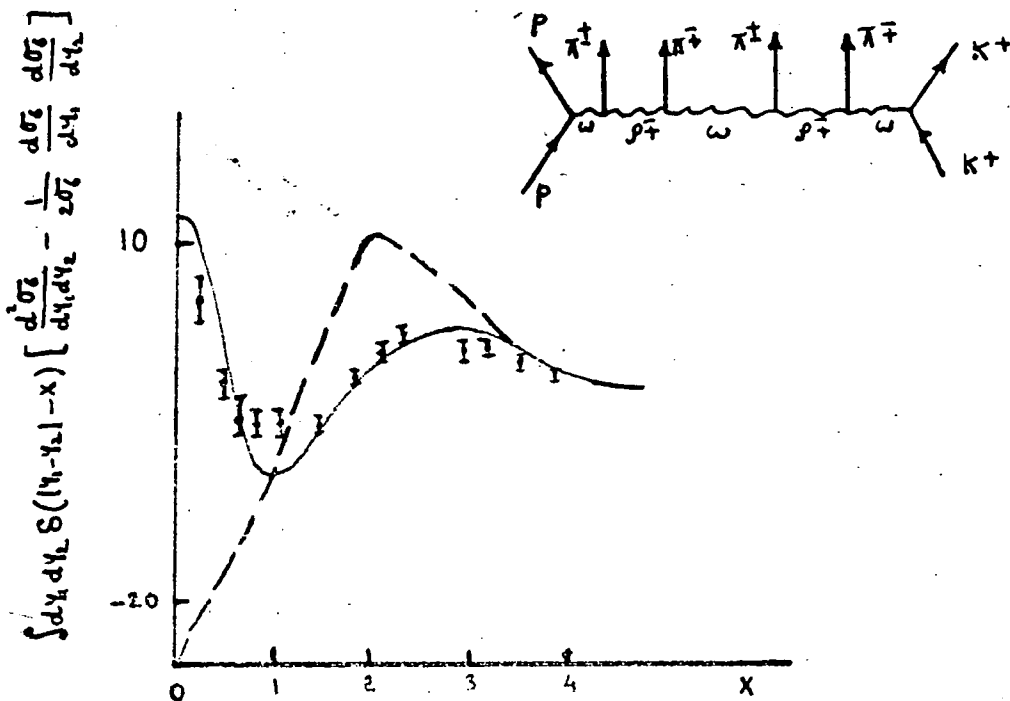
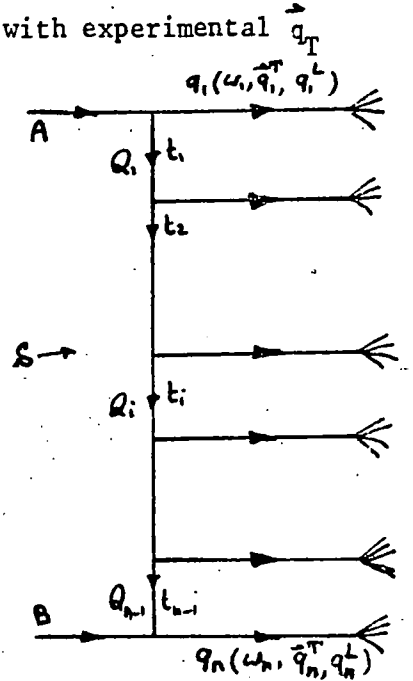


Fig 4.3

4.3. GENERAL TREATMENT OF THE DIAGRAMS

The input to the model is shown in fig (3.4), where the t-dependence of the amplitude arises from a factor $e^{\lambda t_i}$, associated with each internal line. The value of λ can be found by comparing with experimental q_T distribution in inclusive processes. The other parameter of the model is the mass of the produced objects and their multiplicity. If we assume that they are pions then the mass is known and we can read the multiplicity directly from data. However it is well known that studies of correlation require the production of clusters decaying into several pions, so it is necessary to assume a value of the cluster mass and the average multiplicity of each cluster



(Fig. 4.4)

(a mass of $\sqrt{S_0} = 1$ gev has been allocated for the cluster mass).

Let us rewrite two of the equations of the third chapter here again,

$$\tilde{A}(\vec{b}_j, q_{Lj}) = \int \prod_{j=1}^n \left[d^2 q_{Tj} e^{i(\vec{q}_{Tj} \cdot \vec{b}_j)} \right] A(\vec{q}_{Tj}, q_{Lj}) \delta^{(2)} \left(\sum_{i=1}^n \vec{q}_{Ti} \right) \quad (4.2)$$

$$I_m \tilde{A}_d(\vec{b}) = \int \prod_{j=1}^n \left[d^2 b_j dy_j \right] \delta(\sum q_{Lj}) \delta(\sum \omega_j - \sqrt{S}) \delta^{(2)}(\sum \vec{b}_j)$$

$$\delta^{(2)}(\vec{b} - \sum \frac{q_{Lj}}{p} \vec{b}_j) \left| \tilde{A}(\vec{b}_j, q_{Lj}) \right|^2 \quad (4.3)$$

where the rapidity is defined by

$$y_j = \frac{1}{2} \ln \frac{\omega_j + q_{Lj}}{\omega_j - q_{Lj}},$$

and P is the centre of mass momentum ($S \approx 4P^+$).

As mentioned earlier the amplitude will be supposed to have the following form,

$$\tilde{A}(\bar{q}_{Tj}, q_{Lj}) = \exp \lambda \sum_{j=1}^{n-1} t_j, \quad (4.4)$$

where

$$\begin{aligned} t_j &= \left(P_a - \sum_{i=1}^j q_i \right)^2 \\ &= \left(P_a^+ - \sum_{i=1}^j q_i^+ \right) \left(P_a^- - \sum_{i=1}^j q_i^- \right) - \left(\sum_{i=1}^j \bar{q}_{T_i} \right)^2 \end{aligned}$$

We have defined the longitudinal variables q_i as

$$q_i^\pm = \omega_i \pm q_{L_i},$$

which are related to the cluster mass, So, by

$$q_i^+ q_i^- = S_0. \quad (4.5)$$

Using the momentum conservation,

$$t_j = \left(\sum_{i=j+1}^n q_i^+ \right) \left(P_a^- - \sum_{i=1}^j q_i^- \right) - \left(\sum_{i=1}^j \bar{q}_{T_i} \right)^2. \quad (4.6)$$

An important property of the components q_i^\pm is that under Lorentz transformations along the longitudinal directions they transform like³⁸

$$q_i^\pm \rightarrow e^{\pm \phi} q_i^\pm$$

so that their ratios will be invariant under those transformations.

4.3.a. The Longitudinal Calculation

For the time being we shall not consider the transverse part in equation (4.6). In the same equation $P_a^- (= E_a - P_a^L)$ is small so that with a very good approximation we can write (4.6) as

$$t_j = - S_0 \left(\sum_{i=j+1}^n X_i \right) \left(\sum_{i=1}^j X_i^{-1} \right), \quad (4.6a)$$

where we have defined

$$X_i = q_i^+$$

We shall define the matrix $M_{ij}^{(w)}$ by the following equation,

$$\sum_{j=1}^{n-1} t_j = - S_0 M_{ij}^{(w)} X_i X_j^{-1} \quad ; (i, j = 1, n) \quad (4.7)$$

$M_{ij}^{(w)}$ is an $n \times n$ matrix and can be easily calculated

$$M_{ij}^{(w)} = \begin{pmatrix} 0 & 0 & 0 & \dots & 0 & 0 \\ 1 & 0 & 0 & \dots & 0 & 0 \\ 2 & 1 & 0 & \dots & 0 & 0 \\ 3 & 2 & 1 & 0 & \dots & 0 & 0 \\ \vdots & \vdots & \vdots & \vdots & \vdots & \vdots & \vdots \\ n-1 & n-2 & n-3 & \dots & 1 & 0 \end{pmatrix}$$

As the imaginary part of the amplitude depends on the square of the amplitude, there shall be another t -dependence in the exponent which may conveniently be written as

$$\sum_{j=1}^{n-1} t_j' = - S_0 M_{ij}^{(w')} X_i X_j^{-1} \quad ; (i, j = 1, \dots, n) \quad (4.8)$$

where $M^{(w')}$ of (4.8) in general will be a permutation of $M^{(w)}$ in (4.7),

$$M^{(w')} = \mathcal{P} (M^{(w)})$$

We define a new matrix M as the sum of these two matrices,

$$M_{ij} = M_{ij}^{(v)} + M_{ij}^{(w)}$$

Therefore

$$\lambda (\sum t_k + \sum t_k') = -\lambda S_0 M_{ij} X_i X_j^{-1}$$

is the exponential of the amplitude squared in (4.3).

Realizing that

$$dY_i = \frac{dX_i}{X_i}$$

we can write the longitudinal part of equation (4.3) in the following form.

$$\mathcal{L} = \int_{-\infty}^{\infty} \prod_{i=1}^n \left[\frac{dX_i}{X_i} \right] e^{-\lambda S_0 M_{ij} X_i X_j^{-1}} \delta\left(\sqrt{S} - \sum_{j=1}^n X_j\right) \delta\left(\sqrt{S_0} - \sum_{j=1}^n \frac{S_0}{X_j}\right)$$

Defining a new dimensionless variable \mathfrak{z}_i in place of X_i by

$$\mathfrak{z}_i = \frac{X_i}{\sqrt{S}}$$

we get

$$\mathcal{L} = \int_{-\infty}^{\infty} \prod_{i=1}^n \left(\frac{d\mathfrak{z}_i}{\mathfrak{z}_i} \right) e^{-\lambda S_0 M_{ij} \mathfrak{z}_i \mathfrak{z}_j^{-1}} \delta\left(\frac{\sqrt{S}}{\sqrt{S}} - \sum \mathfrak{z}_j\right) \delta\left(\frac{\sqrt{S_0}}{\sqrt{S_0}} - \sum \mathfrak{z}_j^{-1}\right) \quad (4.9)$$

Unfortunately there seems to be no exact analytic way of doing this integral. So to proceed we maximize the exponential by those \mathfrak{z}_i , say \mathfrak{z}_i^0 , which minimize $M_{ij} \mathfrak{z}_i \mathfrak{z}_j^{-1}$,

$$\mathfrak{z}_i = \mathfrak{z}_i^0 + \epsilon_i$$

and keep only the terms which are of the order of ϵ or ϵ^2 .

\mathfrak{z}_i^0 are subject to the two constraints which are imposed by the two delta functions of (4.9).

Hence,

$$\mathcal{L} = \prod_{i=1}^n [\dot{\beta}_i^{-1}] e^{-\lambda S_0 M_{ij} \dot{\beta}_i \dot{\beta}_j^{-1}} \int \prod_{i=1}^n [d\xi_i] e^{-\lambda S_0 Z_{ij} \xi_i \xi_j} \delta(\sum \xi_j) \delta(\sum \frac{\xi_j}{\dot{\beta}_j^2}) ,$$

where

$$Z_{ij} \xi_i \xi_j = M_{ij} \dot{\beta}_i \dot{\beta}_j^{-3} \xi_j^2 - M_{ij} \dot{\beta}_j^{-2} \xi_i \xi_j .$$

Note that the terms linear in ξ_i , because of the choice of the $\dot{\beta}_i$, cancel. Writing the δ -functions in their integral form

we get,

$$\mathcal{L} = \prod_{i=1}^n (\dot{\beta}_i^{-1}) e^{-\lambda S_0 M_{ij} \dot{\beta}_i \dot{\beta}_j^{-1}} \int dk dl \int \prod [d\xi_i] e^{i(k + \frac{l}{\dot{\beta}_i^2}) \xi_i - \lambda S_0 Z_{ij} \xi_i \xi_j} \quad (4.10)$$

The ξ_i integration gives*

$$\mathcal{L} = \frac{\exp(-\lambda S_0 M_{ij} \dot{\beta}_i \dot{\beta}_j^{-1})}{\pi(\dot{\beta}_i)} \frac{\pi^{1/2}}{(\lambda S_0)^{1/2} \sqrt{\det Z}} \int dk dl \exp\left(-\frac{1}{4\lambda S_0} Z_{ij}^{-1} (k + \frac{l}{\dot{\beta}_i^2})(k + \frac{l}{\dot{\beta}_j^2})\right) \quad (4.11)$$

Now doing the k and l integration one concludes that

$$\mathcal{L} = \frac{\exp(-\lambda S_0 M_{ij} \dot{\beta}_i \dot{\beta}_j^{-1})}{\pi(\dot{\beta}_i) \sqrt{\det Z}} \cdot \frac{2\pi}{(\lambda S_0 \pi^1)^{1/2} (4\pi^1 \pi_2 - \pi_3^2)^{1/2}} \quad (4.12)$$

* proceeding from (4.10) to (4.11) we have assumed that Z is not a singular matrix. If it were singular we must have proceeded in a different way. See the appendix C for the latter case.

where

$$\Gamma_1 = \frac{1}{4\lambda s_0} \sum z_{ij}^{-1}$$

$$\Gamma_2 = \frac{1}{4\lambda s_0} \sum z_{ij}^{-1} \delta_i^{-2} \delta_j^{-2}$$

$$\Gamma_3 = \frac{1}{4\lambda s_0} \sum z_{ij}^{-1} \left(\frac{1}{\delta_i^{-2}} + \frac{1}{\delta_j^{-2}} \right)$$

L, as we shall see, will serve the purpose of weighing different interference diagrams and will appear as a coefficient of the term which includes the radius.

4.3.b. The Transverse Calculation

Having dealt with the longitudinal part of the amplitude we shall discuss the transverse part here. The procedure will be more or less as before. We are mainly concerned with the term which we suppressed in (4.6),

$$t_j = - \left(\sum_{i=1}^j \vec{q}_{\tau_i} \right)^2,$$

which corresponds to the transverse part of the amplitude,

$$A(\vec{q}_{\tau_j}) = \prod_{j=1}^n \exp \left[-\lambda \left(\sum_{i=1}^j \vec{q}_{\tau_i} \right)^2 \right].$$

As before let us define an $n \times n$ and symmetric matrix L_{ij}^{ω} by the following equation,

$$L_{ij}^{\omega} \vec{q}_{\tau_i} \cdot \vec{q}_{\tau_j} = \sum_{j=1}^n \left(\sum_{i=1}^j \vec{q}_{\tau_i} \right)^2.$$

The amplitude, now, looks like,

$$A(\vec{q}_{\tau_j}) = \exp \left(-\lambda \sum_{i,j} L_{ij}^{\omega} \vec{q}_{\tau_i} \cdot \vec{q}_{\tau_j} \right).$$

One can transform this to the b_i space using equation (4.2),

$$\tilde{A}(\vec{b}_j) = \frac{4\pi^2}{(\lambda/\pi)^{n-1} \det L^{\omega} \left(\sum_{i,j=1}^n L_{ij}^{-1} \right)} \exp \left(-\frac{1}{\lambda} B_{ij}^{\omega} \vec{b}_i \cdot \vec{b}_j \right)$$

where

$$B_{ij}^{\omega} = \frac{1}{4} \left[L_{ij}^{\omega-1} - \frac{1}{\left(\sum L_{ij}^{\omega-1} \right)} L_{ir}^{-1} \int_{rs} L_{sj}^{-1} \right] \quad (4.13)$$

and

$$\int_{rs} = 1, \quad \forall r, s = 1, n.$$

Matrix $B^{(1)}$ is $n \times n$ and symmetric.

Let us rewrite the transverse part of equation (4.3) again,

$$T(\hat{b}) = \int \prod_{j=1}^n [d^4 b_j] \delta^{(n)}(\sum \hat{b}_j) \delta^{(n)}(\hat{b} - \sum \alpha_j \hat{b}_j) |\tilde{A}(b_j)|^2. \quad (4.14)$$

Once more we need to permute (4.13)

$$\mathcal{B}_{ij}^{(v)} = \mathcal{P}(\mathcal{B}_{ij}^{(u)})$$

and

$$B_{ij} = \mathcal{B}_{ij}^{(u)} + \mathcal{B}_{ij}^{(w)}$$

Hence,

$$|\tilde{A}(\hat{b}_i)|^2 = h_1 \exp\left(-\frac{1}{\lambda} B_{ij} \hat{b}_i \cdot \hat{b}_j\right),$$

where,

$$h_1 = \frac{16 \pi^4}{(\lambda/\pi)^{2(n-1)}} \cdot \left[\left(\sum_{ij} L_{ij}^{-1} \right)^2 \det L^{(u)} \det L^{(w)} \right]^{-1}.$$

Matrix B_{ij} is n by n and symmetric. It could be, and in most cases is, singular. In what follows we shall assume that it is singular. For the other case refer to appendix D. The fact that B_{ij} is singular does not mean that the integral (4.14) will be divergent at all. The reason for this is the existence of the δ -functions. This makes it possible to get rid of the zero eigenvalue corresponding to matrix B as is explained below. Writing the delta function of (4.14) in its integral form we get,

$$T(\hat{b}) = h_1 \int d^4 x d^4 y e^{i\hat{y} \cdot \hat{b}} \int \prod [d^4 b_i e^{i(\hat{x} - \alpha_i \hat{y}) \cdot \hat{b}_i}] \exp\left(-\frac{1}{\lambda} B_{ij} \hat{b}_i \cdot \hat{b}_j\right)$$

According to appendix E one can do the integration over $d^4 b_i$ to get

$$T(\hat{b}) = h_2 \int d^4 x d^4 y e^{i\hat{y} \cdot \hat{b}} \delta^{(n)}\left(\hat{x} - \frac{\sum C_{in} \alpha_i}{\sum C_{in}} \hat{y}\right) \exp\left[-\lambda F_{ij}(\hat{x} - \alpha_i \hat{y})(\hat{x} - \alpha_j \hat{y})\right],$$

where

$$h_2 = h_1 (\lambda \lambda)^{n-1} \left[\prod_{i=1}^{n-1} [\lambda_i] \left(\sum_{j=1}^n C_{jn} \right) \right]^{-1},$$

and C_{ij} is the matrix which diagonalizes B_{ij} to produce the eigenvalues λ_i . Matrix F_{ij} is defined in the appendix E. Using the δ -function, one can easily do the integration over \vec{x} ,

$$T(\vec{b}) = h_2 \int d^4y \ e^{i\vec{y}\cdot\vec{b}} \ e^{-\lambda\theta\vec{y}^2},$$

where

$$\theta = \sum_{i,j=1}^n F_{ij} (\mathcal{P} - \chi_i)(\mathcal{P} - \chi_j),$$

and

$$\mathcal{P} = \left(\sum_{i=1}^n C_{in} \chi_i \right) / \left(\sum_{i=1}^n C_{in} \right).$$

One, therefore, finally ends up with

$$T(\vec{b}) = \frac{\lambda}{\lambda\theta} h_2 \exp\left(-\frac{\vec{b}^2}{4\lambda\theta}\right). \quad (4.15)$$

The radius is customarily defined according to

$$R^2 = 4\lambda\theta. \quad (4.16)$$

It is this that Henyey finds to increase very sharply as energy increases and indeed we confirm and see the same effect (Fig. 4.5) using his parameter values (for uncrossed diagrams).

Before going to compare different diagrams and see what their effects are, it seems most appropriate to say a few words on the parameter λ . The next section is devoted to this and the way one assigns a value by considering the transverse momentum distribution.

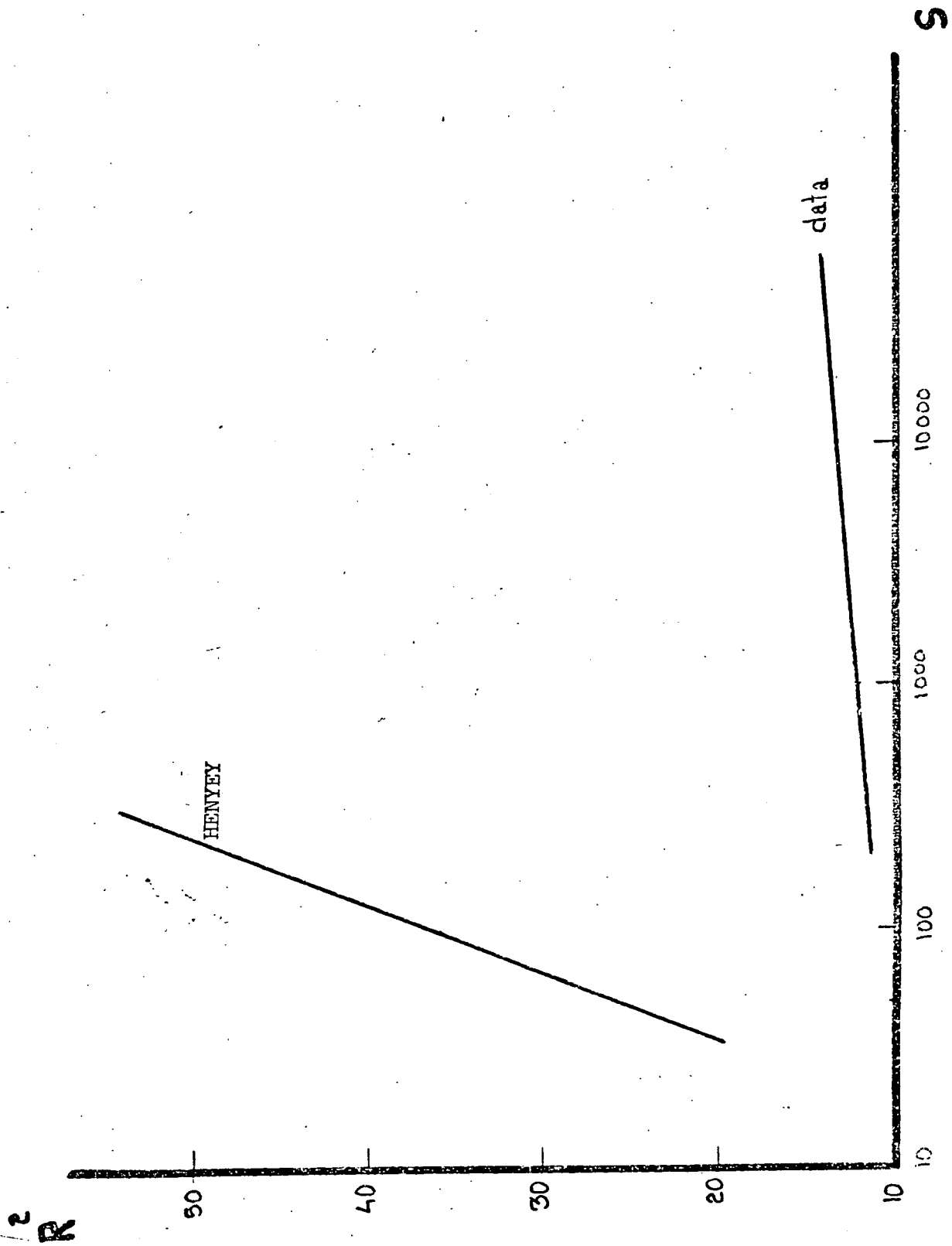


Fig 4.5

4.4. TRANSVERSE MOMENTUM DISTRIBUTION

We, in this chapter, introduced the parameter λ in equation (4.4). It is clear in there that λ governs the t-distribution of the amplitude. According to what t should be approximated to, referring to Henyey or Jedach-Turnau calculations, λ can take values as high as 5.5 or as small as 0.5. We shall assign that value for λ which gives the best fit to the transverse momentum distributions.

The invariant cross-section is defined as ⁸ (with the notations of fig. 4.4)

$$\begin{aligned} \rho_{ab}^c &= \omega_c \frac{d^2\sigma}{dq^2} = \frac{d^2\sigma}{d^4 d^2q_T} \\ &= \frac{1}{2S} \sum_{n=2}^{\infty} \sum_f \int \prod_{i=1}^n \left[\frac{d^2q_i}{(2\pi)^2 2\omega_i} \right] \omega_f \delta^{(3)}(\vec{q}_f - \vec{q}) \delta^{(4)}(p_a + p_b - \sum q_i) |A|^2 \\ &\quad \text{↳ type c momenta} \end{aligned}$$

Since we are interested in the transverse part of the calculation we shall consider that first,

$$\rho_{ab}^c = \int \left[\prod_{i=1}^n d^2q_{T_i} \right] \delta^{(2)}(\vec{q}_{T_f} - \vec{q}_T) \delta^{(2)}\left(\sum_{i=1}^n \vec{q}_{T_i}\right) |A(\vec{q}_{T_i})|^2,$$

where

$$|A(\vec{q}_{T_i})|^2 = \exp(-\lambda L_{ij} \vec{q}_{T_i} \cdot \vec{q}_{T_j}),$$

is the squared amplitude in Henyey Case ($t \approx t^T$).

L_{ij} is sum of two symmetric matrices,

$$L_{ij} = L_{ij}^{(v)} + \mathcal{P}(L_{ij}^{(u)}).$$

Splitting the matrix L_{ij} to a lower matrix N_{ij} and the remaining

we get

$$\rho'_{ab} = \int \left[\prod_{i \neq f}^n d^2 q_{\tau_i} \right] \exp \left(-\lambda \sum_{i,j \neq f} N_{ij} \bar{q}_{\tau_i} \cdot \bar{q}_{\tau_j} \right)$$

$$\int d^2 q_{\tau_f} \exp \left[-\lambda (L_{ff} \bar{q}_{\tau_f}^2 + 2 \sum_{i \neq f} L_{if} \bar{q}_{\tau_i} \cdot \bar{q}_{\tau_f}) \right] \delta^{(4)}(\bar{q}_{\tau_f} - \bar{q}_{\tau_f}) \delta^{(4)}\left(\sum_{i \neq f} \bar{q}_{\tau_i} + \bar{q}_{\tau_f}\right)$$

The first δ -function makes the integration over \bar{q}_{τ_f} easy,

$$\rho'_{ab} = \int \left[\prod_{i \neq f}^n d^2 q_{\tau_i} \right] e^{-\lambda \sum_{i,j \neq f} N_{ij} \bar{q}_{\tau_i} \cdot \bar{q}_{\tau_j}} e^{-\lambda (L_{ff} \bar{q}_{\tau_f}^2 + 2 \bar{q}_{\tau_f} \cdot (\sum_{i \neq f} L_{if} \bar{q}_{\tau_i}))} \delta^{(4)}(\sum_{i \neq f} \bar{q}_{\tau_i} + \bar{q}_{\tau_f})$$

Writing the delta function in the integral form and doing the integration over \bar{q}_{τ_f} and ignoring the uninteresting numbers like 2π we obtain,

$$\rho'_{ab} = \lambda^{1-n} (\det N)^{-1} e^{-2\theta \bar{q}_{\tau_f}^2} \int d^4 \bar{x} e^{i \bar{x} \cdot \tau \bar{q}_{\tau_f}} e^{-\frac{1}{4\lambda} \sum_{i,j \neq f} N_{ij} \bar{x}^2},$$

where

$$\theta = L_{ff} - \sum_{i,j \neq f}^n N_{ij}^{-1} (L_{if} L_{jf})$$

$$\eta = 1 - \frac{1}{2} \sum_{i,j \neq f}^n N_{ij}^{-1} (L_{if} + L_{jf})$$

The integration over \bar{x} is straightforward now; we get,

$$\rho'_{ab} = \alpha_1 \exp(-\lambda \beta \bar{q}_{\tau_f}^2), \quad (4.17)$$

with

$$\alpha_1 = \frac{4\pi}{\lambda^{n-2} \det N} \left(\sum_{i,j \neq f}^n N_{ij}^{-1} \right)^{-1} \quad (4.18)$$

and

$$\beta = \theta + \frac{\eta^2}{\sum_{i,j \neq f}^n N_{ij}^{-1}}$$

Fortunately the longitudinal calculation is what we have already performed. Therefore the only effect we may get from that is the

following transformation for α_1 of (4.18),

$$\alpha_1 \rightarrow \mathcal{L} \alpha_1 ,$$

where \mathcal{L} is given in (4.12).

Averaging over all final state transverse momentum distributions we fit the data³⁹ in both Henyey and Jedach-Turnau* type of calculations (fig. 4.6). The best values one gets in the two cases are,

$$\text{Henyey type} \quad \lambda = 4.1$$

$$\text{Jedach-Turnau type} \quad \lambda = 2.8$$

We would like to point out that in determining these values we have considered only the uncrossed diagrams. Another point worth mentioning here is that energy variation has little effect on the parameter λ as is clear from figure (4.7).

Obviously the transverse momentum distribution seen experimentally is that of the observed particles, yet we fit the data with the calculations based on the clusters. Of course we might expect that there would be some effect due to the decay of the clusters into the observed particles but we anticipate that this will not be too important.

* For Jedach-Turnau calculations see the next section.

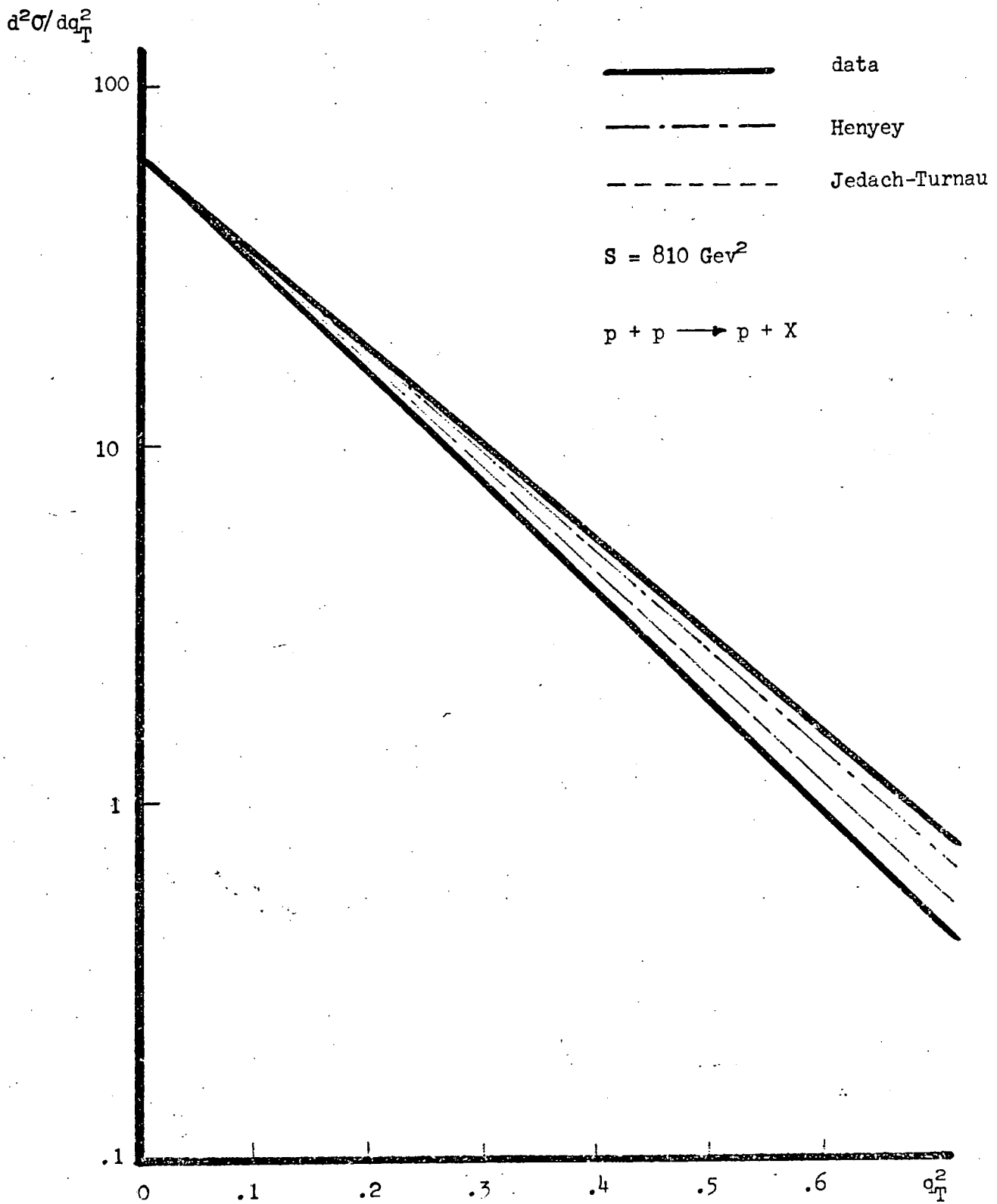


Fig 4.6

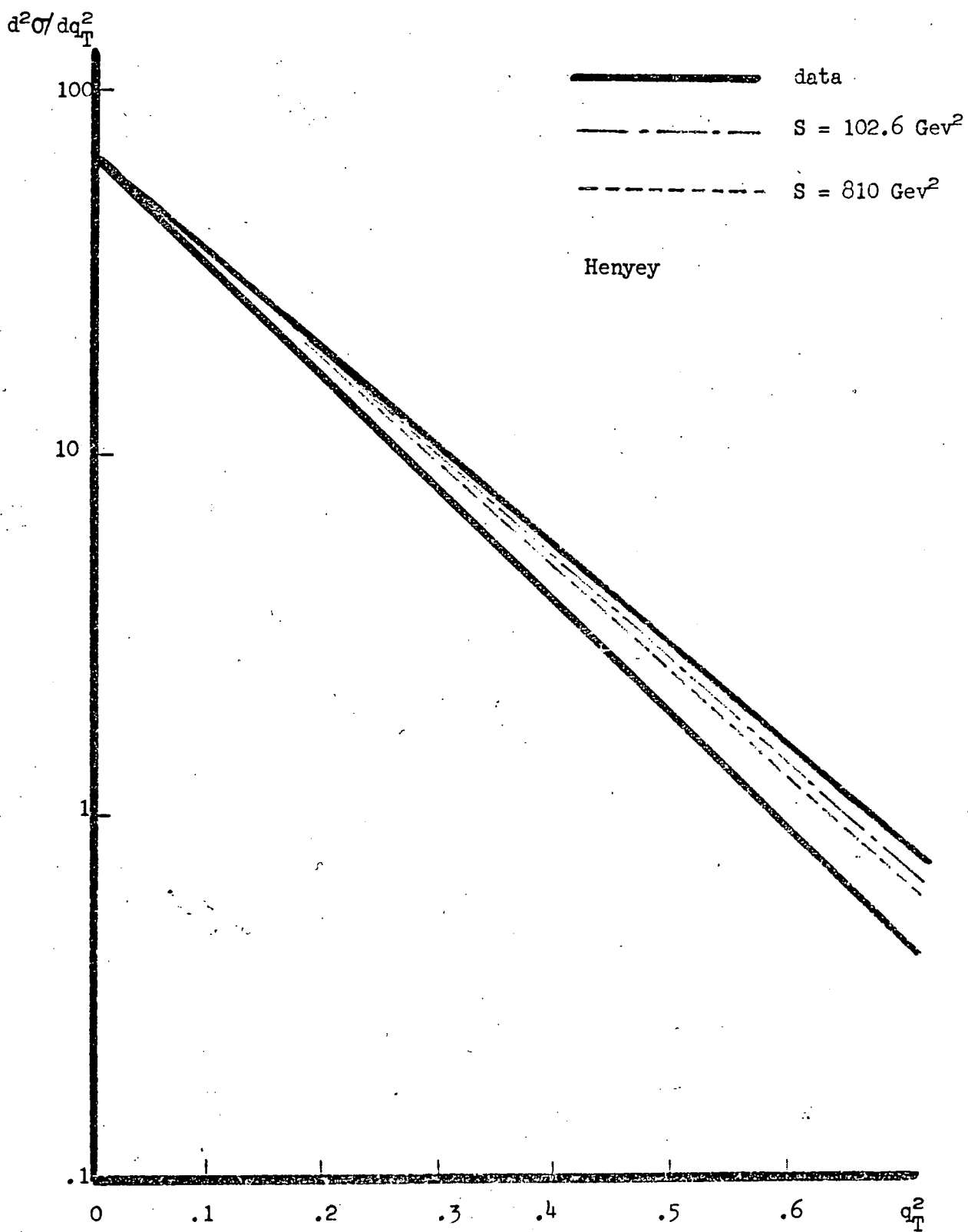


Fig 4.7a

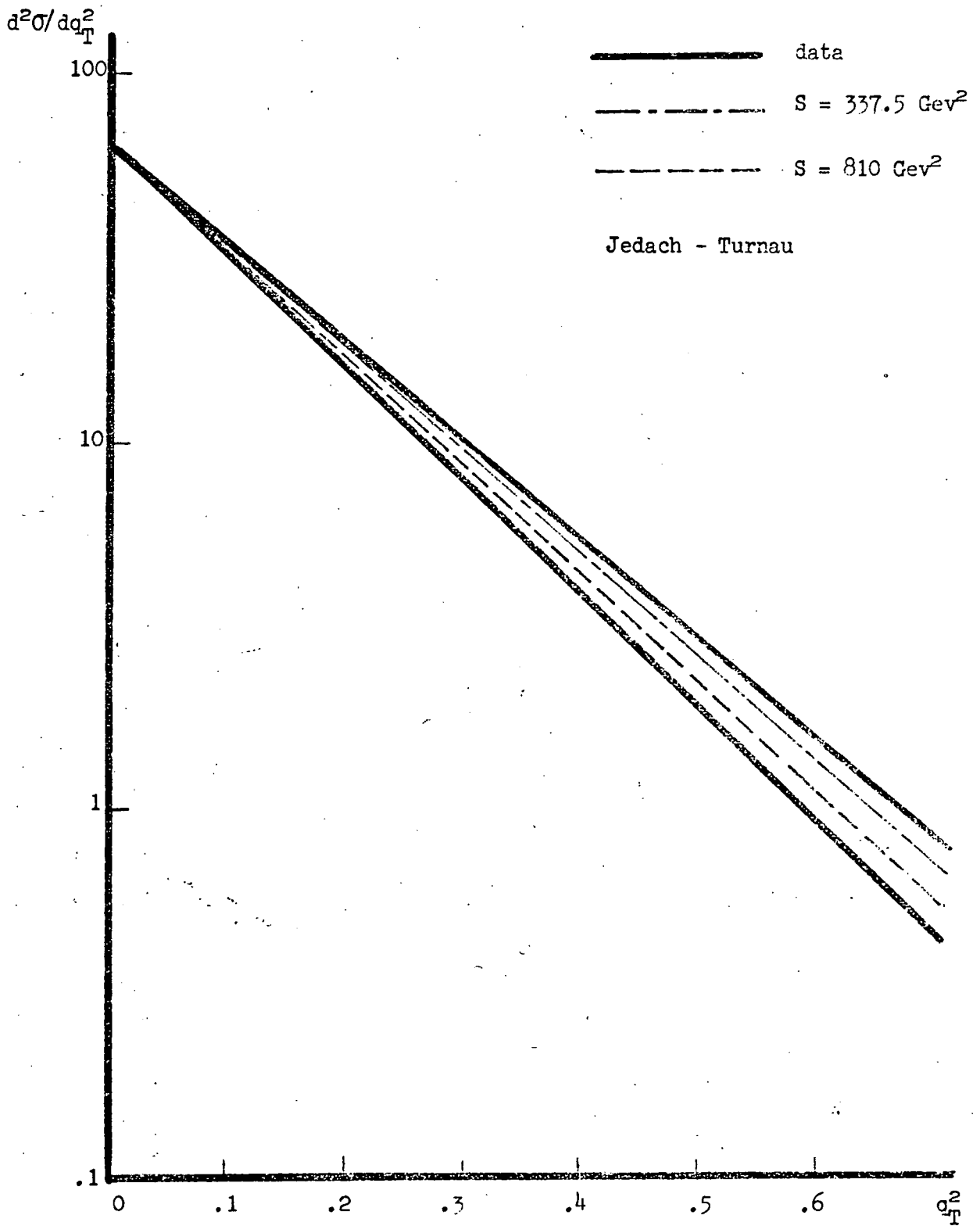


Fig 4.7b

4.5. THE JEDACH AND TURNAU EFFECT

As it was mentioned in section 3 of the third chapter one gets a transverse dependence from the longitudinal momentum transfer, t_i^L . This is suggested to be taken into consideration as well. Here we shall demonstrate the change the additional term imposes on the calculations of the previous two sections in short.

Inserting

$$\begin{aligned}\omega_k + q_{Lk} &= \chi_k \\ \omega_k - q_{Lk} &= m_k^\pi \exp \ln \frac{m_k^\pi}{\chi_k} \\ &= \frac{m_k^2}{\chi_k} + \frac{q_{Lk}^2}{\chi_k}\end{aligned}$$

in equation (2.14) we get

$$t_i^L \approx -m^2 \sum_{k=i+1}^n \chi_k \sum_{k=1}^i 1/\chi_k - \sum_{k=i+1}^n \chi_k \sum \frac{q_{Lk}^2}{\chi_k}$$

The first term on the right hand side is essentially same as (3.6a). Therefore the longitudinal calculations are left unchanged under this effect. The second term is new and must be added to t_i^T ,

$$t_i^T = - \left(\sum_{j=1}^i q_{Tj} \right)^2 - \left(\sum_{j=i+1}^n \chi_j \right) \left(\sum_{j=1}^i \frac{q_{Tj}^2}{\chi_j} \right)$$

Hence, the inclusion of the Jedach and Turnau effect will only change the diagonal entries of the matrix $L^{(1)}$ in the subsections (3.3b) and (3.4) and, therefore, the remaining calculations will be as they stand.

4.6. THE EFFECT OF INTERFERENCE DIAGRAMS

Now that we have developed a method such that every individual diagram could be calculated separately we turn to its application. The numerical calculation has been performed in the Rutherford High Energy Laboratories (RHEL) 360 computer where CERN minimization routines have been ^{extensively} used. The program has been developed in such a way that given the parameter values and the type of permutation, it calculates transverse momentum distribution and the radius as well as the other required quantities automatically. Then it averages over all interference diagrams, at a given energy, to give the effective quantities.

To cut down the computer time and since omission of some diagrams such as those in figure (4.8) are justified according to the results one gets from the numerical calculations, we have reduced the number of diagrams corresponding to 3, 4, 5 intermediate states to 28 out of possible 150 ones. These interference diagrams have been shown in fig. (4.9). Of course some of the diagrams, by symmetry, are representatives of two or four terms. For example, there are three more terms similar to diagram number 7 of fig (4.9). Thus, by considering these extra terms, we in actual fact are dealing with some 65 diagrams.

The cluster production has been invoked both in Henyey and Jedach-Turnau papers to improve the situation. Here we too shall consider the effect of clusters as well and check how important they play a role in achieving a better agreement with data.

The central aim is to see how the radius behaves as compared to data. In figures (4.10) and (4.11) we plot the radius of uncrossed diagram, with and without the formation of clusters, for Henyey and Jedach-Turnau cases respectively. It is evident from the pictures that cluster formation improves the situation slightly but does not solve the problem. This is one of the conclusions of the reference 32 as well.



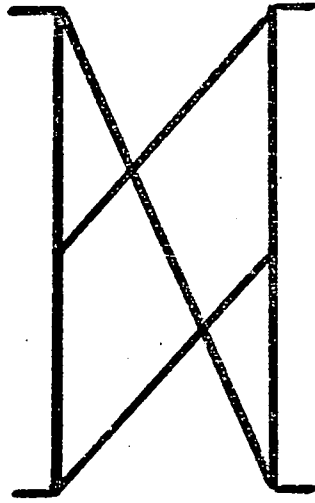
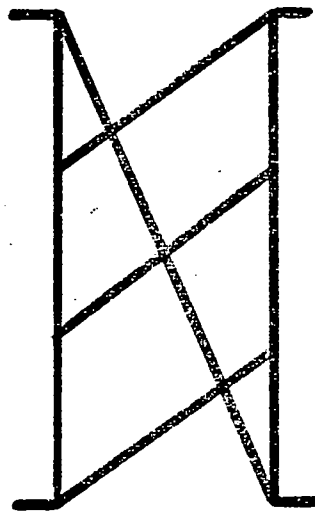
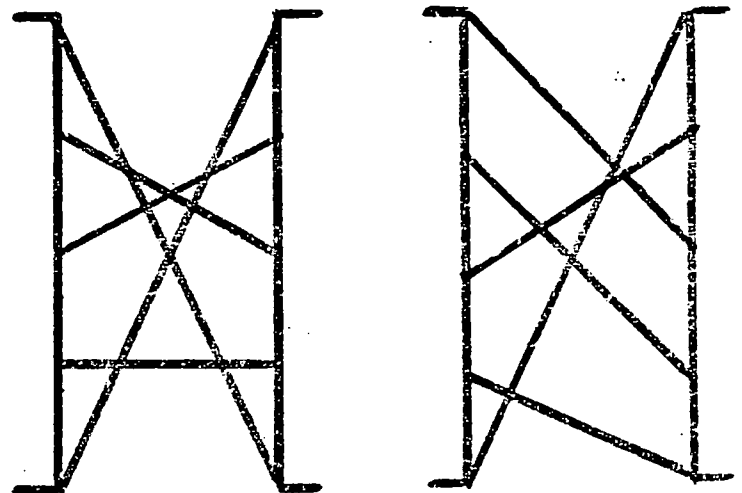
$n = 3$  $n = 4$  $n = 5$ 

Fig. 4.8

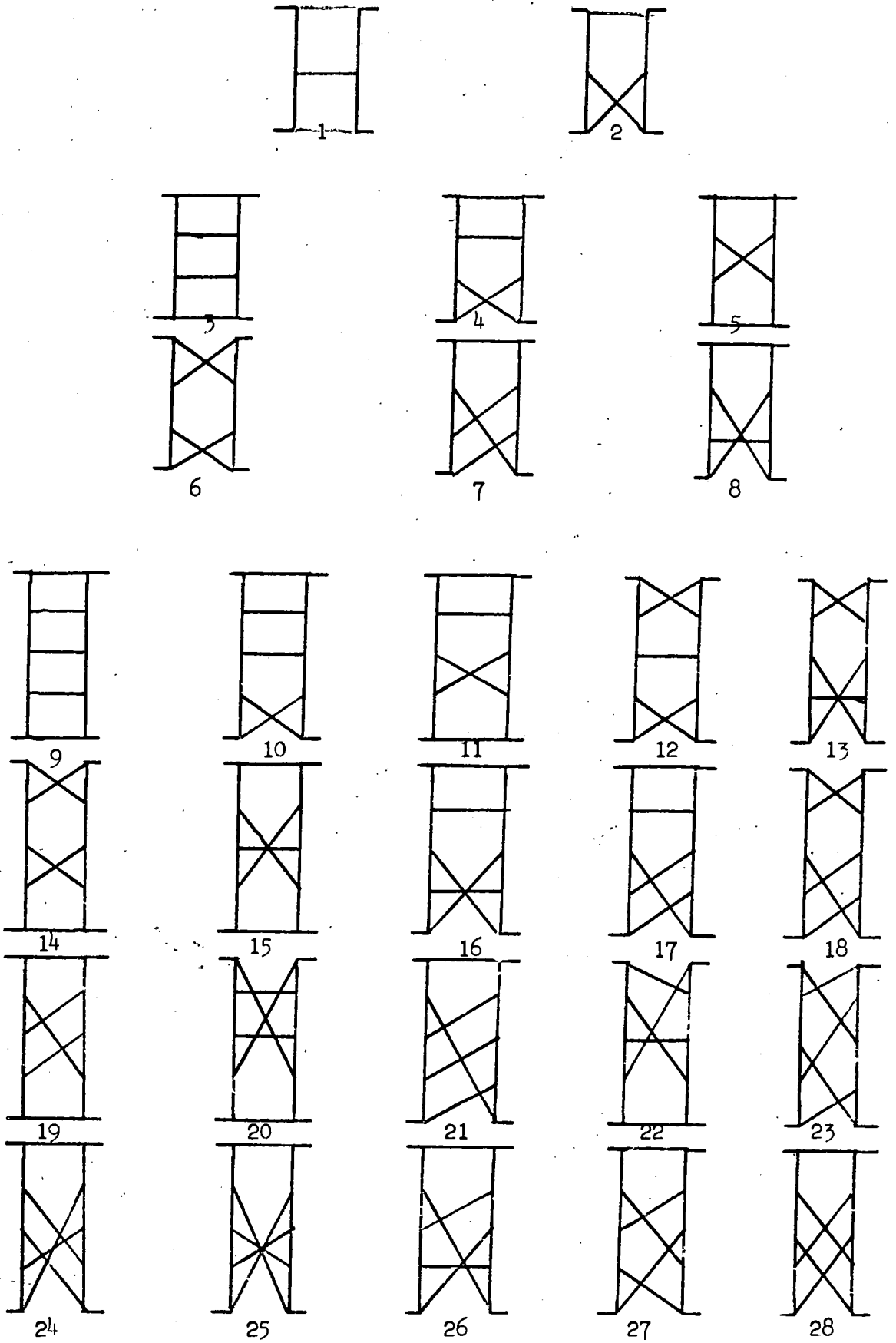


Fig 4.9

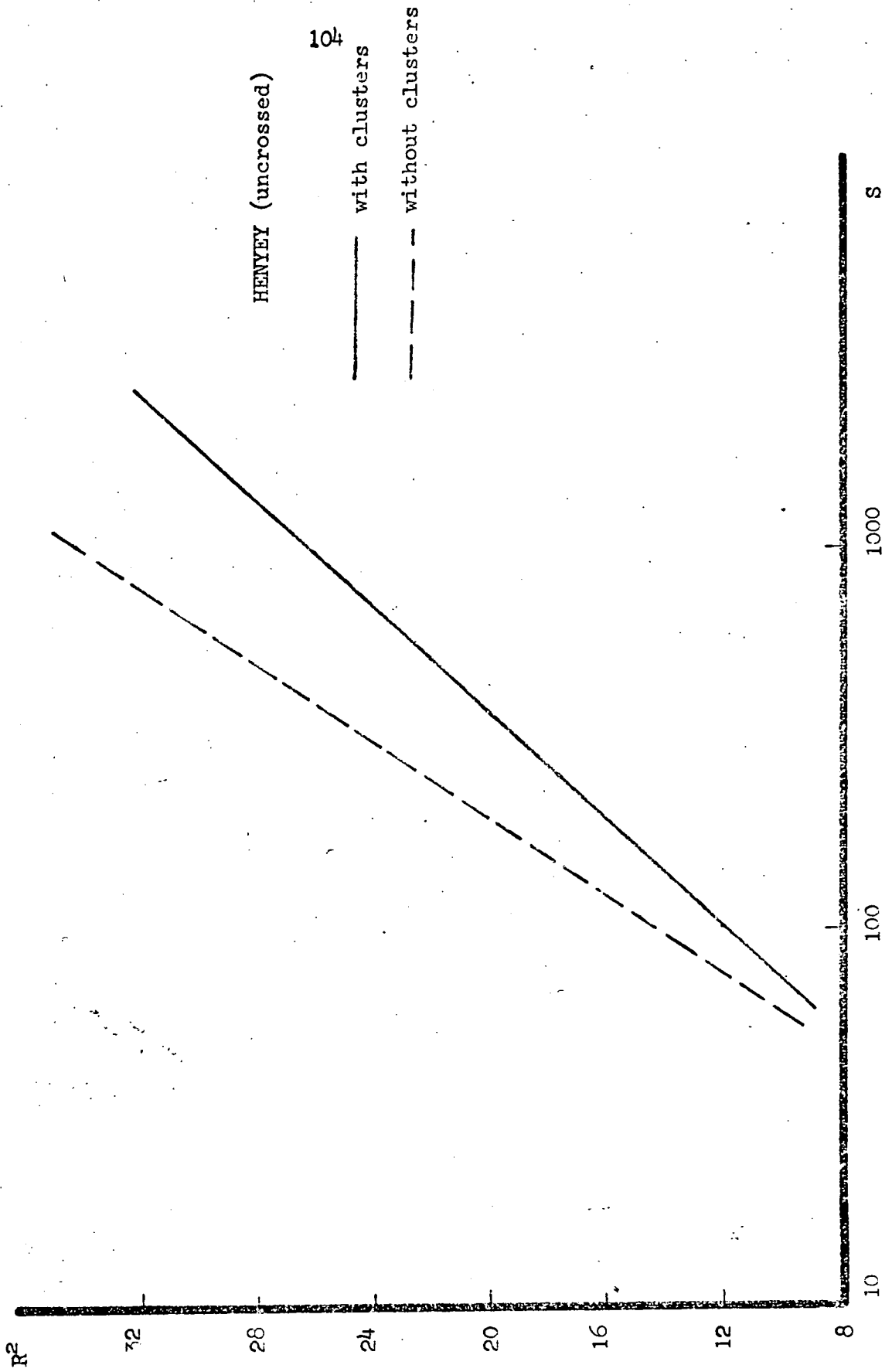


Fig 4.10

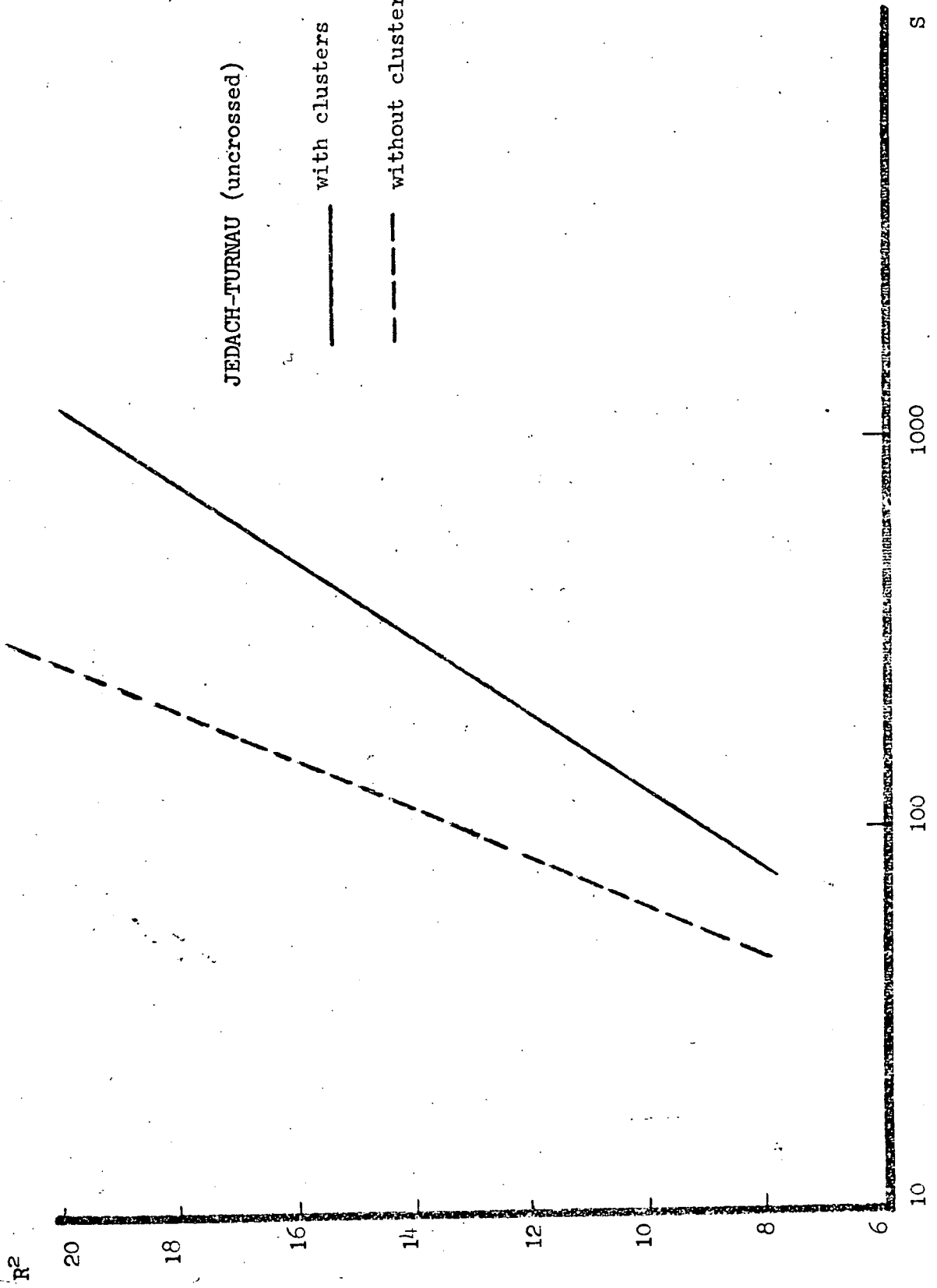


Fig 4.11

Taking into account the interference diagrams we arrive at the figure (4.12) where cluster formation is also included. Surprisingly enough, for the realistic values of λ the inclusion of the interference diagrams does not overcome the problem either. In fact, their contribution is so little that as far as R^2 is concerned one could neglect all of the crossed diagrams.

The parameter λ plays a crucial role in the evaluation of the importance of the crossed diagrams. This seems to be part, if not all, of the reason for the Teper's conclusion of up to 30% contribution to the slope from the crossed diagrams. To support this idea we plot α^2 as a function of λ in (4.13) where

$$\alpha^2 = \frac{R_{\text{uncrossed}}}{R_{\text{eff}}}$$

The rapid variation of α^2 at small λ justifies the point, at least partially. Using different values for S_0 does not improve the case much either. In figure 4.14, for the sake of completeness, we plot R^2 versus S for different values of the parameters λ and S_0 .

Therefore, we, disappointingly, come to the conclusion that adding the interference diagrams leaves the problem of sharp increase of radius, or alternatively the slope of the pomeron, unchanged. We shall try to demonstrate another dynamics, in the next chapter, which may be a solution to the problem.

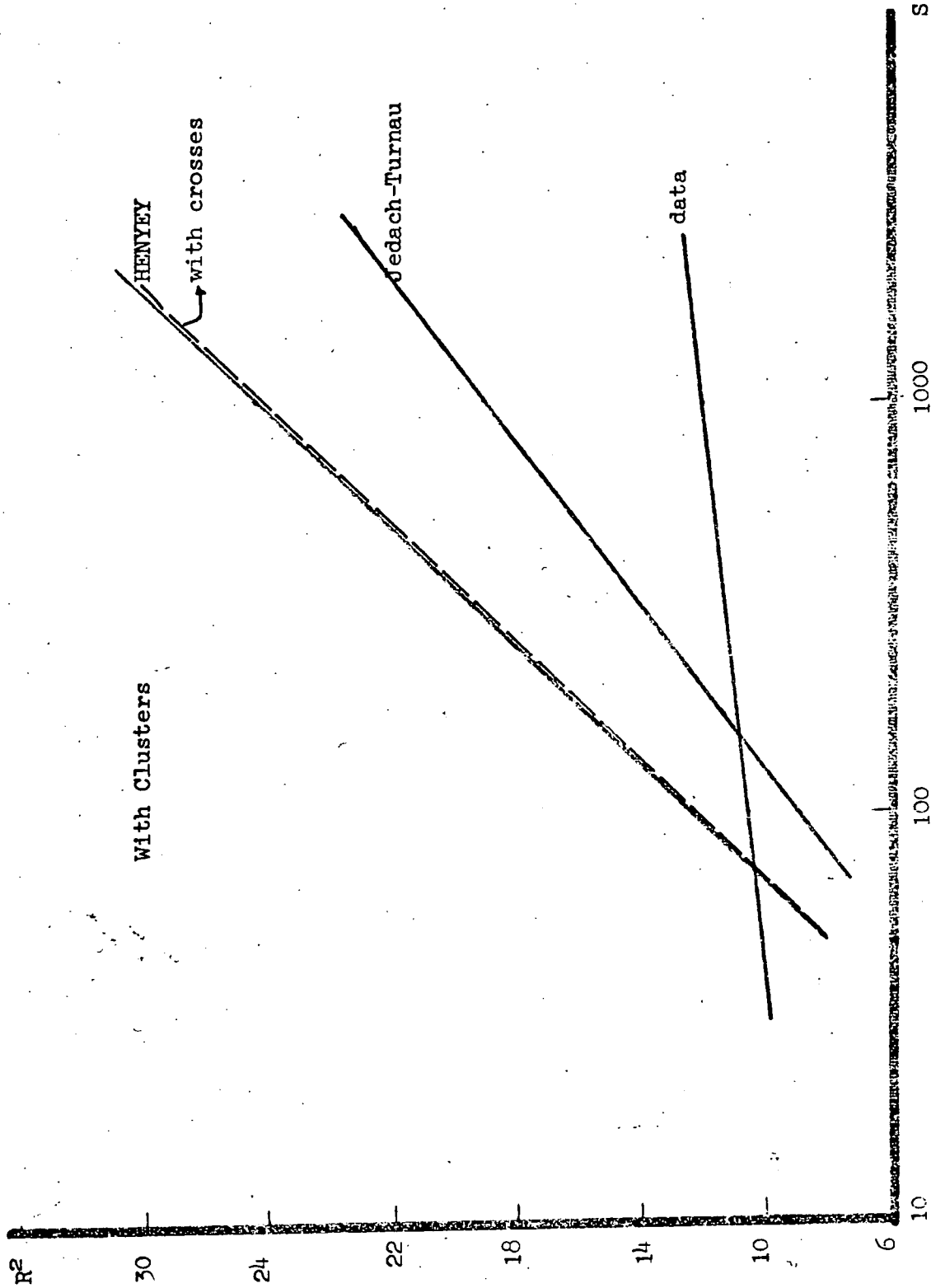


Fig 4.12

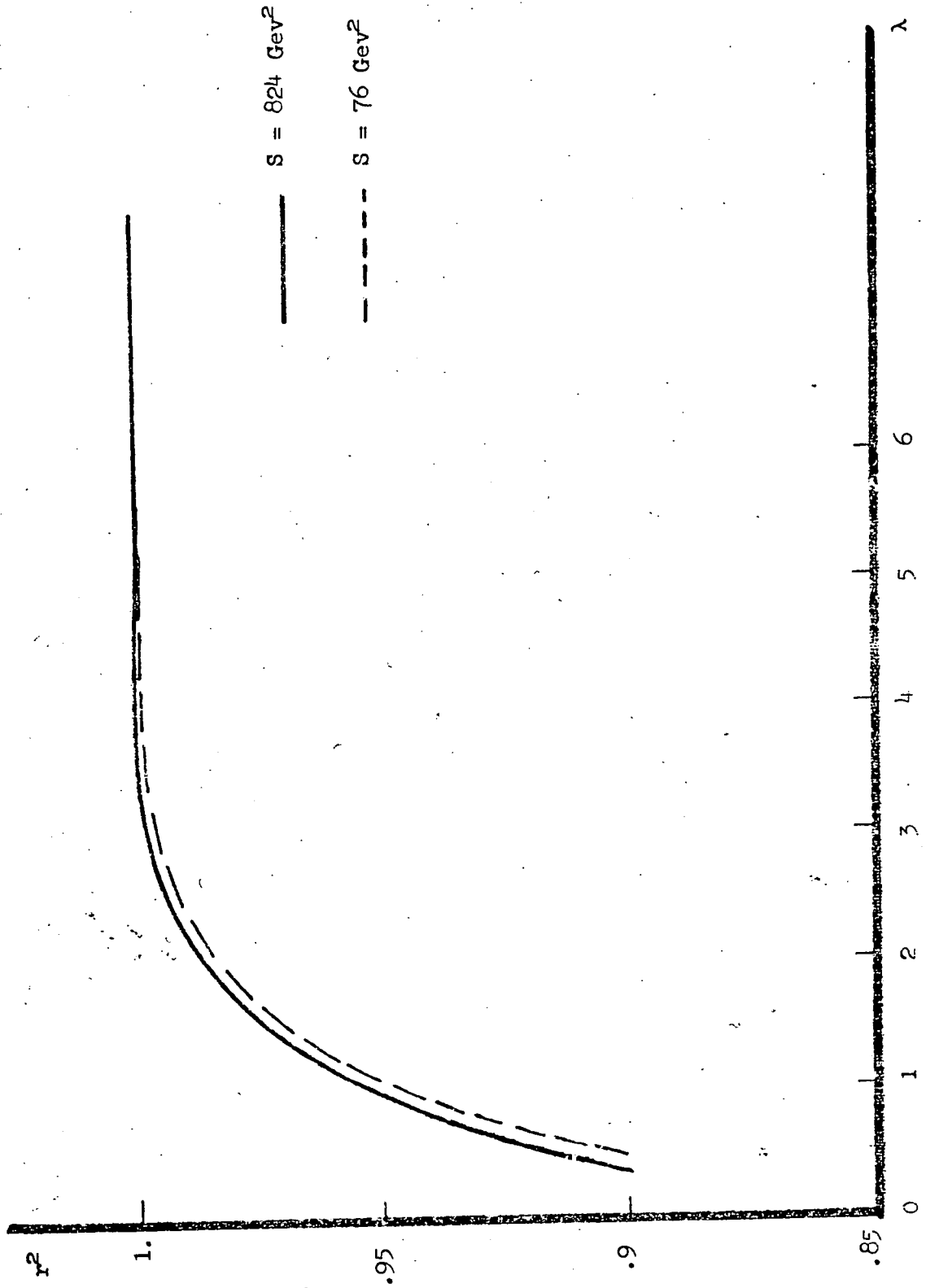


Fig 4.13

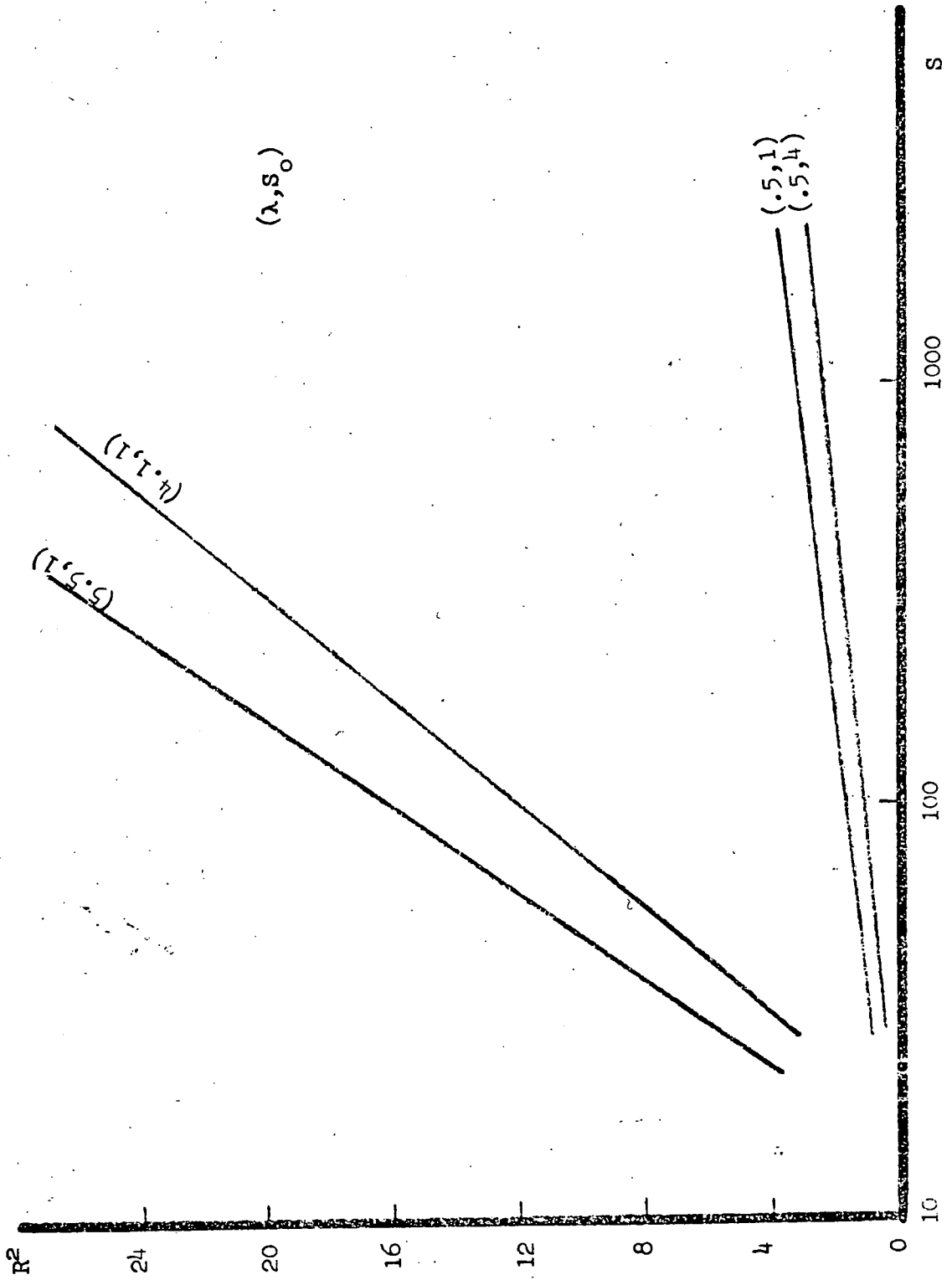


Fig 4.14

CHAPTER FIVE

A LINK DEPENDENT MODEL

5.1. INTRODUCTION

We tried to fit the data of the radius as a function of energy for the reasonable values of λ which satisfied the transverse momentum distribution in Chapter 4, with due regard to the interference diagrams. But, sadly enough, we concluded that these extra terms could not help us in removing the difficulty which was introduced in Chapter three. Therefore one should seek the answer somewhere else. But before going to introduce the new model, let us briefly sketch some of the attempts which have been made towards improving the problem of α_P during the last two years or so.

5.2. WHAT HAS HAPPENED DURING THE LAST TWO YEARS?

The situation studied so far, briefly, is as follows. The result of Henyey on the problem of the slope of the pomeron, which could be derived model independently as well,⁴³ is

$$\alpha'_P = \frac{\nu}{2 \langle q_T^2 \rangle}, \quad (5.1)$$

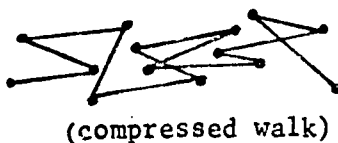
where

$$\nu \approx \frac{\langle n \rangle}{2 \ln S},$$

is the density of particles per unit rapidity in the central region. This result was criticised by Jedach and Turnau on the ground that one should use full momentum transfer and therefore (5.1) no longer holds. But, of course, then one would have some undesirable correlations between the transverse and longitudinal components.

Since then there have been a number of attempts and out of them the works of Kubar-André et al,⁴⁰ C. Michael⁴¹ and Bialas and Sakai⁴² have thrown some light onto the problem.

For instance, allowing some correlations between neighbouring transverse momentum transfers Kubar-André et al⁴⁰ conclude that each step in the impact parameter space is followed by a step in the opposite direction and therefore the radius remains small. This, in turn, means that the random walk should be replaced by the compressed walk:



This easily follows by transforming the amplitude from \vec{Q}_{T_j} - space to its conjugate \vec{B}_j - space; that is from

$$A_n \propto \prod_{i,j} \exp \left[-\frac{1}{2} c A_{ij} \vec{Q}_{T_i} \cdot \vec{Q}_{T_j} \right]$$

to

$$\tilde{A}_n \propto \prod_{i,j} \exp \left[-\frac{1}{2} A_{ij} \vec{B}_i \cdot \vec{B}_j \right]$$

The symmetric matrix is defined by the following,

$$A_{ij} = \begin{pmatrix} 1 & \epsilon & 0 & 0 & 0 & \dots & 0 \\ \epsilon & 1 & 0 & 0 & 0 & \dots & 0 \\ 0 & \epsilon & 1 & 0 & 0 & \dots & 0 \\ 0 & 0 & \epsilon & 1 & 0 & \dots & 0 \\ \vdots & \vdots & \vdots & \vdots & \vdots & \ddots & \vdots \\ 0 & \dots & \dots & \dots & \dots & \dots & 1 \end{pmatrix}$$

One, now, gets for the average $\langle \vec{B}_i \cdot \vec{B}_j \rangle$:

$$\langle \vec{B}_i \cdot \vec{B}_j \rangle = \frac{1}{2} c A_{ij} = \begin{cases} \frac{1}{2} c & \text{if } i=j \\ \frac{1}{2} c \epsilon & \text{if } |i-j|=1 \\ 0 & \text{elsewhere} \end{cases}$$

This is the compressed walk as ϵ is negative.

The accommodation of spin in the both ends of the multiperipheral model, on the other hand, seems to produce a non negligible effect. Bialas and Sakai⁴² find that the contribution to the overlap slope arising from the spin of the leading clusters is around 8 gev^{-2} . They also conclude that the shrinkage could only be determined by the central region of the multiperipheral model. The points mentioned here have been best summed up in a paper by B.R. Weber.⁴⁴

5.3. THE MODEL

The form of the link dependent amplitude which is considered here and corresponds to the figure 5.1 is supposed to be of the following form,

$$A = \prod_j e^{\lambda t_j + \gamma Q_j Q_{j+2}} \quad (5.2)$$

where

$$t_j = Q_j^2.$$

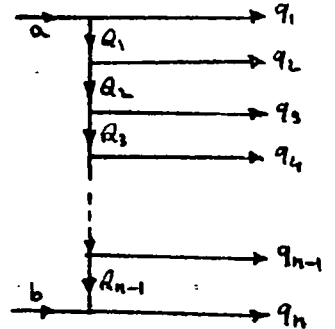


(fig. 5.1)

The reason why the term $Q_j Q_{j+1}$ is not taken into consideration is due to the following reason,

$$(Q_j - Q_{j+1})^2 = q_{j+1}^2$$

$$Q_j^2 + Q_{j+1}^2 - 2 Q_j Q_{j+1} = 2 \text{ const.}$$

$$Q_j Q_{j+1} = \frac{1}{2} (Q_j^2 + Q_{j+1}^2) - \text{const.},$$

which means that as $s_0/2$ is a constant and Q_j^2 - type terms have already been considered therefore $Q_j Q_{j+1}$ produces nothing new. So the obvious thing to do at this stage is to consider $Q_j Q_{j+2}$ type terms. To proceed we write Q_{j+2} in terms of Q_j ,

$$Q_{j+2} = Q_j - (q_{j+1} + q_{j+2}). \quad (5.3)$$

t_j according to (4.6) may be written in the following form,

$$t_j = - \left(\sum_{r=j+1}^n q_r^+ \right) \left(\sum_{r=1}^j q_r^- \right) - \left(\sum_{r=1}^j \bar{q}_{Tr} \right)^2$$

$$= - s_0 \left(\sum_{r=j+1}^n x_r \right) \left(\sum_{r=1}^j x_r^{-1} \right) - \left(\sum \bar{q}_{Tr} \right)^2. \quad (5.4)$$

The two terms in brackets of (5.3) in terms of x 's become,

$$\begin{aligned} q_{j+1} + q_{j+2} &= \left[(q_{j+1}^+ + q_{j+2}^+) (q_{j+1}^- + q_{j+2}^-) - (\bar{q}_{T_{j+1}} + \bar{q}_{T_{j+2}})^2 \right]^{1/2} \\ &= \left[S_0 \left(2 + \frac{x_{j+1}}{x_{j+2}} + \frac{x_{j+2}}{x_{j+1}} \right) - (\bar{q}_{T_{j+1}} + \bar{q}_{T_{j+2}})^2 \right]^{1/2} \end{aligned}$$

Since

$$\begin{aligned} y_j &= \ln x_j, \\ \frac{x_{j+1}}{x_j} &= \exp(y_{j+1} - y_j) \\ &= \exp(-\delta), \end{aligned}$$

where δ is the rapidity gap size,

$$\delta = \ln S / n - 1,$$

therefore,

$$\frac{x_{j+1}}{x_j} = S^{-\frac{1}{n-1}}.$$

Hence,

$$q_{j+1} + q_{j+2} \approx \alpha_1 - \frac{1}{2\alpha_1} (\bar{q}_{T_{j+1}} + \bar{q}_{T_{j+2}})^2, \quad (5.5)$$

where

$$\alpha_1 = \sqrt{S_0} \left(2 + S^{1/n-1} + S^{-1/n-1} \right)^{1/2}.$$

Going back to Q_j we write,

$$\begin{aligned} Q_j &= \sum_{r=1}^j q_r \\ &= \left[\left(\sum_{r=1}^j q_r^+ \right) \left(\sum_{r=1}^j q_r^- \right) - \left(\sum_{r=1}^j \bar{q}_{T_r} \right)^2 \right]^{1/2} \\ &= \sqrt{S_0} \left[\left(\sum_{r=1}^j x_r \right) \left(\sum_{r=1}^j x_r^{-1} \right) \right]^{1/2} - \frac{1}{2} \frac{\left(\sum_{r=1}^j \bar{q}_{T_r} \right)^2}{\sqrt{S_0} \left[\left(\sum_{r=1}^j x_r \right) \left(\sum_{r=1}^j x_r^{-1} \right) \right]^{1/2}} \quad (5.6) \end{aligned}$$

The $Q_j Q_{j+2}$ term requires the calculation of $Q_j (q_{j+1} + q_{j+2})$ due to (5.3). Using (5.5) and (5.6),

$$Q_j (q_{j+1} + q_{j+2}) = \sqrt{s_0} \alpha_1 \left[(\dot{\Sigma} X_r) (\dot{\Sigma} X_r^{-1}) \right]^{1/2} - \\ - \frac{1}{2} \left[\frac{\sqrt{\alpha_1} (\dot{\Sigma} \hat{q}_{T_r})^2}{\sqrt{s_0} \left[(\dot{\Sigma} X_r) (\dot{\Sigma} X_r^{-1}) \right]^{1/2}} + \right. \\ \left. + \frac{\sqrt{s_0} \left[(\dot{\Sigma} X_r) (\dot{\Sigma} X_r^{-1}) \right]^{1/2}}{\alpha_1} (\hat{q}_{T_{j+1}} + \hat{q}_{T_{j+2}})^2 \right]$$

Bearing in mind that $t_j = Q_j^2$, the exponential term of (5.2) could conveniently be written as, using 5.4 as well,

$$F_j \equiv \lambda t_j + \pi Q_j q_{j+2} \\ = \left\{ -\lambda s_0 (\dot{\Sigma} X_r) (\dot{\Sigma} X_r^{-1}) + \pi s_0 (\dot{\Sigma} X_r) (\dot{\Sigma} X_r^{-1}) - \pi \alpha_1 \sqrt{s_0} \left[(\dot{\Sigma} X_r) (\dot{\Sigma} X_r^{-1}) \right] \right\} \\ + \left\{ -\mu_j \left(\dot{\Sigma} \hat{q}_{T_r} \right)^2 + \frac{\pi \sqrt{s_0}}{2 \alpha_1} \left[(\dot{\Sigma} X_r) (\dot{\Sigma} X_r^{-1}) \right]^{1/2} (\hat{q}_{T_{j+1}} + \hat{q}_{T_{j+2}})^2 \right\}$$

(5.7)

where

$$\mu_j = \lambda + \pi - \frac{\alpha_1 \pi}{2 \sqrt{s_0}} \left[(\dot{\Sigma} X_r) (\dot{\Sigma} X_r^{-1}) \right]^{-1/2}$$

Let us split F_j into transverse and longitudinal parts,

$$F_j = F_j^L + F_j^\pi,$$

where

$$F_j^L = -\lambda s_0 \left(\dot{\Sigma}_{r=j+1} X_r \right) \left(\dot{\Sigma}_{r=1} X_r^{-1} \right) - \pi \alpha_1 \sqrt{s_0} \left[(\dot{\Sigma} X_r) (\dot{\Sigma} X_r^{-1}) \right]^{1/2} + \pi s_0 (\dot{\Sigma} X_r) (\dot{\Sigma} X_r^{-1})$$

(5.8)

$$F_j^\pi = -\mu_j \left(\dot{\Sigma}_{r=1} \hat{q}_{T_r} \right)^2 + \frac{\pi \sqrt{s_0}}{2 \alpha_1} \left[(\dot{\Sigma} X_r) (\dot{\Sigma} X_r^{-1}) \right]^{1/2} (\hat{q}_{T_{j+1}} + \hat{q}_{T_{j+2}})^2$$

Now we shall be dealing with each of them in the same way as in the fourth chapter.

5.3a LONGITUDINAL PART OF THE CALCULATION

The procedure here will be almost exactly as the calculations of

4.3a. Transforming x 's by,

$$X_r = x_r^{\circ} + \varepsilon_r$$

F_j^L becomes,

$$F_j^L = -\lambda_1 \left[\left(\sum x_r^{\circ} \right) \left(\sum x_r^{\circ -1} \right) - \left(\sum \varepsilon_r \right) \left(\sum x_r^{\circ -2} \varepsilon_r \right) + \left(\sum \varepsilon_r^2 x_r^{\circ -3} \right) \left(\sum x_r^{\circ} \right) \right. \\ \left. - \lambda_2 \left\{ \left(\sum x_r^{\circ} \right) \left(\sum x_r^{\circ -1} \right) + \sum_{rs} \varepsilon_r \varepsilon_s \right\}^{1/2} + \rho S_0 \left(\sum x_r^{\circ} + \sum \varepsilon_r \right) \left(\sum x_r^{\circ -1} - \sum x_r^{\circ -2} \varepsilon_r + \sum x_r^{\circ -3} \varepsilon_r^2 \right) \right]$$

where

$$\lambda_1 = \rho S_0$$

$$\lambda_2 = \rho \sqrt{S_0} \alpha_1$$

and

$$\sum_{rs} \varepsilon_r \varepsilon_s = \left(\sum x_r^{\circ} \right) \left(\sum x_r^{\circ -3} \varepsilon_r^2 \right) - \left(\sum \varepsilon_r \right) \left(\sum x_r^{\circ -2} \varepsilon_r \right)$$

Summing over all j 's we get,

$$\sum_{j=1}^{n-1} F_j^L = \left\{ -\lambda_1 M_{rs}^{(j)} x_r x_s^{-1} - \lambda_2 \sum_{j=1}^{n-1} \left[\left(\sum x_r^{\circ} \right) \left(\sum x_r^{\circ -1} \right) \right]^{1/2} + \rho S_0 \sum_{j=1}^{n-1} \left[\left(\sum x_r^{\circ} \right) \left(\sum x_r^{\circ -1} \right) \right] \right. \\ \left. + \lambda_1 H_{rs}^{(j)} \varepsilon_r \varepsilon_s - \frac{1}{2} \lambda_2 \sum_{j=1}^{n-1} \frac{\sum_{rs} \varepsilon_r \varepsilon_s}{\sqrt{\left(\sum x_r^{\circ} \right) \left(\sum x_r^{\circ -1} \right)}} + \rho S_0 \sum_{rs} y_{rs}^{(j)} x_r x_s^{-1} \right\} \\ = -\alpha^{(j)} - \lambda_1 M_{rs}^{(j)} \varepsilon_r \varepsilon_s \quad (5.9)$$

where

$$\alpha^{(j)} = \lambda_1 M_{rs}^{(j)} x_r x_s^{-1} + \lambda_2 \sum_{j=1}^{n-1} \left[\left(\sum x_r^{\circ} \right) \left(\sum x_r^{\circ -1} \right) \right]^{1/2} - \rho S_0 y_{rs}^{(j)} x_r x_s^{-1} \\ H_{rs}^{(j)} \varepsilon_r \varepsilon_s = \sum_{j=1}^{n-1} \left\{ \left(\sum_{j=1}^n \varepsilon_r \right) \left(\sum_{j=1}^n x_r^{\circ -2} \varepsilon_r \right) - \left(\sum_{j=1}^n x_r^{\circ} \right) \left(\sum_{j=1}^n x_r^{\circ -3} \varepsilon_r^2 \right) \right\}$$

and

$$M_{rs}^{(j)} \varepsilon_r \varepsilon_s = \frac{\lambda_2}{2\lambda_1} \sum_{j=1}^{n-1} \frac{\sum_{rs} \varepsilon_r \varepsilon_s}{\sqrt{\left(\sum x_r^{\circ} \right) \left(\sum x_r^{\circ -1} \right)}} - H_{rs}^{(j)} \varepsilon_r \varepsilon_s - \frac{\rho S_0}{\lambda_1} y_{rs}^{(j)} \varepsilon_r \varepsilon_s$$

Remembering that the original idea was to evaluate,

$$L = \int \prod_{j=1}^n \frac{dx_j}{x_j} |A(s, t)|^2 \delta(\sqrt{s} - \sum x_i) \delta(\sqrt{s} - s_0 \sum x_i^{-1})$$

or alternatively, using 5.9,

$$L = \frac{e^{-a}}{s_0 \prod x_j} \int \prod_{j=1}^n d\xi_j e^{-\lambda_1 M_{rs} \xi_r \xi_s} \delta\left(\frac{\sqrt{s}}{\sqrt{s_0}} - \sum x_i\right) \delta\left(\frac{\sqrt{s}}{\sqrt{s_0}} - \sum x_i^{-1}\right)$$

where the following transformation has been applied,

$$x_i \rightarrow \sqrt{s_0} x_i$$

and

$$M = M^{(1)} + \mathcal{P}(M^{(2)})$$

$$a = a^{(1)} + \mathcal{P}(a^{(2)}),$$

one, making use of the results obtained in section 5.3a, obtains,

(the matrix Z there has been replaced by M here),

$$L = \frac{e^{-a}}{s_0 \prod x_j} \frac{2\pi}{(\det M)^{n/2}} \left(\frac{\pi}{\lambda_1}\right)^{n/2} \frac{1}{4\pi\Gamma_2 - \Gamma_3^2}, \text{ if } M \text{ not singular} \quad (5.10)$$

$$L = \frac{e^{-a}}{s_0 \prod x_j} \frac{2(\pi)^{n/2}}{(\det f)^{n/2}} \frac{1}{(\lambda s_0)^{1+n/2}} \left[\sum_{ij}^{-1} (x_i^{-2} - x_n^{-2})(x_j^{-2} - x_n^{-2}) \right]^{-1}, \text{ if } M \text{ singular}$$

where Γ_1 , Γ_2 and Γ_3 have been defined according to (4.12). In doing this calculation we did not take into effect the dependence on transverse momenta, \vec{q}_{T_i} , of F_j^L . This will be dealt with at subsection 5.3c. Now we turn to the transverse part of the theory.

5.3b TRANSVERSE PART OF THE CALCULATION

Let us define

$$\beta_j = \frac{\sqrt{S_0}}{2\alpha_1} \left[\left(\sum_{r=1}^j X_r \right) \left(\sum_{r=1}^j X_r^{-1} \right) \right]^{1/2},$$

then the transverse part of the exponential, F_j^T , becomes,

$$F_j^T = -\mu_j \left(\sum_{r=1}^j \bar{q}_{T_r} \right) + \beta_j \left(\bar{q}_{T_{j+1}} + \bar{q}_{T_{j+2}} \right)^2,$$

hence,

$$\sum_{j=1}^{n-1} F_j^T = -L_{ij}^{(u)} \bar{q}_{T_i} \bar{q}_{T_j} + \Delta_{ij}^{(u)} \bar{q}_{T_i} \bar{q}_{T_j},$$

where the symmetric ($n \times n$) matrix $\Delta_{ij}^{(u)}$ is defined by,

$$\Delta_{ij}^{(u)} \bar{q}_{T_i} \bar{q}_{T_j} = \sum_{j=1}^{n-1} \left(\bar{q}_{T_{j+1}} + \Theta(n-2+j) \bar{q}_{T_{j+2}} \right)^2 \beta_j$$

with

$$\Theta(x) = \begin{cases} 1 & \text{if } x \geq 0 \\ 0 & \text{if } x < 0 \end{cases}$$

The matrix $L^{(u)}$, with the exception of the inclusion of the factor μ_j , is the same matrix as in 4.3b.

The final form of $\sum_j F_j^T$ now looks like,

$$\sum_{j=1}^{n-1} F_j^T = L_{ij}^{(u)} \bar{q}_i \bar{q}_j \quad (5.11)$$

where the $n \times n$ and symmetric matrix $L^{(u)}$ is defined by

$$L_{ij}^{(u)} = L_{ij}^{(u)} - \Delta_{ij}^{(u)}$$

This form of the transverse part (5.11) falls into the previously defined category (section 4.3b) and, thus, shall not be treated in full here.

The final answer is

$$T(\hat{b}) = \int \prod [\alpha^i b_i] \delta^{(n)}(\Sigma \hat{b}_i) \delta^{(n)}(\hat{b} - \Sigma \alpha_i \hat{b}_i) |\tilde{A}(\hat{b}_i)|^2 \\ = h \exp\left(-\frac{b^2}{4\theta}\right)$$

where

$$\theta = \sum F_{ij} (\tau - \alpha_i)(\tau - \alpha_j)$$

with the notations already been used in Chapter 4.

The radius, accordingly, is defined as,

$$R^2 = 4\theta$$

5.3c THE JEDACH-TURNAU EFFECT

The effect enters the calculation through S_0 ,

$$S_0 = m^2 + \hat{q}_{Tr}^2.$$

We write F_j^T , with this in mind,

$$\begin{aligned} F_j^L &= -\lambda \left(\sum_{r=1}^n \dot{X}_r \right) \left(\dot{\Sigma} \frac{S_0}{X_r} \right) + \tau \left(\dot{\Sigma} X_r \right) \left(\dot{\Sigma} \frac{S_0}{X_r} \right) - \tau \left(2 + s^{\frac{1}{n-1}} + s^{-\frac{1}{n-1}} \right) \left[\left(\dot{\Sigma} X_r \right) \left(\dot{\Sigma} \frac{S_0}{X_r} \right) \right]^{1/2} \\ &= \left\{ m^2 \left(\tau \dot{\Sigma} X_r - \lambda \sum_{r=1}^n X_r \right) \left(\dot{\Sigma} X_r^{-1} \right) - \lambda_4 m^2 \left[\left(\dot{\Sigma} X_r \right) \left(\dot{\Sigma} X_r^{-1} \right) \right]^{1/2} \right\} + \\ &+ \left\{ \left(\tau \dot{\Sigma} X_r - \lambda \sum_{r=1}^n X_r \right) \left(\dot{\Sigma} X_r^{-1} \hat{q}_{Tr}^2 \right) - \lambda_4 \left(\dot{\Sigma} X_r \right)^{1/2} \left[m^2 \left(\dot{\Sigma} X_r^{-1} \right)^{-1} \left(\dot{\Sigma} \frac{m^2 \hat{q}_{Tr}^2}{X_r} \right) \right] \right\} \end{aligned}$$

Finally,

$$\begin{aligned} F_j^L &= -\lambda m^2 \left(\sum_{r=1}^n \dot{X}_r \right) \left(\dot{\Sigma} X_r^{-1} \right) + \tau m^2 \left(\dot{\Sigma} X_r \right) \left(\dot{\Sigma} X_r^{-1} \right) - \lambda_4 m^2 \left[\left(\dot{\Sigma} X_r \right) \left(\dot{\Sigma} X_r^{-1} \right) \right]^{1/2} \\ &+ \left[\left(\tau \dot{\Sigma} X_r - \lambda \sum_{r=1}^n X_r - \lambda_4 \sqrt{\left(\dot{\Sigma} X_r \right) \left(\dot{\Sigma} X_r^{-1} \right)} \right)^{-1/2} \right] \left(\dot{\Sigma} \frac{\hat{q}_{Tr}^2}{X_r} \right) \end{aligned} \tag{5.12}$$

where $\lambda_4 = \tau \left(2 + s^{\frac{1}{(n-1)}} + s^{-\frac{1}{(n-1)}} \right)^{1/2}$,

The last term is the one which was absent from the calculations of subsection (5.3a) and should be added to (5.3b) which will make the diagonal entries of the matrix $L_{ij}^{(u)}$ slightly modified.

Noting that the transverse momentum distribution formula in this case will be same as the one in the fourth chapter, with the replacement by $L_{ij}^{(u)}$, we find the most suitable values for λ and τ (figure 5.2) and then plot the radius as a function of energy in the figures (5.3) and (5.4) in both cases. It is obvious from Fig. 5.3 that, now, the value and the slope of the radius, in Henyey's case, agrees with the experiment very well. For comparison we plot the

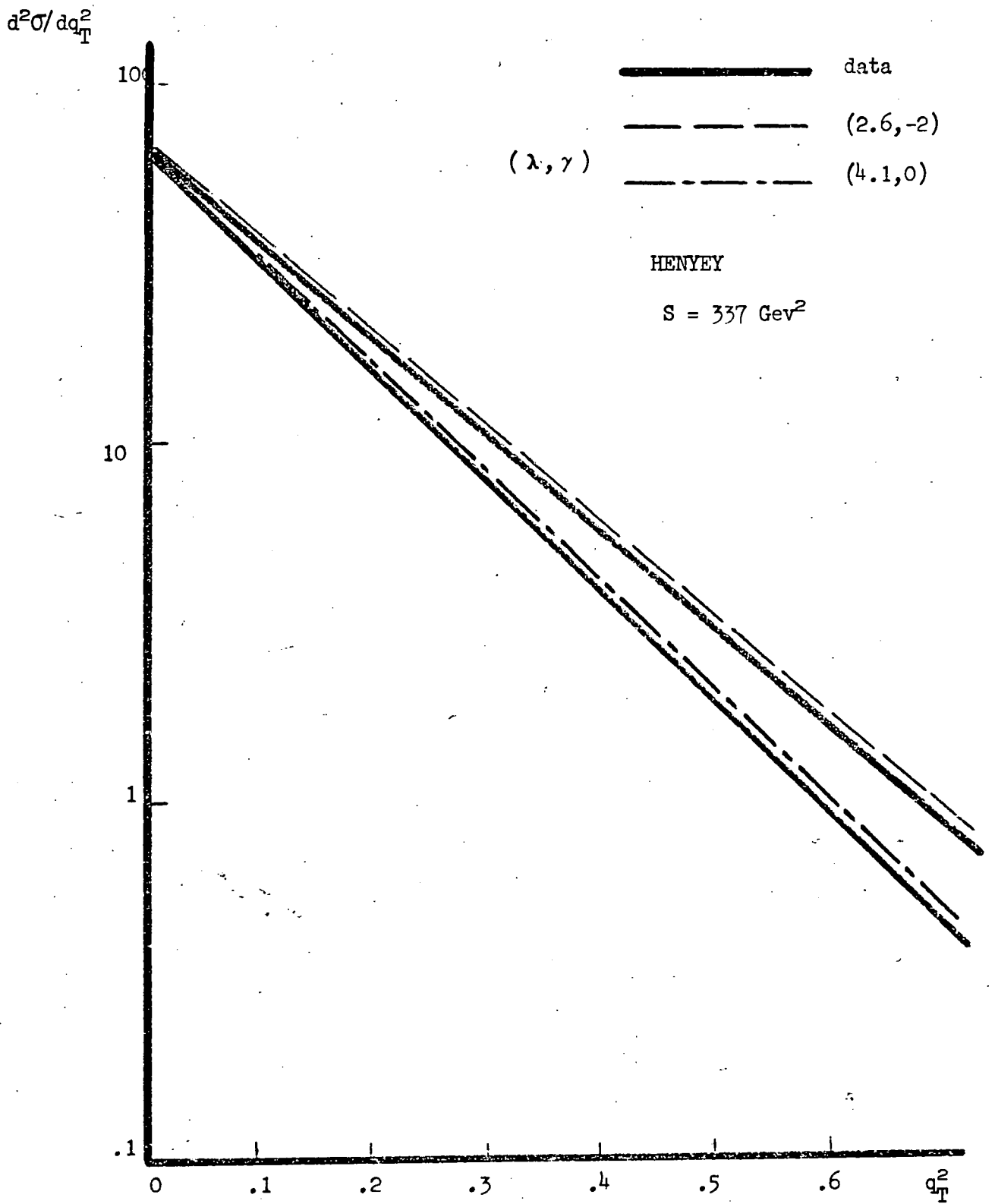


Fig 5.2

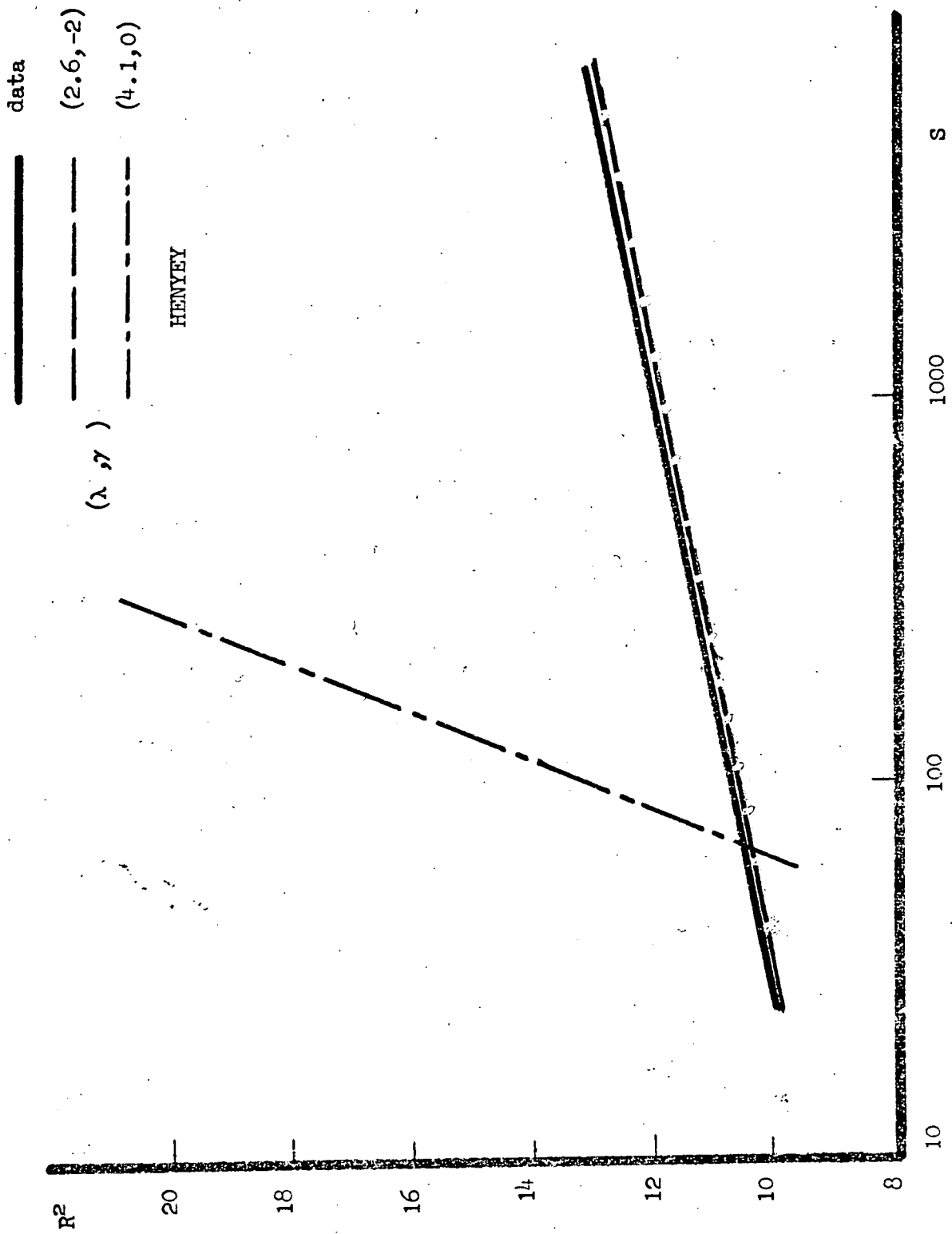


Fig 5.3

data
(2.8,0)
(2.8,-2)
(2,.005)

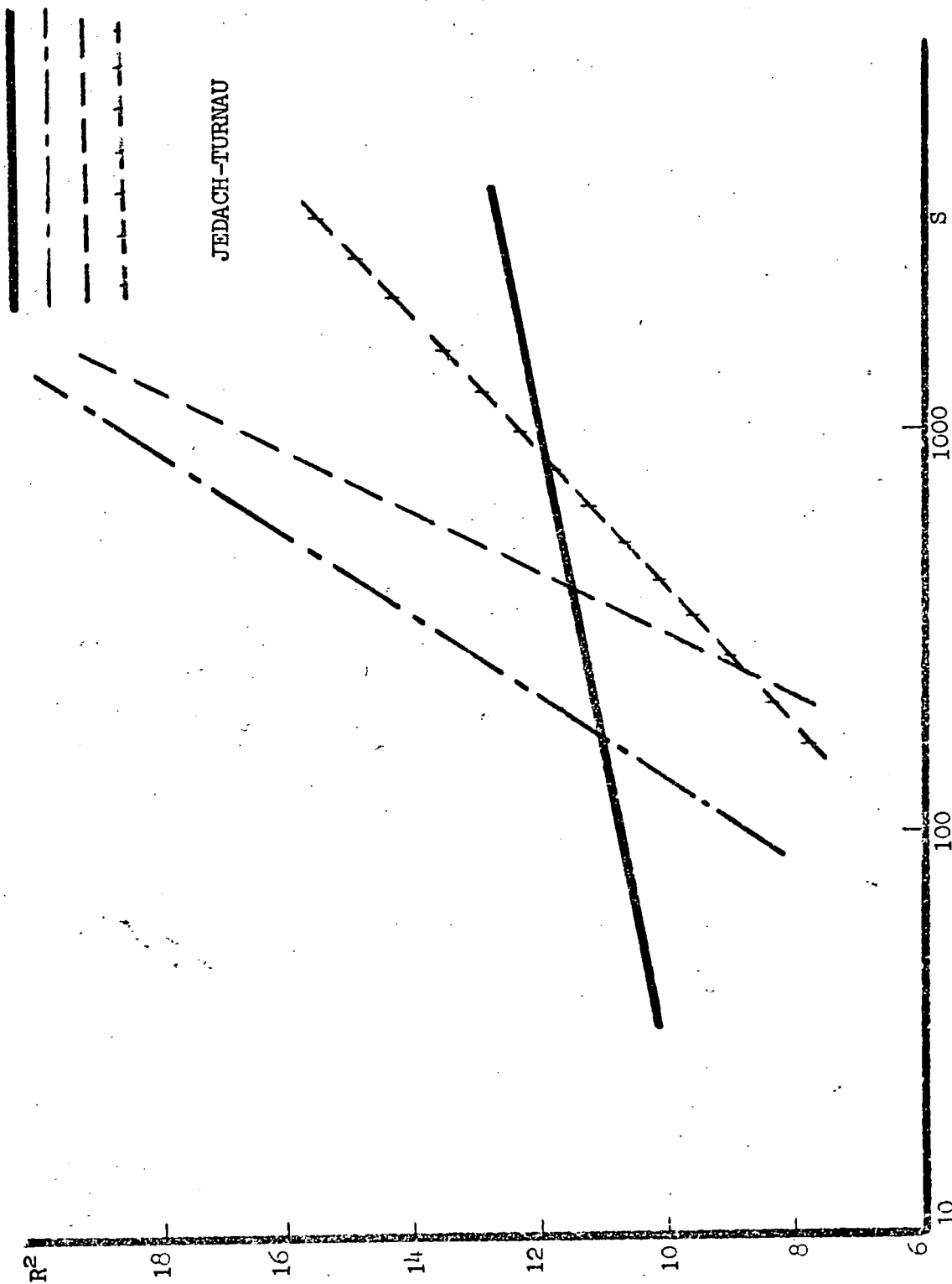


Fig 5.4

result of the fourth chapter as well. In fig. (5.4), where the Jedach-Turnau calculations have been included, still the problem remains unsolved and we get no agreement with data.

5.4 ON THE PARAMETER τ

In this section we would like to see what sort of effect τ introduces and why should it be the case that it adopts an opposite sign to that of the previously defined parameter λ .

We remember that τ was introduced by the following type of equation,

$$A(Q_j) = \prod_j e^{\lambda Q_j^2 + \tau Q_j Q_{j+2}}$$

In order to understand this let us make use of the following,

$$\begin{aligned} \tau Q_j Q_{j+2} &= -\frac{\tau}{2} (Q_j - Q_{j+2})^2 + \frac{\tau}{2} (Q_j^2 + Q_{j+2}^2) \\ &= -\frac{\tau}{2} (q_{j+1} + q_{j+2})^2 + \frac{\tau}{2} (Q_j^2 + Q_{j+2}^2) \end{aligned}$$

As we should sum over j , the summation running from 1 to $n-3$ for the interference term only, we get,

$$\tau \sum_{j=1}^{n-3} Q_j Q_{j+2} = -\frac{\tau}{2} \sum_{j=1}^{n-3} (q_{j+1} + q_{j+2})^2 + \frac{\tau}{2} \sum_{j=1}^{n-3} (Q_j^2 + Q_{j+2}^2)$$

One easily writes,

$$\frac{\tau}{2} \sum_{j=1}^{n-3} (Q_j^2 + Q_{j+2}^2) = \tau \sum_{j=1}^{n-1} Q_j^2 - \frac{\tau}{2} (Q_1^2 + Q_2^2 + Q_{n-2}^2 + Q_{n-1}^2)$$

whence,

$$\tau \sum_{j=1}^{n-3} Q_j Q_{j+2} = -\frac{\tau}{2} \sum_{j=1}^{n-3} (q_{j+1} + q_{j+2})^2 - \frac{\tau}{2} (Q_1^2 + Q_2^2 + Q_{n-2}^2 + Q_{n-1}^2) + \tau \sum_{j=1}^{n-1} Q_j^2$$

Now it is easier to see what is going on since $A(Q_j)$ could now conveniently be written as,

$$A(Q_j) = \exp\left[(\lambda + \tau) \sum_{j=1}^{n-1} Q_j^2\right] \exp\left[-\frac{\tau}{2} (Q_1^2 + Q_2^2 + Q_{n-2}^2 + Q_{n-1}^2)\right] \exp\left[-\frac{\tau}{2} \sum_{j=1}^{n-3} (q_{j+1} + q_{j+2})^2\right]$$

with

$$\begin{aligned} |\lambda| > |\tau| \\ \tau < 0, \lambda > 0 \end{aligned}$$

The first factor is the term which was known from the previous chapter,

with the only difference that the coefficient ($\lambda - |\mathcal{V}|$) is smaller allowing a slow energy variation for the radius. We are not interested in the last term and indeed nothing much could be said about it. The second factor is new. It is obviously not varying with energy and is just a constant. This is the term which gives a constant contribution to the magnitude of the radius. By choosing suitable values for the two parameters one could bring the magnitude and the slope of the radius to the point that would agree with data, as in figure 5.3.

5.5 CONCLUSIONS

We became familiar with the problem the radius is concerned with in the third chapter. There we saw that, by adjusting the parameters to produce the correct transverse momentum distribution, the radius rises too sharply as the energy increases in the multi-peripheral model. There have been some speculations for some time that perhaps the interference diagrams, created by the unitarity, might have been helpful in remedying the sharp increase of the radius and in actual fact there were some attempts along this line which had taken the nearby crossed diagram in the ladder.

In the fourth chapter, treating all prominent diagrams on the same footing, we concluded that, as long as the radius is concerned, the contribution of the $n! - 1$ diagrams, as compared to the one uncrossed diagram, is quite unimportant and therefore this provides us with no solution.

Attempting to solve the problem of the radius, a new alternative was introduced in chapter 5. This time we let the amplitude be link-dependent as well in the multiperipheral context. This idea has been the subject of some recent papers where they take the nearby link correlations into consideration (transverse part of momenta only). It is shown in the text that considering full momenta Q_j, Q_{j+1} type of terms produce essentially nothing new. So we concentrate on Q_j, Q_{j+2} terms. We show that the modification to the basic amplitude is quite adequate in describing the energy dependence of radius along a big range of energy. The agreement with data is very good and may be considered as a support to the model.

APPENDIX A

POISSONIAN σ_n AND f_2

In this part we would like to show that if the distribution of σ_n versus n is poissonian then the two particle correlations function f_2 is zero.

σ_n is of the following form:

$$\sigma_n(s) = \frac{(g^2 \ell s)^n}{n!} s^{-g^2} \sigma_{tot} \quad (A1)$$

and f_2 is defined as

$$\begin{aligned} f_2 &= \langle n(n-1) \rangle - \langle n \rangle^2 \\ &= \frac{\sum_n n(n-1) \sigma_n(s)}{\sum_n \sigma_n(s)} - \left[\frac{\sum_n n \sigma_n(s)}{\sum_n \sigma_n(s)} \right]^2 \quad (A2) \end{aligned}$$

Substituting (A1) in (A2)

$$f_2 = \frac{\sum_n n(n-1) \frac{(g^2 \ell s)^n}{n!}}{\sum_n \frac{(g^2 \ell s)^n}{n!}} - \left[\frac{\sum_n n \frac{(g^2 \ell s)^n}{n!}}{\sum_n \frac{(g^2 \ell s)^n}{n!}} \right]^2$$

since we have

$$\sum_n \frac{(g^2 \ell s)^n}{n!} = e^{g^2 \ell s}$$

$$\sum_n n(n-1) \frac{(g^2 \ell s)^n}{n!} = (g^2 \ell s)^2 e^{g^2 \ell s}$$

and

$$\sum_n n \frac{(g^2 \ell s)^n}{n!} = (g^2 \ell s) e^{g^2 \ell s}$$

thus

$$f_2 = \frac{(g^2 \ell s)^2 e^{g^2 \ell s}}{e^{g^2 \ell s}} - \left[\frac{g^2 \ell s e^{g^2 \ell s}}{e^{g^2 \ell s}} \right]^2$$

$$= 0$$

APPENDIX B

THE INVERSE TRANSFORMATION OF (3.8)

The equation 2 of chapter 3, suppressing the longitudinal variables, is

$$\tilde{A}(\vec{b}_j) = \int \prod_{j=1}^n [d^2 \vec{q}_j e^{i \vec{q}_j \cdot \vec{b}_j}] A(\vec{q}_j) \delta^{(n)}(\Sigma \vec{q}_j) \quad (B1)$$

We have ignored the uninteresting factors of 2. We shall make the ansatz that equation 3 of the same chapter is the inverse transformation of (B1) and then verify that it is allright.

$$A(\vec{q}'_j) = n^2 \int \prod_{j=1}^n [d^2 \vec{b}_j e^{-i \vec{q}'_j \cdot \vec{b}_j}] \tilde{A}(\vec{b}_j) \delta^{(n)}(\Sigma \vec{b}_j) \quad (B2)$$

(B1) and (B2) could be combined together to produce

$$A(\vec{q}'_j) = n^2 \int d^2 \vec{q}_1 \dots d^2 \vec{q}_n d^2 \vec{b}_1 \dots d^2 \vec{b}_n e^{i(\vec{q}'_j - \vec{q}_j) \cdot \vec{b}_j} \tilde{A}(\vec{q}_j) \delta^{(n)}(\Sigma \vec{q}_j) \delta^{(n)}(\Sigma \vec{b}_j) \quad (B3)$$

The integration over \vec{b}_1 is simple:

$$\begin{aligned} A(\vec{q}'_j) &= n^2 \int d^2 \vec{q}_1 \dots d^2 \vec{q}_n d^2 \vec{b}_2 \dots d^2 \vec{b}_n e^{i(\vec{q}'_2 - \vec{q}'_1) \cdot \vec{b}_2 + \dots + i(\vec{q}'_n - \vec{q}'_1) \cdot \vec{b}_n} \\ &\quad \cdot A(\vec{q}_j) \delta^{(n)}(\Sigma \vec{q}_j) \exp[-i(\vec{q}'_1 - \vec{q}_1) \cdot (\vec{b}_2 + \dots + \vec{b}_n)] \\ &= n^2 \int d^2 \vec{q}_1 \dots d^2 \vec{q}_n d^2 \vec{b}_2 \dots d^2 \vec{b}_n e^{i\vec{b}_2 \cdot (\vec{q}'_2 - \vec{q}'_1 - \vec{q}_1 + \vec{q}'_1) + \dots + i\vec{b}_n \cdot (\vec{q}'_n - \vec{q}'_1 - \vec{q}_1 + \vec{q}'_1)} \\ &\quad \cdot A(\vec{q}_j) \delta^{(n)}(\Sigma \vec{q}_j) \end{aligned}$$

The integration over the remaining \vec{b}_j 's, in turn, will result on:

$$A(\vec{q}'_j) = n^2 \int d^2 \vec{q}_1 \dots d^2 \vec{q}_n A(\vec{q}_j) \delta^{(n)}(\Sigma \vec{q}_j) \delta^{(n)}(\vec{q}'_2 - \vec{q}'_1 - \vec{q}_1 + \vec{q}'_1) \dots \delta^{(n)}(\vec{q}'_n - \vec{q}'_1 - \vec{q}_1 + \vec{q}'_1)$$

Now, leaving $d^2 \vec{q}_j$ out, the integration over $d^2 \vec{q}_j$ by making use of the δ -functions yields

$$A(\vec{q}'_j) = n^2 \int d^4 q_i A(\vec{q}_1, \vec{q}_1 - \vec{q}'_1 + \vec{q}'_2, \vec{q}_1 - \vec{q}'_1 + \vec{q}'_3, \dots, \vec{q}_1 - \vec{q}'_1 + \vec{q}'_n) \delta^2[n(\vec{q} - \vec{q}') + \sum_{j=1}^n \vec{q}'_j]$$

$$= \int d^4 q_i A(\vec{q}_1, \vec{q}_1 - \vec{q}'_1 + \vec{q}'_2, \dots, \vec{q}_1 - \vec{q}'_1 + \vec{q}'_n) \delta^2(\vec{q}_1 - \vec{q}'_1 + \frac{1}{n} \sum_{j=1}^n \vec{q}'_j)$$

Let

$$\sum_{j=1}^n \vec{q}'_j = \vec{\varepsilon}$$

then the \vec{q}_1 integration produces,

$$A(\vec{q}'_j) = A(\vec{q}'_1 - \frac{\vec{\varepsilon}}{n}, \vec{q}'_2 - \frac{\vec{\varepsilon}}{n}, \dots, \vec{q}'_n - \frac{\vec{\varepsilon}}{n}) \quad (\text{B4})$$

The Lorentz invariance implies that l.h.s of (B3) and r.h.s. of (B4) are the same, which this in turn implies (B1) and (B2) are inverse transformations of each other.

APPENDIX C

AN INTEGRATION (CORRESPONDING TO 4.10)

In the process of integrating over ξ_i in (4.10), we had assumed that the matrix Z_{ij} was not singular. There are occasions, such as the uncrossed diagrams, where Z_{ij} becomes singular. The singularity is due to the fact that the last column of the matrix has zero entries. Because of this, the procedure from (4.10) to (4.11) will differ slightly as we shall explain below.

$$L = \left[\prod_i^n z_i \right]^{-1} \exp \left[-\lambda S_0 M_{ij} z_i z_j^{-1} \right] \int \left[\prod_{i=1}^n d\xi_i \right] e^{-\lambda S_0 Z_{ij} \xi_i \xi_j} \delta \left(\sum_{i=1}^n \xi_i \right) \delta \left(\sum_{i=1}^n \frac{\xi_i}{z_i} \right)$$

Separating the last column of Z_{ij} from the others,

$$L = \left[\prod_i^n z_i \right]^{-1} \exp \left[-\lambda S_0 M_{ij} z_i z_j^{-1} \right] \int \prod_{i=1}^{n-1} [d\xi_i] e^{-\lambda S_0 Z'_{ij} \xi_i \xi_j} \int d\xi_n \delta \left[\xi_n - \left(-\sum_{i=1}^{n-1} \xi_i \right) \right] \delta \left[\frac{\xi_n}{z_n} + \sum_{i=1}^{n-1} \frac{\xi_i}{z_i} \right] e^{-\lambda S_0 \left[Z_{nj} \xi_n \xi_j - z_{in} \xi_i \xi_n - z_{nn} \xi_n^2 \right]}$$

Z'_{ij} is one order less than Z_{ij} , where the last row and column of Z are taken off. Since $Z_{in} \forall i = 1, n$, is zero thus

$$L = \frac{\exp \left[-\lambda S_0 M_{ij} z_i z_j^{-1} \right]}{\prod_i^n (z_i)} \int \prod_{i=1}^{n-1} (d\xi_i) e^{-\lambda S_0 Z'_{ij} \xi_i \xi_j + \lambda S_0 Z_{nj} \xi_i \xi_j} \delta \left[\sum \left(\frac{1}{z_i} - \frac{1}{z_n} \right) \xi_i \right]$$

Writing δ -function in its integral form and then doing the ξ_i integral first one finds

$$L = \frac{2\pi^{n/2} \exp \left[-\lambda S_0 M_{ij} z_i z_j^{-1} \right]}{(S_0)^{n/2} \sqrt{\det f} \prod_i z_i} \frac{1}{\sqrt{\prod_{i,j}^{n-1} \left(\frac{1}{z_i} - \frac{1}{z_n} \right) \left(\frac{1}{z_j} - \frac{1}{z_n} \right)}}$$

where

$$f_{ij} = Z'_{ij} - Z_{nj}$$

APPENDIX D

AN INTEGRATION (CORRESPONDING TO 4.3b)

We shall repeat the calculation of subsection 4.3b where the matrix B_{ij} is not singular. Let us rewrite the equation 4.14 here,

$$T(\vec{b}) = h_1 \int \prod_{j=1}^n [d^4 b_j] \delta^{(n)}(\Sigma \vec{b}_j) \delta^{(n)}(\vec{b} - \Sigma \chi_j \vec{b}_j) \exp\left[-\frac{1}{\lambda} B_{ij} \vec{b}_i \cdot \vec{b}_j\right]$$

Rewriting the S-functions in their integral form and performing the \vec{b}_j integration first we get

$$T(\vec{b}) = \frac{h_1}{\det B} (\pi \lambda)^n \int d^4 y e^{i \vec{y} \cdot \vec{b} - \lambda (\Sigma B_{ij}^{-1} \chi_i \chi_j) y^2} \int d^2 x e^{-\lambda B_{ij}^{-1} x^2 + \lambda y B_{ij}^{-1} (\chi_i + \chi_j) \vec{x}}$$

The integrations over \vec{x} and \vec{y} are easy now, they produce,

$$T(\vec{b}) = \pi \frac{h_2}{\lambda \theta} \exp\left[-\frac{b^2}{4 \lambda \theta}\right]$$

where,

$$h_2 = h_1 \frac{(\pi \lambda)^{n-1} \pi^2}{\det B (\Sigma B^{-1})}$$

$$\theta = F_{ij} \chi_i \chi_j$$

and

$$F_{ij} = B_{ij}^{-1} - \frac{1}{\Sigma B_{ij}^{-1}} (\mathcal{J} B \mathcal{J})_{ij}$$

Therefore the radius is

$$R^2 = 4 \lambda \theta$$

APPENDIX E

A GENERAL INTEGRATION

In this part we would like to evaluate the following integral,

$$I = \int_{-\infty}^{\infty} \prod_{i=1}^n [d^4 b_i e^{i \vec{\alpha}_i \cdot \vec{b}_i}] e^{-B_{ij} \vec{b}_i \cdot \vec{b}_j},$$

where B_{ij} is a symmetric and singular matrix. Let C be the matrix which transforms B to D , where D is diagonal,

$$D_{ij} = (C^T B C)_{ij}.$$

Put

$$\vec{\tilde{b}}_i = C \vec{b}_i \quad ; \quad (\vec{\tilde{b}}_i = \sum_j C_{ji} b_j)$$

and

$$\vec{\tilde{\alpha}}_i = C \vec{\alpha}_i.$$

Since

$$B_{ij} \vec{b}_i \cdot \vec{b}_j = D_{ij} \vec{\tilde{b}}_i \cdot \vec{\tilde{b}}_j,$$

and

$$\prod \vec{\alpha}_i \cdot \vec{b}_i = \prod \vec{\tilde{\alpha}}_i \cdot \vec{\tilde{b}}_i,$$

then we can write I in the following way

$$I = \int_{-\infty}^{\infty} \prod_{i=1}^n [d^4 \tilde{b}_i e^{i \vec{\tilde{\alpha}}_i \cdot \vec{\tilde{b}}_i}] e^{-D_{ij} \vec{\tilde{b}}_i \cdot \vec{\tilde{b}}_j}$$

The singularity of matrix B implies that one of the entries of matrix D ,

$$D_{ij} = \begin{pmatrix} \lambda_1 & & & 0 \\ & \lambda_2 & & \\ & & \dots & \\ 0 & & & \lambda_n \end{pmatrix},$$

say λ_n , must be zero. Therefore

$$I = \int_{-\infty}^{\infty} d^4 \tilde{b}_n e^{i \vec{\tilde{\alpha}}_n \cdot \vec{\tilde{b}}_n} \int_{-\infty}^{\infty} \prod_{i=1}^{n-1} [d^4 \tilde{b}_i e^{i \vec{\tilde{\alpha}}_i \cdot \vec{\tilde{b}}_i}] e^{-D_{ij} \vec{\tilde{b}}_i \cdot \vec{\tilde{b}}_j},$$

where

$$D_{ij} = \begin{pmatrix} \lambda_1 & & & 0 \\ & \lambda_2 & & \\ & & \dots & \\ 0 & & & \lambda_{n-1} \end{pmatrix}.$$

The evaluation of first and second integrals are easy enough,

$$I = \frac{\pi^{n-1}}{\det B} \delta^{(n)}(\tilde{\alpha}_n) \exp\left[-\frac{1}{4} B_{ii}^{-1} \tilde{\alpha}_i^2\right]$$

Putting back $\tilde{\alpha}_i$ in $\vec{\alpha}_i$ form,

$$I = \frac{\pi^{n-1}}{\det B} \delta^{(n)}\left(\sum_i C_{in} \vec{\alpha}_i\right) \exp\left[-\frac{1}{4} \sum_{i=1}^{n-1} \frac{1}{\lambda_i} \left(\sum_{j=1}^n C_{ji} \vec{\alpha}_j\right)^2\right]$$

This is the result, but to make it look neater let us define a new

$n \times n$ symmetric matrix, F_{ij} , by

$$F_{ij} \vec{\alpha}_i \cdot \vec{\alpha}_j = \frac{1}{4} \sum_{i=1}^{n-1} \frac{1}{\lambda_i} \left(\sum_{j=1}^n C_{ji} \vec{\alpha}_j\right)^2,$$

then

$$I = \frac{\pi^{n-1}}{\prod_{i=1}^{n-1} \lambda_i} \delta^{(n)}\left(\sum_i C_{in} \vec{\alpha}_i\right) \exp\left[-F_{ij} \vec{\alpha}_i \cdot \vec{\alpha}_j\right]$$

REFERENCES

1. Particle Data Group, Rev. Mod. Phys. 45 (1973) 134.
2. Aubert et al, Phys. Rev. Lett. 33 (1974) 1404.
3. Miettinen, CERN Preprint, TH 1906 (1974).
4. Jacob, CERN Preprint, TH 1683 (1973).
5. Froissart, Phys. Rev. 123 (1961) 1053.
6. Pomeranchuk, Soviet Phys. JETP 3 (1956) 307.
7. Bogart et al NAL Conf. 73/30 - EXP (1973).
Whitmore, Phys. Rep. 10C (1974) No. 5.
8. Horn & Zachariasen, Hadron Physics at very high energies (1973),
Pub = Benjamin.
9. Jacob, Chicago Conf., Batavia VI (1972), 373.
10. Miettinen, 4th British Summer School, Durham (1974).
11. Morrison, CERN Preprint, D.Ph.11 /PHYS 73-46 (1973).
12. Frazer et al, Rev. Mod. Phys. 44 (1972) 284.
13. Feynman, Phys. Rev. Lett. 23 (1969) 1415.
14. Bertin et al, Phys. Lett. 42B (1972) 493.
15. A.H. Mueller, Chicago Conf. Batavia I (1971), 347
16. Koba et al, Nuc. Phys. B40 (1972) 317.
17. Jackson, 14th Scottish Summer School, Edinburgh (1973)
Appendix E.
18. Mueller, Phys. Rev. D4 (1971) 150.
19. Collins & Squires, Regge Poles in Particle Physics (1968) Springer
Collins, Phys. Rep. 1C (1971) 104.
20. Fialkowski & Miettinen PL B43 (1973) 61
Harari and Rabinovici PL B43 (1973) 49.
21. Dolen, Horn, Schmid PR 166 (1968) 1768.
22. Bertocchi, Fubini, NC 25 (1962) 626.
Tonin
Amati, Stanghellini, NC 26 (1962) 896.
Fubini.
23. Balakerishnan JMP 15 (1974) 247.
Dremin & Dunaerskii Phys. Rep. 18C (1975) No. 3.

24. Silverman & Ting, NP B35 (1971) 445.
25. Chan Hong-Mo, Loskiewicz,
Allison NC 57A (1968) 93.
26. Chew and Pignotti PR 176 (1968) 2112
PRL 19 (1967) 614
27. Sohlo Helsinki Univ. Prep. (1968) ISBN 951-45-0367-8.
28. Michejda, Turnau,
Bialas NC 56A (1968) 241
29. F.S. Henyey PLB45 (1973) 469
F.S. Henyey Univ. of Michigan Prep. (1973) UM HE 73-11
R.C. Hwa PR D8 (1973) 1331
C.J. Hamer and R.F. Peierls PR D8 (1973) 1358
we are following the papers by Henyey.
30. Van Hove RMP 36 (1964) 655.
31. S. Jadach and Turnau PLB50 (1974) 369.
32. M. Teper Westfield College Prep. (1974).
33. F.S. Henyey NPB78 (1974) 435.
34. F.S. Henyey Univ. of Michigan Prep. (1974) UM HE 74-2.
35. D.R. Snider and PRD3 (1971) 996.
D.M. Tow.
36. M. Teper Lett NC8 (1973) 929.
37. R.F. Amann and PLB42 (1972) 353
P.M. Shah
38. S. Fubini Scottish Univ. Summer School (1963).
39. Whitmore Phys. Rep. 10C (1974) 324.
40. J. Kubar-Andre', NPB93 (1975) 138.
M.le Bellac &
J.L. Meunier
41. C. Michael Liverpool preprint LTH 4 (1975)
42. A. Bialas & N. Sakai PL 55B (1975) 81.
43. Grassberger & CERN preprint TH 1979 (1975)
Miettinen
44. B.R. Webber Cambridge preprint HEP75110 (1975).
45. R.HWA PRL 26 (1971) 1143.

